

**DESIGN AND DEVELOPMENT OF CERAMIC-BASED
COMPOSITES FOR CUTTING TOOL INSERTS**

BY
TAHA WAQAR

A Thesis Presented to the
DEANSHIP OF GRADUATE STUDIES

KING FAHD UNIVERSITY OF PETROLEUM & MINERALS
DHAHRAN, SAUDI ARABIA

In Partial Fulfillment of the
Requirements for the Degree of

MASTER OF SCIENCE

In

MECHANICAL ENGINEERING

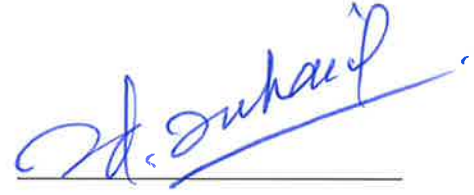
APRIL 2018

KING FAHD UNIVERSITY OF PETROLEUM & MINERALS

DHAHRAN- 31261, SAUDI ARABIA

DEANSHIP OF GRADUATE STUDIES

This thesis, written by **Taha Waqar** under the direction of his thesis advisor and approved by his thesis committee, has been presented and accepted by the Dean of Graduate Studies, in partial fulfillment of the requirements for the degree of **MASTER OF SCIENCE IN MECHANICAL ENGINEERING.**



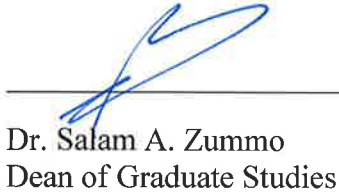
Dr. Syed Sohail Akhtar
(Advisor)



Dr. Zuhair M. Gasem
Department Chairman



Dr. Abul Fazal M. Arif
(Member)



Dr. Salam A. Zummo
Dean of Graduate Studies



Dr. Tahar Laoui
(Member)

21/5/18
Date

© Taha Waqar

2018

Dedicated to my family, for their unwavering support.

ACKNOWLEDGMENTS

I begin in the name of Allah, the most beneficent, the most merciful. I would not have been able to complete my work without the help of Allah who bestowed me with courage, health and the motivation to persevere and realize my academic ambitions.

For the duration of this work, my parents and siblings were a constant source of motivation and support. Their prayers, love and encouragement helped me greatly to achieve this milestone.

I am thankful to *King Fahd University of Petroleum and Minerals* and its Mechanical Engineering department for providing me the opportunity to pursue my graduate studies and for all the support I received in carrying out this research work.

I would like to express my utmost gratitude to my thesis advisor *Dr. Syed Sohail Akhtar* for all I have learned from him, for his patience when progress started to slow down and for his guidance whenever I needed it. I am immensely thankful to *Dr. Abul Fazal M. Arif* for his counseling and encouragement for me to succeed in my academic endeavors. I am also very grateful to *Dr. Tahar Laoui* for his involvement and support since the beginning of my degree. Lastly, acknowledgments are due to *Dr. Abbas Hakeem* for his assistance during the experimental work and to my research group members for their help in achieving my research objectives.

A heartfelt thanks to all my friends and colleagues in the Mechanical Engineering department for making my time at KFUPM a memorable and enlightening experience.

TABLE OF CONTENTS

ACKNOWLEDGMENTS.....	V
TABLE OF CONTENTS.....	VI
LIST OF TABLES.....	IX
LIST OF FIGURES.....	X
LIST OF ABBREVIATIONS.....	XIII
ABSTRACT.....	XV
ملخص الرسالة.....	XVII
CHAPTER 1 INTRODUCTION.....	1
1.1 Background and Motivation.....	1
1.2 Problem Description	8
1.3 Project Objectives	8
1.4 Research Methodology	9
CHAPTER 2 LITERATURE REVIEW	11
2.1 Types of Cutting Tool Insert Materials	11
2.2 Recent Developments in Ceramic Composite Material Design	13
2.3 Research Work Dealing With Enhanced Alumina Composites For Cutting Tools.....	16
2.4 Exploring Other Materials for Inclusion Considerations	21
2.5 High Speed Machining	23
2.6 Computational Models	27
2.7 Spark Plasma Sintering.....	29

2.8	Summary of Chapter	30
 CHAPTER 3 MATERIAL DESIGN		31
3.1	Matrix & Reinforcement Selection	31
3.2	Computational Models	36
	3.2.1. Mean-field homogenization and effective medium approximations	36
	3.2.2 Prediction of fracture toughness and energy release rate	40
3.3	Numerical Simulations	46
3.4	Single Inclusion Results	48
	3.4.1 Effective Thermal Conductivity & CTE Determination.....	48
	3.4.2 Effective Elastic Modulus Determination	50
	3.4.3 Minimum Particle Size of Inclusion Study	51
	3.4.4 Effective Fracture Toughness Determination	52
	3.4.5 Exploring the Effect of Porosity	54
3.5	Double Inclusions.....	55
	3.5.1 Effective Thermal Conductivity & CTE Determination.....	56
	3.5.2 Effective Elastic Modulus Determination	58
	3.5.3 Effective Fracture Toughness Determination	59
	3.5.5 Minimum Particle Size of Inclusions Determination	61
3.6	Summary of Chapter	62
 CHAPTER 4 MATERIAL DEVELOPMENT, CHARACTERIZATION & TESTING.....		63
4.1	Material Development	63
	4.1.1 Manufacturing of Designed Composite	64
	4.1.2 Microstructure and Mechanical Characterization	67
	4.1.3 Thermal Characterization	71
4.2	Microstructure & Mechanical Characterization.....	73
	4.2.1 SEM Analysis.....	73
	4.2.2 X-ray Diffraction Analysis.....	78
	4.2.3 Raman Spectroscopy Analysis	79
	4.2.3 Density & Porosity Determination.....	80
	4.2.4 Micro Hardness, Modulus of Elasticity and Fracture Toughness	81
4.3	Thermal Characterization.....	84
	4.3.1 Effective Thermal Conductivity	84
	4.3.2 Coefficient of Thermal Expansion (CTE)	85
4.4	Summary of Results	87

4.5	Summary of Chapter	88
CHAPTER 5 PERFORMANCE EVALUATION OF THE PROPOSED CUTTING TOOL INSERT.....		89
5.1	Introduction.....	89
5.2	Mathematical Models	90
5.3	Coupled Thermal-Structural Analysis	93
5.4	Finite Element Modelling	94
5.4.1	Geometry Model	94
5.4.2	Material Model.....	95
5.4.3	Boundary Conditions	95
5.4.5	Meshing	97
5.5	Results and Discussion	99
5.5.1	Alumina Insert	100
5.5.2	ZTA Insert.....	106
5.5.3	Designed Ceramic Composite Insert	111
5.6	Model Validation	116
5.7	Summary of Chapter	116
CHAPTER 6 CONCLUSIONS & RECOMMENDATIONS.....		117
6.1	Conclusions.....	117
6.2	Recommendations.....	119
REFERENCES.....		120
VITAE.....		128

LIST OF TABLES

Table 2.1 - Differences between Normal Machining and HSM.	25
Table 2.2 - Key Characteristics of HSM & Industry Applications.....	26
Table 3.1 - Ceramics commonly considered for ceramic-based cutting tool design.	32
Table 3.2 - Pugh's decision matrix for picking the best ceramic matrix.....	33
Table 3.3 - Filler candidates for ceramic-based composite design and their properties of interest with respect to cutting tool inserts.	34
Table 3.4 - Condensed list of potential inclusion candidates.....	35
Table 3.5 - Range of target properties for our proposed composite material design with comparison with pure alumina.....	47
Table 4.1 - Types of samples developed using SPS.	65
Table 4.2 - Measured & theoretical density of samples along with associated porosity..	81
Table 4.3 - Hardness test results and the associated elastic modulus, fracture toughness values.	82
Table 4.4 - Thermal conductivity values of samples determined experimentally and computationally.	84
Table 4.5 - Effective CTE values of samples determined experimentally and computationally.	86
Table 4.6 - Comparison of Computational Results and Experimental Results of alumina- SiC-cBN hybrid composite design with respect to the selected alumina matrix.	87
Table 5.1 - Material properties used to define the material model.	97

LIST OF FIGURES

Figure 1.1 - A cutting tool insert under operation [3].....	2
Figure 1.2 - Hardness values of different tool materials as a function of temperature. [6]	3
Figure 1.3 - Structural performance comparison of various tool materials. [6]	5
Figure 1.4 - Different classes of cutting tool inserts. [6]	6
Figure 1.5 - Schematic explaining research methodology of the proposed work.....	10
Figure 2.1 - A comparison of high hot hardness of various materials. [29]	15
Figure 2.2 - Increase in fracture toughness and strength with addition of SiC [32]	18
Figure 2.3 - Presence of Crater wear on Alumina-SiC cutting tool [22]	19
Figure 2.4 - Comparison of Various Materials HSM Range [39].....	24
Figure 3.1 - Chronological map highlighting each step of the computational material design approach undertaken for ceramic matrix composite design.....	46
Figure 3.2 - Predicted thermal conductivity as a function of volume fraction of alumina based composite material with various independent fillers.....	48
Figure 3.3 - Predicted coefficient of thermal expansion as a function of volume fraction of alumina based composite material with independent fillers.	49
Figure 3.4 - Predicted effective elastic modulus as a function of volume fraction of alumina based composite with the addition of independent fillers.....	50
Figure 3.5 - a) Effective thermal conductivity as a function of particle size of cBN reinforced alumina matrix composite. b) Effective thermal conductivity as a function of particle size of SiC reinforced alumina matrix composite.....	51
Figure 3.6 - Effective Fracture Toughness of Alumina Matrix w/ various inclusion candidates.	53
Figure 3.6 - Effect of porosity on the thermal conductivity of a Alumina-SiC composite.	54
Figure 3.7 - Effect of porosity on the elastic modulus of a Alumina-SiC composite.....	55
Figure 3.8 - Effective thermal conductivity as a function of volume fraction of a hybrid alumina matrix composite with reinforced SiC and cBN as filler materials. 56	
Figure 3.9 - Effective coefficient of thermal expansion as a function of volume fraction of an alumina based matrix composite with reinforced SiC and cBN filler materials.....	57
Figure 3.10 - Predicted effective elastic modulus as a function of volume fraction of an alumina matrix composite with reinforced cBN and SiC reinforced filler materials.....	59
Figure 3.11 - Predicted effective fracture toughness as a function of volume fraction of an alumina matrix composite with reinforced cBN and SiC reinforced filler materials.....	60

Figure 3.12 - Predicted effective thermal conductivity as a function of particle size of a hybrid alumina matrix composite with reinforced filler combinations i) 30% SiC and 20% cBN and ii) 20% SiC and 30% cBN.....	61
Figure 4.1 - Schematic displaying the step-by-step process undertaken for Material Development phase.....	64
Figure 4.2 - Ultrasonic probe sonicator (Model VC750, Sonics).....	65
Figure 4.3 - Spark Plasma Sintering system from FCT, Germany.	66
Figure 4.4 - Jeol JSM-6460LV scanning electron microscope equipped with energy-dispersive spectrometry (EDS).	68
Figure 4.5 - Rigaku desktop x-ray diffractometer model “Miniflex II”.	68
Figure 4.6 - A DXR2 Raman microscope.....	69
Figure 4.7 - Micro Hardness Tester supplied by Buehler instruments.	70
Figure 4.8 - C-Therm TCI Thermal Conductivity Analyzer.....	72
Figure 4.9 - Mettler Toledo Thermal mechanical analyzer (TMA/SDTA 1 LF/1100). ...	72
Figure 4.10 - SEM image of a pure alumina sample.	73
Figure 4.11 - a) SEM image of an Al ₂ O ₃ -30%SiC-20%cBN at 400x magnification. b) SEM image of an Al ₂ O ₃ -30%SiC-20%cBN at 1000x magnification with each constituent specified. c) EDS analysis highlighting the presence of elements within the composite material (performed at 400x).	74
Figure 4.12 - EDS mapping performed at 1000x highlighting the presence and location of each element within the Al ₂ O ₃ -30%SiC-20%cBN composite material.	76
Figure 4.13 - a) SEM image of an Al ₂ O ₃ -20%SiC-30%cBN at 400x magnification. b) SEM image of an Al ₂ O ₃ -20%SiC-30%cBN at 1000x magnification with each constituent specified. c) EDS analysis highlighting the presence of elements within the composite material (performed at 400x).	77
Figure 4.14 - X-ray diffraction analysis/comparison of the three samples a) Pure Al ₂ O ₃ , b) Al ₂ O ₃ -30%SiC-20%cBN, c) Al ₂ O ₃ -20%SiC-30%Cbn (with 42µm avg. particle size).....	78
Figure 4.15 - Raman spectroscopy results of manufactured Al ₂ O ₃ -30%SiC-20%cBN. .	80
Figure 4.16 - E _{eff} /E _{mat} ratios between effective and matrix elastic modulus values (Experimental & Numerical).	83
Figure 4.17 - K _{Iceff} /K _{Icmat} ratios between effective and matrix fracture toughness values (Experimental & Numerical).	83
Figure 4.18 - K _{eff} /K _{mat} ratio of effective and matrix thermal conductivity of samples (Experimental & Numerical).	85
Figure 4.19 - α _{eff} /α _{mat} ratio of effective and matrix CTE of samples (Experimental & Numerical).	86
Figure 5.1 - Geometry model of the cutting tool insert developed using SOLIDWORKS.	94
Figure 5.2 - Heat transfer loading applied onto cutting edge as a function of time. [94].	96

Figure 5.3 - Description of the additional boundary conditions applied onto the insert. .	96
Figure 5.4 - Meshing of the cutting tool insert geometry.	98
Figure 5.5 - Mesh convergence analysis for von-Mises stress and temperature.	99
Figure 5.6 - Temperature profile of the cutting edge during the cutting process.	101
Figure 5.7 - Temperature profile as a function of distance moving away from the cutting edge towards the center.	102
Figure 5.8 - Von-Mises stress distribution at the cutting edge of the tool insert during the cutting process.	103
Figure 5.9 - Temperature profile of the alumina insert at different times during simulated cutting process	104
Figure 5.11 - Von-Mises stress distribution of the alumina insert at different times during the simulated cutting process.....	105
Figure 5.11 - Temperature profile of the cutting edge of ZTA insert during cutting process.	106
Figure 5.12 - Temperature profile as a function of distance moving from cutting edge towards the center of the ZTA insert.	107
Figure 5.13 - Von-Mises stress distribution at the cutting edge of ZTA insert as a function of time.....	108
Figure 5.14 - Temperature profile of ZTA insert at different times during simulated cutting process.	109
Figure 5.15 - Von-Mises stress distribution of ZTA insert at different times during simulated cutting process.....	110
Figure 5.16 - Temperature profile at the cutting edge of the proposed insert as a function of time.....	111
Figure 5.17 - Temperature profile as a function of distance from cutting edge to the center of proposed insert.	112
Figure 5.18 - Von-Mises stress distribution at the cutting edge of proposed insert during the cutting process.	113
Figure 5.19 - Temperature profile of proposed insert at different times during simulated cutting process.	114
Figure 5.20 - Von-Mises stress distribution of the proposed insert at different times of simulated cutting process.....	115

LIST OF ABBREVIATIONS

Al₂O₃	:	Aluminum Oxide (Alumina)
cBN	:	Cubic Boron Nitride
CTE	:	Coefficient of Thermal Expansion
EDS	:	Energy dispersive spectroscopy
EMA	:	Effective Medium Approximation
FEM	:	Finite Element Modelling
HRC	:	Rockwell Hardness
hBN	:	Hexagonal Boron Nitride
HSM	:	High Speed Machining
KPI	:	Key Performance Indicator
MTPS	:	Modified Transient Plane Source
R&D	:	Research & Development
SiC	:	Silicon Carbide
SPS	:	Spark Plasma Sintering
SEM	:	Scanned Electron Microscopy
TiC	:	Titanium Carbide

Ti[C,N]	:	Titanium Carbo-nitride
TiB₂	:	Titanium Diboride
TMA	:	Thermal Mechanical Analyzer
XRD	:	X-ray Diffraction
ZrO₂	:	Zirconium Dioxide
ZTA	:	Zirconia Toughened Alumina

ABSTRACT

Full Name : Taha Waqar
Thesis Title : Design and Development of Ceramic-Based Composites for Cutting Tool Inserts.
Major Field : Mechanical Engineering
Date of Degree : April, 2018

Successful development of enhanced cutting tool materials requires the application of innovative concepts at every phase of the manufacturing process. In this work, a computational design approach is applied in the development of reinforced ceramic based cutting tool inserts with tailored structural and thermal properties. Several potential filler materials are considered at the material design stage for the improvement of structural and thermal properties of a select matrix material. Properties, such as an improved thermal conductivity and reduced coefficient of thermal expansion are essential for an effective cutting tool insert to absorb thermal shock at varying temperatures. In addition, structural properties such as fracture toughness and elastic modulus should be enhanced or maintained within a moderate range. A mean-field homogenization theory and effective medium approximation along with fracture toughness determination through J-integral evaluation approach using an in-house code are applied for predicting potential optimum structural and thermal properties for the required application. This is achieved by considering the effect of inclusions as a function of volume fraction and particle size in the ceramic base matrix. Development of composites is done using the Spark Plasma Sintering process; structural and thermal properties are measured experimentally in order to validate the computational results. From the results, it is found that the computational material

design approach is precise enough in predicting the targeted properties of a designed hybrid composite material for cutting tool inserts. The designed composite cutting tool insert material's performance is evaluated during a cutting process through the use of FEM. Comparative studies showed more robust performance of the composite when compared to benchmark materials due to its enhanced thermal and structural target properties.

ملخص الرسالة

الاسم الكامل: طه وقار

عنوان الرسالة: تصميم وتطوير السيراميك المستندة إلى المركبة لقطع أداة إدراجات

التخصص: الهندسة الميكانيكية

تاريخ الدرجة العلمية: أبريل 2018

يتطلب التطوير الناجح لمواد أدوات القطع المحسنة تطبيق مفاهيم مبتكرة في كل مرحلة من مراحل عملية التصنيع. في هذا العمل ، يتم تطبيق نهج التصميم الحسابي في تطوير إدخالات أداة قطع السيراميك المقواة مع الخصائص الهيكلية والحرارية المصممة. يتم النظر في عدة مواد حشو محتملة في مرحلة تصميم المواد لتحسين الخصائص الهيكلية والحرارية لمواد مصفوفة مختارة. تعتبر الخصائص مثل التوصيل الحراري المُحسَّن وانخفاض معامل التمدد الحراري ضرورية لإدخال أداة القطع الفعالة لامتصاص الصدمات الحرارية عند درجات حرارة متفاوتة. بالإضافة إلى ذلك ، يجب تعزيز أو الحفاظ على الخصائص التركيبية مثل صلابة الكسر ومعامل المرونة ضمن نطاق معتدل. يتم تطبيق نظرية تجانس المجال الوسطي وتقريب متوسط الفعالية بالإضافة إلى تحديد صلابة الكسر من خلال منهج التقييم J المتكاملة باستخدام كود داخلي للتنبؤ بالخصائص الهيكلية والحرارية المحتملة المثلى للتطبيق المطلوب. ويتحقق ذلك من خلال النظر في تأثير الادراج كدالة لكسر حجم وحجم الجسيمات في مصفوفة قاعدة السيراميك. يتم تطوير المواد المركبة باستخدام عملية Spark Plasma Sintering ؛ يتم قياس الخصائص الهيكلية والحرارية تجريبيا من أجل التحقق من صحة النتائج الحسابية. من النتائج ، وجد أن نهج تصميم المواد الحسابية دقيق بما فيه الكفاية في التنبؤ بالخصائص المستهدفة لمركب هجين مركب مصمم لإدخال أداة القطع. يتم تقييم أداء أداة القطع المركبة المصممة للمادة أثناء عملية القطع من خلال استخدام FEM. أظهرت الدراسات المقارنة أداء أكثر قوة للمركب عند مقارنته بالمواد القياسية بسبب خصائصه المستهدفة الحرارية والهيكلية المحسنة.

CHAPTER 1

INTRODUCTION

1.1 Background and Motivation

In today's ever changing global manufacturing market, there is an increasing requirement for ultimate product quality. The need for economical and efficient production techniques is of utmost requirement; the designing of innovative products ranging widely in intricacy, composition of material, size, and surface finish quality has driven the industry to develop and design new composite materials and to adopt these new materials into strategies for optimizing the machining process. The demand has meant increased revenues for the global machine tools and cutting tools market, reportedly worth \$15.72bn in 2012 [1]. Main contributors to this surge in the rise of this particular growth is from the automotive, aerospace and defensive industries.

Due to the design of products with advanced materials, innovative cutting tools have also been developed and adopted for economic and performance optimization in high speed machining conditions, especially high cutting speed and higher feeds [2]. The main aim of this work is to explore the material design aspects of cutting tool inserts with enhanced properties through a computational model approach.



Figure 1.1 - A cutting tool insert under operation [3]

Cutting tools are typically divided into five main classes of tool materials. Choosing which type of material for use as cutting tool requires careful consideration because this can greatly affect the final quality of the machined workpiece. Therefore, when selecting which material to use for machining it is important to consider which process type is in consideration and the material composition of the workpiece that requires machining [3–5]. To be more aware of the differences between the different cutting tool materials five main classes of tool materials are described as the following:

- Ceramics – Ceramic based cutting tools are usually considered in the form of disposable tips. This is possible due to the relative cheaper costs associated with most ceramics when compared with the alternatives. Due to the high hot hardness possessed by ceramics they are able to operate at higher speeds in comparison to tungsten carbide[6]. Due to their brittle nature and good wear resistance they are exceptional at resisting crater damage. Ceramics are typically more brittle compared to carbides and are fitted with rigid tool holders in order to avoid failure

due to shock. The hot hardness and chemical stability of ceramics make them a good material for high speed cutting of various high strength workpieces. However due to their poor ability to withstand thermal and mechanical shock, continuous and insufficient use of coolant can lead to failure of tools.

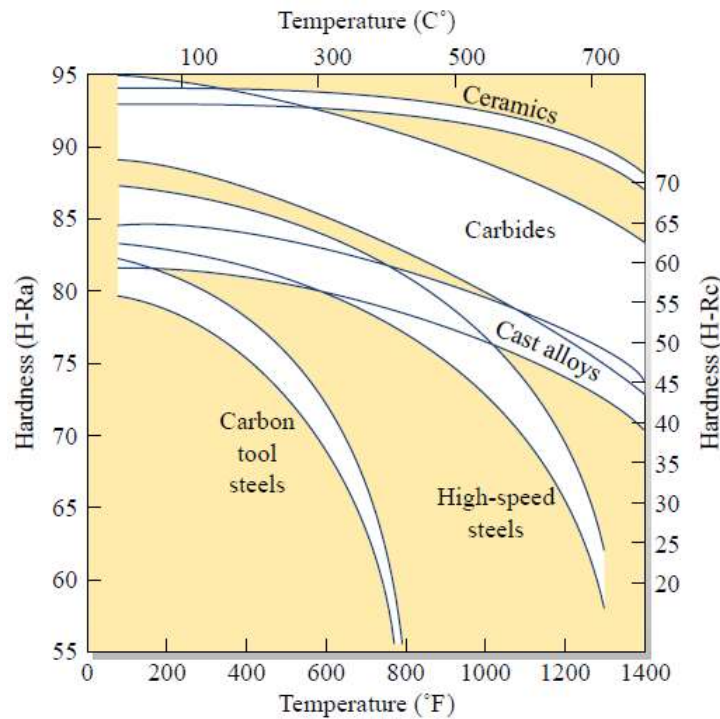


Figure 1.2 - Hardness values of different tool materials as a function of temperature. [6]

- Carbides – Carbide based tools are one of the most commonly used tool materials and are considered the standard choice of material for nearly 50% of all cutting processes. They are manufactured using powder metallurgy methods by reinforced various forms of carbides into a tough iron group based matrix. Commonly used carbides are tungsten carbide, titanium carbide, tantalum carbide among others. Cobalt is also considered to enhance the binding quality of the material. Carbide tool inserts are categorized into two groups. Tungsten based grades are applied in

light finishing to heavy roughing cutting processes involving most ferrous and non-ferrous metals. Grades containing titanium, tantalum are considered only for finishing and semi-finishing of ferrous based workpieces due to their chemical affinity with ferrous materials at high temperature.

- Cermets – A hybrid class of tool materials which consists of a ceramic and a reinforced metallic alloy. Cermets possess superior wear resistance, greater tool life and are able to operate at high cutting speeds. They possess higher hot hardness and oxidation resistance compared to cemented carbides. Therefore, they are able to apply a better finish due to its reduced chemical affinity with iron. However, due to their low toughness, lower thermal conductivity and high thermal expansion coefficient can make them prone to failure due to thermal cracking.
- Carbon-based – Development of super hard materials was begun in the early 1970s with the introduction of tool materials formed from super hard materials such as diamond, cBN; these are being used in the industry for the machining of aluminum and various plastics due to the reduced cutting forces generated during machining compared to carbides. Their key properties which include high hardness, good thermal conductivity, the ability to form sharp edged finishes and good wear resistance. However, diamond based tools wear when used for machining of steel-based workpieces. This is due to the chemical affinity diamond has with iron based workpieces at high temperatures which causes the diamond to change its atomic structure.
- High-speed Steels – Need for tool materials which are able to handle high cutting speeds and temperatures have led to the development of high speed steels. One of

the key advantages is the possibility of reinforcing additional elements to boost the hardness and strength the steel based tool when exposed to hot hardness, i.e. maintenance of hardness at elevated temperatures. Few of the commonly considered alloying elements are: manganese, molybdenum, chromium, cobalt etc. Each inclusion is considered to improve the desired target properties. These enhanced properties will allow machining at higher speeds and better performance as compared to stand-alone steels. High speed steels contain varying amounts of carbon, which reacts with refractory metal to form hard carbides which provides greater wear resistance. However, the alloying elements considered for high speed steels are not to be found in abundance and the cost of these elements is rising.

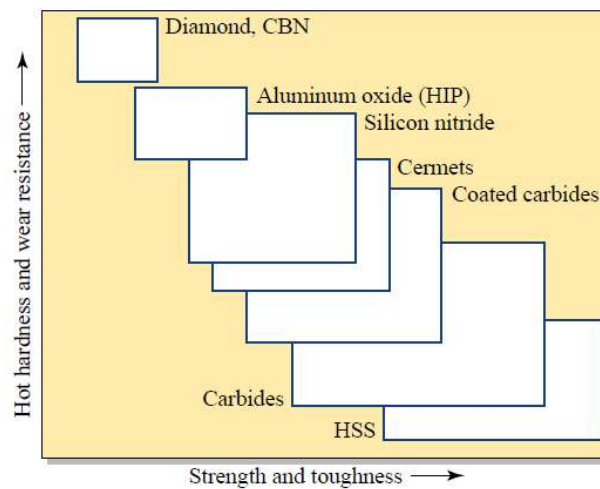


Figure 1.3 - Structural performance comparison of various tool materials. [6]

Cutting tools are quite frequently designed with fit-in replaceable inserts. In such a scenario, the cutting edge consists of a separate piece of desired material fitted onto the tool body via either clamping, welding or blazing the insert onto the tool body [4]. Common materials considered as candidates for cutting inserts include ceramics, cemented carbides,

polycrystalline diamond, cubic boron nitrides, etc. Tools that are used with these fitted inserts include tool inserts, milling cutters & saw blades.



Figure 1.4 - Different classes of cutting tool inserts. [6]

Furthermore, due to the advancing nature of technology, products are directly machined to their final dimensions' post heat treatment [3]. This leads to hard cutting which depends especially on the features of the cutting tool materials and the cutting speed.

Ceramic tools are usually considered for high-cutting speed, finishing of ferrous alloys and cast iron workpieces. They are considered due to their high hot hardness and chemical stability when working with ferrous alloys [3]. However, due to poor fracture toughness and resistance to thermal shock, this leaves room for improvement which may be possible with the fabrication of ceramic-based composite materials [4]. The most widely used form of ceramic cutters is that of the ceramic cutting tool insert, this due to relative ease with which it can be manufactured and into the desired shape. Current trends show research of ceramic materials shifting from single phase to multiphase composite materials in order to obtain the best effective properties for the required application. Ceramic tools based on Alumina are of particular interest due to their exhibition of high hot hardness and good wear resistance, which makes it an ideal candidate for high speed machining.

Therefore, it is notable that there is a significant increase in R&D of ceramic based tools [1,6]. This is because ceramics are considered a cost-effective yet efficient option for a cutting tool material dealing with a wide range of workpiece material. However, it is found that there is a need to improve fracture toughness and thermal shock resistance parameters to improve the efficiency and applicability [7]. Reinforced ceramic matrix composites are a viable to enhance the target properties and achieve a cheap yet effective option for a high performance cutting tool insert.

Design of a cutting tool material is an essential part of determining the overall quality of the tool design process. This is because these tools are subjected to strenuous conditions such as high wear conditions, severe contact stresses and high temperatures [2]. Consequently, the materials selected should possess the properties in order to cope with these demanding conditions. Mentioned below are the key target properties that are taken into consideration during the material design process: [3]

- 1) High hot hardness
- 2) Good wear resistance
- 3) High fracture toughness
- 4) Chemical Stability – Inert to reaction with workpieces
- 5) High thermal conductivity
- 6) High thermal shock resistance
- 7) Reduced coefficient of thermal expansion

1.2 Problem Description

For effective development, it is important to utilize innovative concepts during the design process of a composite material used for cutting tool inserts. Key target properties for cutting tool design are high wear and thermal shock resistance, chemical stability, fracture toughness. An enhanced composite material is designed and developed for the tool insert application using a computational based approach keeping the target properties in focus.

1.3 Project Objectives

In this work, a base matrix is selected based on a comparison analysis with other potential candidates. Furthermore, selection of inclusions will be done based on the desired target properties. Next, computational modelling is used to predict the effective properties and the corresponding required inclusion volume fractions and particle sizes. Furthermore, experimental work is performed to validate the computational results followed by a performance evaluation. In order to achieve the set objective, the following KPIs have been constructed:

- 1) To design a ceramic based composite material with enhanced target properties for the cutting tool application through a computational approach.
- 2) Manufacture the selected ceramic based composites using the spark plasma sintering process.
- 3) Validate the findings from the numerical simulations with experimental data in terms of their effective properties and morphologies.

- 4) Carry out performance evaluation of the designed composites through simulation of various cutting conditions.
- 5) To develop a computational model which could be used to predict the effective fracture toughness of the prepared composite and to compare these findings with experimental testing and existing literature.

1.4 Research Methodology

Shown in the schematic (Figure 1.5) on the next page is a step-by-step plan prepared to achieve the problem objectives that have been set. Each target of the set objectives required the utilization of various resources ranging from the university library resources, powerful computational workstations to the experimental equipment.

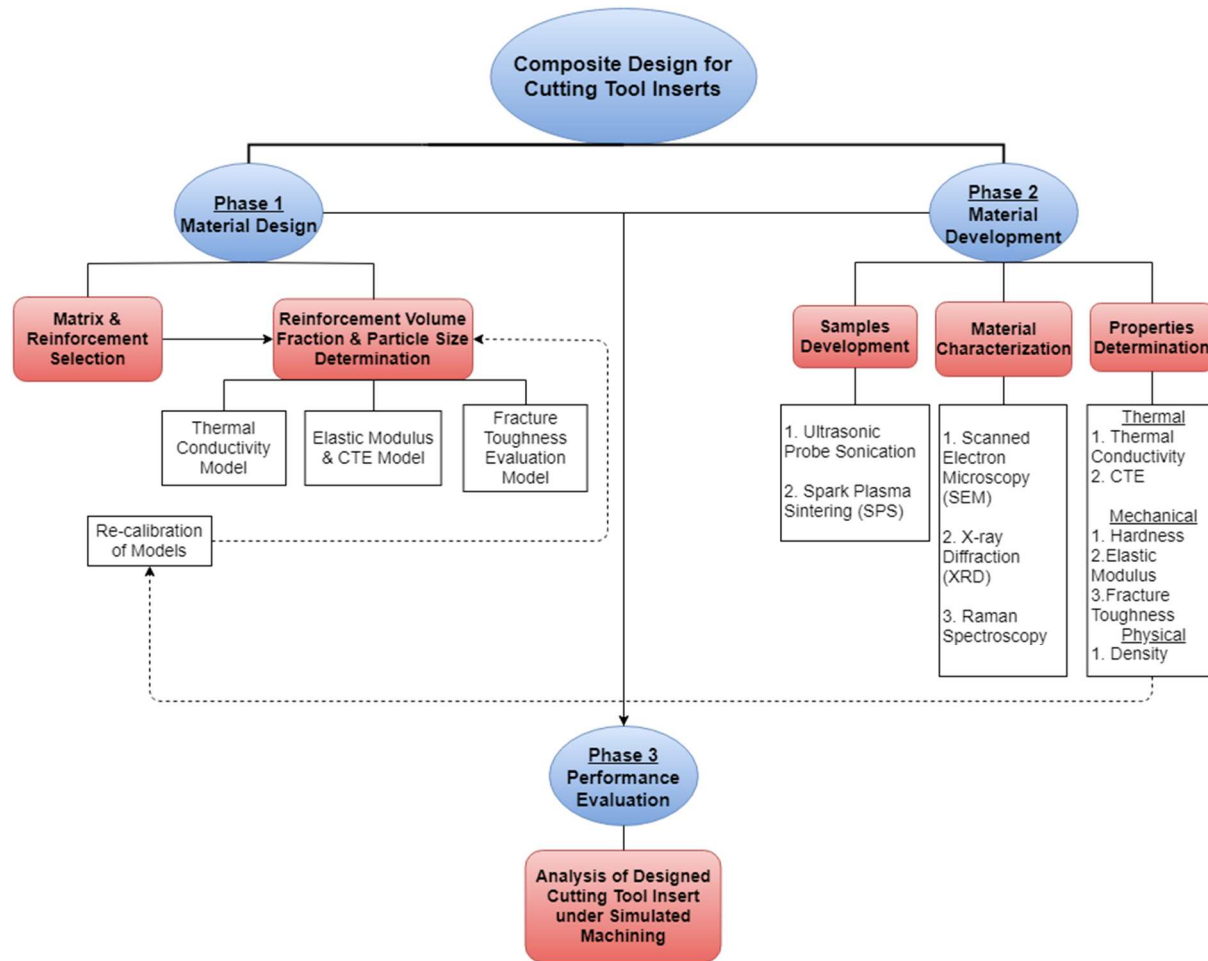


Figure 1.5 - Schematic explaining research methodology of the proposed work.

CHAPTER 2

LITERATURE REVIEW

The need for cost efficiency in production and the development of complex products have raised the requirement for the industry to design new cutting tool with enhanced material properties. New materials have been designed for cost and performance optimization in high-speed machining conditions. New materials are also designed for dry cutting which is increasingly becoming a favored process. If machining can be performed without the use of coolant there is a significant saving in cost.

2.1 Types of Cutting Tool Insert Materials

Ceramic based tools are generally considered for high speed cutting, finish machining of ferrous alloys or machining of various cast iron workpieces [5,8]. Various reinforcements are used to improve the thermal shock resistance without much loss to the effective hardness.

Cutting tools are quite often designed with replaceable inserts. For cutting tool inserts, the cutting edge consists of a separate piece of material which is either brazed, welded or clamped on to the tool body. Common materials considered for inserts include cemented carbide, polycrystalline diamond and cubic boron nitride. Tools using inserts include tool

bits, milling cutters. An effective cutting tool insert would be possessing good wear resistance, superior fracture toughness and thermal shock resistance.

There are various materials available that can be considered for the usage as cutting tool inserts. Materials range from metals, cemented carbides and ceramics. Ceramics and carbon based materials are considered in applications such as turning, milling of cast iron and super alloys as well as in finishing of hardened materials[5,8–10]. For cutting tool applications, there are two kinds of ceramic composite materials that are used, alumina and silicon nitride. The advantage of ceramic based tools is their ability to withstand heat relatively better than its rivals. For example, ceramic based tools will soften at 2200°C as opposed to carbide tools that will soften at about 870°C, this allows machining processes to be performed at higher temperatures [5,8].

Ceramic cutting tools have developed greatly during the past few years and have begun replacing carbide based tools in various high-speed machining applications [11]. In addition, the mechanical properties possessed by ceramics are deemed superior to those of carbides at high temperatures (800°C). They can maintain excellent hardness and stiffness at temperatures greater than 1000°C and are chemically stable with various workpiece materials at temperatures greater than 1000°C. Ceramics provide high quality finishing cuts due to their ability to provide better dimension control at lower tool wear rates [12]. However, they also possess several deficiencies such as low strength compared to other candidates of material, minimal resistance to thermal and mechanical shock, and a habit to fail by chipping. Various ceramic based materials do not prove to possess decisive failure times and may fail catastrophically that may lead to the damaging of the workpiece [3,4].

2.2 Recent Developments in Ceramic Composite Material Design

In the recent times, continued progress has been made in the development of ceramic matrix composites with particulate or whisker reinforcements. This development has been in the search for enhancement in the mechanical properties of ceramics to obtain enhanced properties [13]. Particular attention has been paid to the thermal and elastic properties, which are critical in the material design for high temperature cutting applications. The addition of multiple phases can improve the fracture behavior and the “field” properties. These are elastic modulus, thermal conductivity, coefficient of thermal expansion [3]. These properties will play a significant role in the overall target properties of cutting inserts. During machining, a SiC reinforced alumina composite exhibited longer tool life as compared to that of standalone alumina. The reinforced composite exhibits greater hardness than the reinforced matrix due to the presence of a hard-secondary phase [14,15][16]. As the main drawback of ceramic inserts is their brittleness, increasing their toughness is a key aspect. Thermal shock tests of an alumina with reinforced 20% SiC composite resulted in relatively no fall in flexural strength with a temperature difference up to 900°C which showed significant improvement to pure alumina. Alumina-TiC designed have reported to have improved the effective toughness with addition of TiC [17]. Incorporating a ductile phase into a brittle ceramic composite can assist in improvement of toughness and dissipate the energy of crack propagation. Inclusion of cobalt, ZrO₂ into a Al₂O₃-TiC composite exhibits a comparatively higher toughness[18,19]. Inclusion of Ti[C,N] into Al₂O₃ fabricated via repetitious hot-pressing exhibited enhanced structural properties with a decreased coefficient of friction [20][21]. Kumar et al report a designed

alumina-ceria ceramic composite which shows improvement in hardness and fracture toughness properties when in comparison with pure alumina and comparable with ZTA cutting inserts [22]. Fabrication of Al_2O_3 -cBN composites were fabricated through SPS by Irshad et al, where they reported enhanced structural properties until 30% cBN content [23]. Jianxin et. al produced Al_2O_3 - TiB_2 cutting tools through hot pressing which led to the formation of a self-lubricating oxide film which resulted in the improvement of wear resistance [24]. This film also offers cost reduction and an environmental advantage in machining because of lack of need of coolant. Furthermore, Jianxin et. al carried his Al_2O_3 - TiB_2 design forward and developed hybrid composites with additional SiC inclusion. His results showed the structural properties continually improved with increased SiC content [25]. Alumina-Graphene Oxide composites fabricated using spark plasma sintering by Bronizewski et. al were reported to possess enhanced structural properties with good cohesion between matrix and inclusion [26].

Thermal properties are key aspect for design of cutting tool composites as this will influence the thermal shock resistance of the designed insert. For improved thermal shock resistance, an increase in thermal conductivity while a decrease in coefficient of thermal expansion is desirable [3]. Akhtar et. al fabricated Alumina-SiC composites using spark plasma sintering and reported enhanced properties for thermal shock resistance when in comparison with pure alumina [27]. In addition, Al_2O_3 -cBN composites fabricated by SPS also demonstrated improved thermal conductivity and reduced coefficient of thermal expansion. These are expected results due to the enhanced thermal properties of filler materials. It is noteworthy that almost all reviewed publications have designed the composite materials via an experimental approach. Design of material through a

computational approach can prove to be beneficial in many ways as this will reduce amount of resources, material and time consumed experimentally along with the time required to perform the design process.

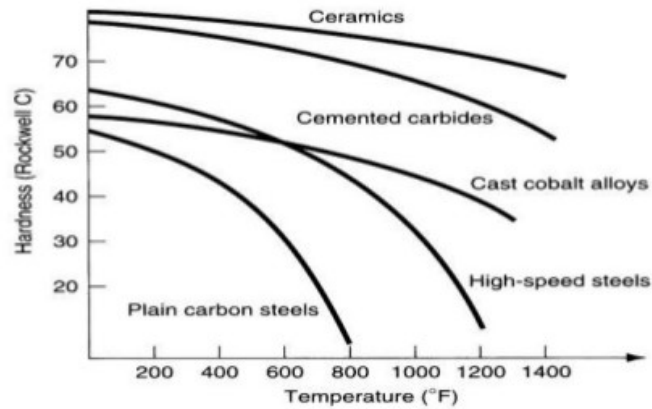


Figure 2.1 - A comparison of high hot hardness of various materials. [28]

Ceramic cutting tools have developed greatly during the past few years and have begun replacing carbide based tools in various high-speed machining applications [7]. In addition, the mechanical properties possessed by ceramics are deemed to be superior to those of carbides at high temperatures (800°C). They can maintain excellent hardness and stiffness at temperatures greater than 1000°C and are chemically stable with various workpiece materials at temperatures greater than 1000°C. Ceramics provide high quality finishing cuts due to their ability to provide better dimension control at lower tool wear rates [7]. However, they also possess several deficiencies such as low strength compared to other candidates of material, minimal resistance to thermal and mechanical shock, and a habit to fail by chipping. Various ceramic based materials do not prove to possess decisive failure times and may fail catastrophically that may lead to the damaging of the workpiece.

To be able to deal with weaknesses, research is being carried out extensively to develop ceramic based composite materials that enhance their properties and design a more

effective cutting tool. For the basis of my study, Attention is focused on Alumina due to its high hot hardness and wear resistance properties while being cheap to manufacture and produce. Alumina matrix based tools are used due to their relatively low cost and a wide range of workability.

2.3 Research Work Dealing With Enhanced Alumina Composites For Cutting Tools

Alumina (Al_2O_3) based cutting tools have been used since the turn of the 20th century in machining of low hardness steels and grey cast iron [29]. Cutting tools of pure alumina are considered due to their cheap cost in mass production [8,12]. It possesses hot hardness and compression strength larger than that for cemented carbides while also being chemically stable at high temperatures. However, its fracture toughness is low (K_{IC} around $4.3 \text{ MPa}\cdot\text{m}^{1/2}$) which is considerably lower than that of carbides [30]. Therefore, there is a need to develop alumina based composites which deals with the deficiencies while keeping the production process cost effective. There have been various publications regarding production of alumina composites with enhanced properties which will be discussed.

In the recent times, continued progress has been made in the development of ceramic matrix composites with particulate or whisker reinforcements. This development has been in the search for enhancement in the mechanical properties of ceramics to obtain enhanced properties. Particular attention has been paid to the thermal and elastic properties, which are critical in the material design for high temperature cutting applications. The addition of a second phase can improve the fracture behavior and the “field” properties. These are

elastic modulus, thermal conductivity, coefficient of thermal expansion. These properties will play a large role in the overall target properties for a cutting insert.

Materials consisting of an alumina matrix reinforced with silicon carbide have garnered particular attention and are considered successful functioning as cutting tools. Silicon carbide is chosen due to its high thermal conductivity which is needed to reduce thermal shock failures and high fracture toughness capabilities [14]. The SiC reinforcement can be reinforced as powder, whiskers or as nano composite. During machining, the composite exhibited the longest tool life, a tool life seven times longer than that of an Al₂O₃-TiC composite. Typically, it is done in the whisker format. The reinforced composite exhibits greater hardness than the unreinforced matrix due to the small grain structure (presence of hard secondary phase as well grain growth) [15,16].

As the main drawback of ceramic inserts is their brittleness, increasing the toughness is a key aspect. Tieggs prepared Al₂O₃-SiC whiskers composites and then observed the effective properties obtained [31]. It was observed that Al₂O₃-SiC whisker composites possesses minorly high fracture toughness as compared to pure alumina due to mainly crack deflection by the whiskers with some contribution from crack bridging and whisker pullout. Increasing whisker volume concentration lead to increase in crack deflection mechanism as was expected. This increase is further highlighted as shown in Figure 2.2.

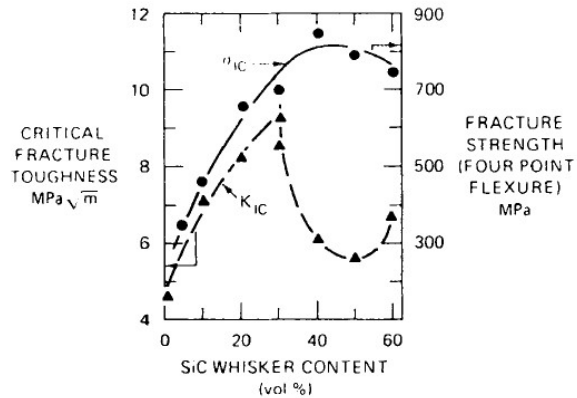


Figure 2.2 - Increase in fracture toughness and strength with addition of SiC [32]

In addition, thermal shock tests of an alumina based w/ 20% SiC composite resulted in relatively no fall in flexural strength with a temperature difference of up to 900°C. In comparison, standalone alumina, experiences a significant decrease in flexural strength above temperatures than 400°C [16]. Research has shown that the reasoning behind the improvement is a result of interactions between the SiC whiskers and the microcracks present within the alumina matrix halt the dispersion of the cracks into critical flaws.

Furthermore, it is essential to understand the wear properties of developed composites as these will determine the quality of cut and life of each insert. El-Wardany et al reported that, during machining of hardened steel using ceramic cutting tools, the presence of plastic deformation of the ceramic cutting edge lead to the deterioration of the surface roughness which later lead to edge failure [33]. However, it is reported that these composites exhibit good resistance to notch wear as opposed to stand-alone alumina.

The random distribution of the whiskers in the alumina matrix assists the matrix to have predictable wear patterns on the inserts. These composites are at their best when being used

with hard ferrous steel and nickel alloys as will be discussed later on. The wear resistance of these reinforced ceramics will be reduced as the volume fraction of SiC is increased.

The performance of these composites can vary depending on the workpiece material. Alumina-SiC is found to suffer from chemically initiated wear due to the presence of high chemical affinity of silicon carbide with iron and this results in SiC being removed from the alumina base. SiC whisker reinforced alumina ceramic cutting tools exhibit good resistance to notch wear despite the chemical affinity wear mechanism. Gatto observed the pull-out whisker phenomenon due to the temperature difference on the tool-chip interface when cutting Inconel 718 with SiC whisker however the performance was still considered adequate compared to regular alumina [21]. Richards observed the limitation of tool life of the composite tool due to extreme depth of cut notch wearing while machining Nickel based alloys [21]. Tests conducted on the composite material showed improved notch and crater wear compared to alumina.

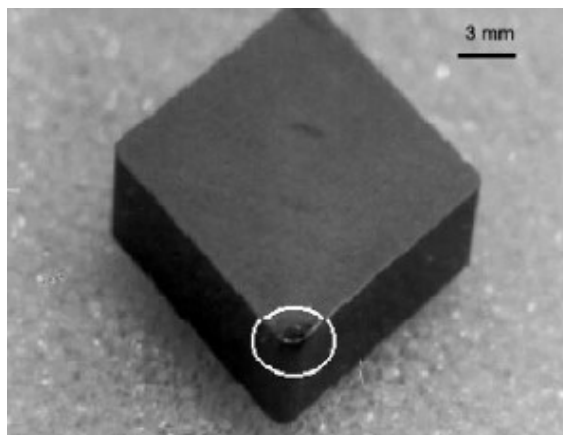


Figure 2.3 - Presence of Crater wear on Alumina-SiC cutting tool [21]

Hardness tests show an increase in the hardness. It is observed with increase in SiC content within the alumina matrix there will be a rise in the Vicker's hardness. This is due to the

presence of harder and firmly bonded SiC particles in the Alumina matrix which impedes the dislocation movements which in turn lead to the rise in hardness.

Next, the relationship of tensile strength and SiC volume fraction is explored. From the finding, it is evident that the tensile strength increases with greater reinforcement of SiC. This is attributed to transferring of tensile load to the strongly bonded SiC reinforcements in the matrix, which lead to the increase in the dislocations density near matrix-inclusion interface and initiated the grain strengthening effect [16]. Therefore, in a strong reinforced matrix, the crack must spread across both matrix and reinforcement. These mechanisms along with strong interfacial bonds contribute in enhancing the tensile strength of the composite material.

Double inclusions can also be considered to enhance the target properties. One such case that will be discussed is reinforcing TiB₂, SiC into alumina. Various volume fractions of both reinforcements were considered which were manufactured by hot pressing. Results entailed that fracture toughness and hardness of the composite based tools uninterruptedly increased with increasing SiC content [33].

Jianxin et al report that these double inclusion composites also exhibited improved wear resistance due to the superior fracture toughness and hardness of TiB₂, SiC; Increasing SiC content improved wear resistance even further. Abrasive wear was found to be dominant mechanism in flank wear. While adhesion and diffusion due to high cutting temperature were deemed responsible for crater wear [25].

2.4 Exploring Other Materials for Inclusion Considerations

In a case where the hardness is relatively high, such as in the production of quenched steels or hardened cast iron, nickel based super alloys and some metallic composite materials it becomes important to use suitable cutting tools which deal with the requirements [9]. Therefore, the tool used needs to have high wear resistance along with high hardness and for these reasons ultra-hard tools based on cubic boron nitride are considered. Cubic boron nitride is only second to diamond when it comes to hardest materials that are known to man. Following is a review of published work discussing the performance of cBN based tools.

cBN based tools have been widely applied in the cutting of hard materials at high speeds. This is due to its high temperature stability, superior hot hardness, high thermal conductivity, low CTE and good chemical stability with iron [34]. It is observed that during the cutting of hard steels that the lifecycle of cBN tools showed an ascending and then a descending trend when cutting speed is increased. This behavior is significantly different than that is ascribed by the Taylor's tool life equation. It is reported that the wear behavior of cBN at low cutting speeds takes the form of abrasion. Increase of cutting speed results in the formation of a layer on the tool face which helps in protection from wear [35]. However, further increase will cause the friction forces to remove the layer which will

promote diffusion at high speeds which will lead to a rise in wear on rake face of the cutting tool.

Chou et al. researched the machining quality and wear behavior of various CBN tools which are used for finishing turning of hardened steel. They established that materials with low percentage of cBN content provides the optimum performance in regards to quality of surface finish and tool life. The cause of failure of these tools is attributed to the result of plastic deformations under the combination of thermal and mechanical stresses around the edge area and the small wear rate of the cBN based tool is ascribed to a condensed chemical affinity when in contact with certain alloys. It is concluded that the wear resistance behavior of the cBN is benefited by the reduced solubility of boron.

Luo et al. investigated the wear behavior in hard turning of alloy steel using both ceramic and cBN based tools and it was reported that the flank wear in cBN was reduced as work material hardness was increased upto 50 HRC beyond this limit the wear rate began to increase; this phenomenon has led to great activity of research in this area. It is observed that the most influencing factor on the tool wear is due to the occurrence of carbide elements within the workpiece steel microstructure which assist the abrasion and diffusion mechanisms. Lahiff et al were able to conclude that there are varying theories regarding the tool wear mechanisms however there is a general consensus that wear is due to a combination of mechanisms and not one can be singled out. An experimental study carried

out by Yallese et al concluded that hard turning of steel alloys with cBN inserts showed an acceptable wear resistance for comparatively high cutting speeds.

Another interesting proposition is to consider cubic boron nitride as a reinforcement within an Alumina matrix to enhance fracture toughness and other target properties. cBN on its own possesses a high elastic modulus, thermal conductivity, fracture toughness and a low coefficient of thermal expansion. This makes it an ideal candidate for a reinforcement. Its disadvantageous because it changes form into a hexagonal shape if exposed to high temperature during sintering therefore different techniques are used to manufacture. It is formed from the synthesis of boron nitride into cubic form & if synthesized with alumina and/or additional reinforcements could potentially make an effective cutting tool insert.

2.5 High Speed Machining

High Speed Machining is considered to be of special significance to the industry and the researching community in recent times due to the benefits it provides in comparison to conventional machining processes [36]. The boundary between conventional machining and HSM depends on factors such as the workpiece material and the process. The highest cutting speeds can be achieved for non-ferrous materials that exhibit good machinability, such as aluminum, but they are limited by the attained cutting speeds of the machine tools [36,37]. For machining some different factors are taken into consideration, such as cutting speed, spindle speed, feed, the cutting operation, workpiece material, cutting forces and cutting tool.

The notion of high speed machining was first conceived in the early 20th century by Salomon in the year 1931 [36]. He proposed that at a particular cutting speed which is 5 - 10 times higher as compared to conventional machining, the chip tool interface temperature will start to decrease. He used these findings to generate a curve to highlight the chip removal temperature for various materials. It was observed that at increased cutting speeds the chip interfacial temperature would drop and thus he was able to back his theory.

It is reported that at high cutting speeds required for a constant cutting power, there will be less required cutting forces to carry out the machining process [38]. Therefore, high speed machining is a cost-effective option among the machining processes and if used properly with careful considerations of material can be a great cutting method. For each material, the transition range to enter the high-speed machining range as shown in the figure below.

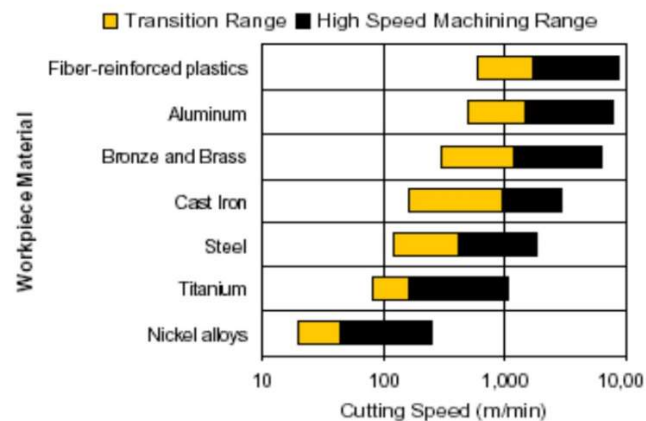


Figure 2.4 - Comparison of Various Materials HSM Range [39]

Therefore, it is shown that through the usage of high speed machining leads to an improvement in accuracy, efficiency, reduced machining time, improved quality of workpieces and decreased costs in production [37].

Differences of Normal and HSM:

Table 2.1 - Differences between Normal Machining and HSM.

Normal	HSM
Long contact time	Short contact time
Low accuracy	High accuracy
Higher cutting forces needed	Less cutting forces needed
Poor quality surface finish	Good quality surface finish
Low rate of material removal	High rate of material removal
Requirement of cutting cooling fluid	Cooling fluid is not required

There are three key process parameters that are considered during high speed machining [37]:

- 1) Actual cutting speed

Cutting speed is a function of both the spindle speed and the diameter of the tool.

- 2) Metal Removal rate
- 3) Surface finish

Surface finish quality relies upon the cutting tool geometry, coating (if applied) on the cutting tool and the wear resistance properties of tool.

Various Examples of HSM [30]:

Table 2.2 - Key Characteristics of HSM & Industry Applications

Attributes	Type of application	Industrial examples
High rate of metal removal	Light metals	Aerospace
	Steel and cast iron	Die forming
High surface finish quality	Precisions machining	Die forming
	Special components	Components of precision mechanics
Low cutting forces	Machining of thin-walled components	Aerospace
		Automotive industry
		Household appliances
High exciting frequencies	Vibration free machining of difficult components	Precision components Optical Industry
Heat dissipation through chips	Distortion-free machining	Precision components
	Colder workpieces	Magnesium alloys

So, high speed machining is not simply dependent on a high cutting speed. It should be regarded as a process where the processes are precision and application specific methods [38]. It does not essentially depend on machining at a high spindle speed. Various HSM

applications are performed considering moderate spindle speeds and cutters of large size [38]. It is highly productive machining in small sized components in roughing to finishing of components of all sizes. Further research is still being carried out to build on the development to further improve the quality of the process.

2.6 Computational Models

Simulations of practical material design and testing have become feasible due to the powerful computational tools at hand. Composite materials targeted for a certain application are characterized by a variety of phases, defects, interfaces and other microstructural features. These simulations provide a cost-effective alternative approach in order to understand the response of a material's structural and thermal behavior of a material under various combinations of matrix and filler materials.

There are several computational models that have been proposed over the years for the prediction of key material properties [40–60]. For thermal conductivity, Hesselman and Johnson proposed a model using a self consistent scheme incorporating the effect of particle size and thermal interfacial resistance between matrix and interface; however this model can handle low inclusion cases and spherical shape particles. Another thermal conductivity model proposed by Jiajun et al. carried forward the work of Hesselman and Johnson and included the shape factor and could be considered for non-percolating, micron sized inclusion in random orientation [45]. Nan et. al utilize the effective medium theory which incorporates the effect of particle orientation and alignment along with the

dependency of aspect ratio. Siddique and Arif modified the work of Nan to include the incorporation of nano-sized percolating inclusions and non-uniform distributions [49].

For the determination of elastic modulus and the coefficient of thermal expansion CTE there are various models proposed by renowned researchers. A numerical model proposed by Doghri and Tinel incorporates the Mori-Tanaka method to formulate a model which allows to determine effective elastic modulus and CTE for cases dealing with multiple inclusions, wide range of inclusion particle size and can be extended to include constitutive relationships [42]. The generalized method of cells approach has been limited to fiber inclusion and frequently arranged filler composites. Using Voigt and Reuss bounds approach allows the determination of properties in wider bounds [47]. Various analytical and numerical models have been proposed to quantify the effective fracture toughness of brittle matrix composites. These models require the knowledge of the in-situ fracture toughness of the inclusions. Values needed for modelling are usually unavailable which is why the effective properties can vary significantly. Li & Zhou have proposed analytical and numerical model for the prediction of fracture toughness of ceramic composites as a function of microstructure [59,60]. This is done by evaluating the associated J-integral through determining the probability of occurrence of different fracture mechanisms and energy release rate.

2.7 Spark Plasma Sintering

Traditionally, cutting tool material have been manufactured through either hot rolling or cold rolling. Spark plasma sintering (SPS) is a relatively new sintering process that allows compaction of ceramics and powdered metals at low temperature while using short holding times [61,62]. Loading of the precursors into the die and application of axial pressure make it similar it hot pressing technique. SPS makes it possible to apply very fast heating rates for small holding times which sinters highly dense sintered samples.

Al_2O_3 has been previously sintered in several published works along with other materials. Al_2O_3 -SiC composites have been fabricated using spark plasma sintering and the effect of the sintering parameters have been investigated [63–68]. Similarly, Al_2O_3 -cBN composites have been sintered using SPS [23,69–76]. The effect of sintering parameters is investigated and how phase transformation of cBN can be minimized.

2.8 Summary of Chapter

In Chapter 2, an extensive literature review in relation to the project objectives has been presented with the following key points.

- Key concepts of cutting tool inserts & various materials used as cutting tools; pros and cons.
- Advancements of ceramic composite design in recent times and how various inclusions can lead to improvement in various processes.
- Research work dealing the design of alumina based composites for use as enhanced cutting tools was discussed and how certain inclusion candidates can help improve performance.
- The basics of high speed machining and what are the key parameters that can affect the quality of the machining process.
- Computational models needed to carry out the material design were discussed. Mean field homogenization and effective medium theory based models were considered for the evaluation of thermal conductivity, CTE and elastic modulus. While fracture toughness based parameters can be determined through the evaluation of a J-integral and energy release rate.

CHAPTER 3

MATERIAL DESIGN

Simulations of practical material design and testing have become feasible due to the powerful computational tools at hand. Composite materials targeted for a certain application are characterized by a variety of phases, defects, interfaces and other microstructural features. These simulations provide a cost-effective alternative approach in order to understand the response of a material's structural and thermal behavior under various combinations of matrix and filler materials.

3.1 Matrix & Reinforcement Selection

There are various commercially available ceramics available within the cutting tool market. Among them, alumina stands out due to its structural properties and economical cost [12]. Therefore, an alumina based composite having enhanced properties is considered in this work. The main objective for designing this particular composite is to improve the thermal shock resistance. This will be achieved by obtaining a high thermal conductivity and low CTE while maintaining its structural properties. Our approach integrates thermal and structural properties of composites as a constraint on the design process. Table 3.1 highlights the properties of commercially available alumina and the desired properties of our proposed material [77].

Table 3.1 - Ceramics commonly considered for ceramic-based cutting tool design.

Properties	Alumina	Silicon Nitride	Zirconia
Hardness (Mohs)	8	8.5	3
Fracture Toughness (MPa.m^{1/2})	4	8	8.5
Flexural Strength (MPa)	400	750	900
Modulus of Elasticity (GPa)	150	297	94.5
Thermal Conductivity W/m.K	25	43	16.7
CTE 10⁻⁶/K	7.1	2.8	12.2
Wear Resistance	Good	Good	Poor
Affordability	Good	Poor	Poor
Thermal Shock Resistance	Poor	Good	Poor
Chemical Stability	Good	Poor	Good

After tabulating the properties found from literature, Pugh's decision matrix method is used to select the best possible material for matrix consideration with Alumina kept as datum.

Table 3.2 - Pugh's decision matrix for picking the best ceramic matrix.

Properties	Alumina (Datum)	Silicon Nitride	Zirconia
Hardness (Moh's Scale)	8	+1	-1
Fracture Toughness K_{IC} (Mpa.m^{1/2})	4	+1	+1
Flexural Strength (MPa)	400	+1	+1
Modulus of Elasticity (Gpa)	150	-1	-1
Thermal Conductivity W/m.K	25	+1	-1
CTE 10⁻⁶/K	7.1	+1	-1
Wear Resistance	Good	-1	-1
Affordability	Good	-2	-1
Thermal Shock Resistance	Poor	+1	0
Chemical Stability	Good	-2	0
Availability	Good	-1	0
Total	0	-1	-5

From the Pugh's/decision-matrix method results, alumina has been selected as matrix material due to its greater availability, relatively cheap cost and good properties. It also promotes cohesiveness between the matrix and the filler inclusions. However, it has poor resistance to thermal shock therefore the objective here is to improve properties which will

enhance thermal shock resistance while maintaining structural integrity. Selection of filler materials listed in Table 3.3 will be done by picking the best possible filler candidates for our hybrid composite with the aid of numerical simulations.

Candidate filler materials are listed in Table 3.3; these have been chosen based on their ability to enhance the targeted properties. For the application of cutting tool inserts, the reinforcements chosen have to improve the thermal shock resistance as well as the structural properties. Therefore, the filler materials should possess the material properties required to achieve the set target.

Table 3.3 - Filler candidates for ceramic-based composite design and their properties of interest with respect to cutting tool inserts.

Candidates	Modulus of Elasticity E (GPa)	Poisson's Ratio	Hardness (Moh's)	Fracture Toughness K_{IC} (Mpa.m ^{1/2})	Density (g/cm ³)	Melt. Temp (C)	CTE 10 ⁻⁶ /K	Thermal Cond. W/m.K
Alumina	150	0.22	8	4	3.96	2054	7.1	25
Titanium Carbide	450	0.18	9.4	4.4	4.94	3065	7.7	30.9
Cubic Boron Nitride	367	0.15	9.8	4	3.35	3027	4.8	42.1
Titanium Carbonitride	473	0.23	7.8	6	5.50	2930	9.4	19.0
Silicon Nitride	297	0.28	8.5	8	3.25	2769	2.80	43
Silicon Carbide	410	0.14	9.2	4.6	3.1	2730	4.0	120
Diamond	1000	0.29	10	3.40	3.52	3550	1.18	2000
Graphene	1000	0.18	10	4	2.25	4727	4.30	500
Zirconia	94.5	0.34	3	8	5.68	2973	12.2	16.7

Next, the same steps are taken to select the best filler materials. Best candidates are bundled and then through the process of elimination the list is condensed. The properties shaded in yellow are eliminated because they are not within the range and therefore the associated will be eliminated. This leads to the condensed list of inclusion candidates.

Table 3.4 - Condensed list of potential inclusion candidates.

	Alumina	TiC	cBN	Si ₃ N ₄	SiC	Graphene	TiB ₂	ZrO ₂
Modulus of Elasticity E (GPa)	370	450	550	297	410	1000	367	94.2
Poisson's Ratio	0.22	0.18	0.15	0.28	0.14	0.18	0.12	0.34
Hardness (Moh's)	8	9.4	9.8	8.5	9.2	10	9.4	3
K _{IC} (MPa.m ^{1/2})	4	4.4	4	8	4.6	4	8	8
Density (g/cm ³)	3.96	4.94	8.8	3.25	3.1	2.25	4.52	5.68
Melt. Temp (°C)	2054	3.65	3027	2769	2730	4727	2970	2973
CTE 10 ⁻⁶ /K	8.1	7.7	4.8	2.8	4	4.3	6.7	12.2
Thermal Cond. W/m.K	25	30.9	42.1	43	120	500	54	16.7

Despite high structural properties of titanium carbonitride, it was eliminated from the list due to its inferior thermal conductivity and CTE values. Zirconia was considered to be eliminated because of its low thermal conductivity and elastic modulus but retained for fracture toughness. Diamond was not considered due to its brittleness and incompatibility with cast iron at high temperatures.

To validate our material elimination process, the computational design tool is used to predict the effective properties that have been discussed when the various selected reinforcements are considered. Based on the computational results, the most effective fillers were selected as shown in Table 3.4 that were deemed to be the most suitable to achieve the target properties required for the designed composites. For the basis of this work, we have selected silicon carbide and cubic boron nitride as filler materials because of their enhanced target properties and due to availability of material. The target properties have been set as functions of volume fraction and particle size. The volume fraction of filler material in a reinforced composite material has a direct effect on the properties of the composite; the filler volume fraction may lead to an increase or reduction in certain properties of the material. Therefore, it is important to investigate the effect of these parameters on the target properties such as thermal conductivity, CTE, elastic modulus and fracture toughness parameters.

3.2 Computational Models

3.2.1. Mean-field homogenization and effective medium approximations

The term homogenization is used to refer a method of estimating the properties of an inhomogeneous material which provides a higher-level approximation. Homogenization is broken down into two different phases: A microscale problem is solved over a representative volume of the heterogeneous material to determine the microscale solution. Secondly, an averaging of the of the local microscale solutions is carried out to determine the macroscale response of the heterogeneous material. A multi inclusion effective medium

theory is used in the current study to predict the thermal conductivity of a composite material. The model takes into account the properties of the matrix and reinforcement, particle size, volume fraction and interfacial thermal resistance; the effect of the shape and of orientation of inclusion on the effective thermal conductivity is accounted for. The volume fraction of the dispersions is assumed sufficiently dilute that interactions between the local temperature fields of neighboring dispersions are absent. The effect of material mismatch and imperfect interfaces is taken into account as an interfacial thermal resistance. The multi-inclusion EMA is expressed through the following equations. For complete descriptions, refer to Siddiqui [49]:

$$k_{eff,11} = k_{eff,22} = k_{mat} \frac{2 + \sum_{i=2}^N \varphi_i \left[\beta_{11}^i (1 - L_{11}^i) (1 + \langle \cos^2 \theta \rangle^i) + \beta_{33}^i (1 - L_{33}^i) (1 - \langle \cos^2 \theta \rangle^i) \right]}{2 - \sum_{i=2}^N \varphi_i \left[\beta_{11}^i L_{11}^i (1 + \langle \cos^2 \theta \rangle^i) + \beta_{33}^i L_{33}^i (1 - \langle \cos^2 \theta \rangle^i) \right]} \quad 3.1$$

$$k_{eff,33} = k_{mat} \frac{1 + \sum_{i=2}^N \varphi_i \left[\beta_{11}^i (1 - L_{11}^i) (1 - \langle \cos^2 \theta \rangle^i) + \beta_{33}^i (1 - L_{33}^i) \langle \cos^2 \theta \rangle^i \right]}{1 - \sum_{i=2}^N \varphi_i \left[\beta_{11}^i L_{11}^i (1 - \langle \cos^2 \theta \rangle^i) + \beta_{33}^i L_{33}^i \langle \cos^2 \theta \rangle^i \right]} \quad 3.2$$

$$\langle \cos^2 \theta \rangle^i = \frac{\int \rho^i(\theta) \cos^2 \theta \sin \theta d\theta}{\int \rho^i(\theta) \sin \theta d\theta} \quad 3.3$$

$$L_{11}^i = L_{22}^i = \begin{cases} \frac{(p^i)^2}{2((p^i)^2 - 1)} - \frac{p^i}{2((p^i)^2 - 1)^{1.5}} \cosh^{-1} p^i, & \text{for } p^i \geq 1 \\ \frac{(p^i)^2}{2((p^i)^2 - 1)} + \frac{p^i}{2(1 - (p^i)^2)^{1.5}} \cosh^{-1} p^i, & \text{for } p^i < 1 \end{cases} \quad 3.4$$

$$p^i = a_3^i / a_1^i \quad 3.5$$

$$L_{33}^i = 1 - 2L_{11}^i \quad 3.6$$

$$\beta_{kk}^i = \frac{k_{c,kk}^i - k_{mat}}{k_{mat} + L_{kk}^i (k_{c,kk}^i - k_{mat})} \quad 3.7$$

$$k_{c,11}^i = \begin{cases} k_{inc}^i / (1 + \gamma_{11}^i L_{33}^i k_{inc}^i / k_{mat}), & \text{for platelet inclusions} \\ k_{inc}^i / (1 + \gamma_{11}^i L_{11}^i k_{inc}^i / k_{mat}), & \text{for other shapes} \end{cases} \quad 3.8$$

$$k_{c,33}^i = \begin{cases} k_{inc}^i / (1 + \gamma_{33}^i L_{11}^i k_{inc}^i / k_{mat}), & \text{for cylindrical inclusions} \\ k_{inc}^i / (1 + \gamma_{33}^i L_{33}^i k_{inc}^i / k_{mat}), & \text{for other shapes} \end{cases}$$

$$\gamma_{kk}^i = \begin{cases} \alpha_k (2 + 1/p^i), & \text{for } p^i \geq 1 \\ \alpha_k (1 + 2p^i), & \text{for } p^i < 1 \end{cases} \quad 3.9$$

$$\alpha_k^i = R_{TB}^i k_m / a_k^i \quad 3.10$$

Where, $K_{eff,11}$, $K_{eff,22}$ and $K_{eff,33}$ are the effective thermal conductivity values of the composites in all three directions; φ_i is the volume fraction, a_1^i and a_3^i are particle radii. R_{TB}^i is the interfacial thermal resistance, p^i is the aspect ratio. $K_{inc,i}$ is the thermal conductivity of inclusion of type i . $\langle \cos^2 \theta \rangle^i$ is the factor which defines the orientation of inclusion of type i . k_m is the thermal conductivity of the base matrix. L_{11} and L_{22} , L_{33} are the phonon mean free paths of matrix and inclusions, respectively.

The coefficient of thermal expansion is calculated using the Mori-Tanaka mean-field homogenization theory using the base equation:

$$\alpha_{eff} = \alpha_i I_2 + c_i (C_i^{-1} - C_M^{-1}) W ((1 - c_i) I_4 + c_i W)^{-1} (C_i^{-1} - C_M^{-1})^{-1} (\alpha_i I_2 - \alpha_M I_2) \quad 3.11$$

$$\text{where, } W = C_i A_i C_M^{-1} \text{ and } A_i = [I + S_M C_M^{-1} (C_{I,i} - C_M)]^{-1} \quad 3.12$$

α_{eff} is the effective coefficient of thermal expansion of the reinforced composites. α_M is the thermal expansion of the base matrix material, while α_i is the thermal expansion of the reinforcement, C_M is the stiffness tensor of the base matrix, C_i is the stiffness tensor of the inclusion and S is the Eshelby tensor. c_i is the inclusion volume fraction. I_2 and I_4 are the second and fourth stiffness tensors respectively. A_i is the strain localization tensor for the inclusion type i which is determined by Mori-Tanaka scheme [78]. It is used to predict the average strain field in inclusion i using the macroscopic strain field that is applied onto the composite.

The model used for predicting the modulus of elasticity is based on the seminal work done by Eshelby in 1965 along with utilizing the mean-field homogenization theory to predict the effective modulus of elasticity of a particulate reinforced composite. The strain distribution at the micro scale is related to the macro scale strains using the equation of strain localization $E(x) = A(x)\bar{E}_M$. The homogenized elasticity tensor can be solved using the equation: $\bar{C}_M = \sum_i c_i C_i A_i$. Through Mori-Tanaka scheme we can further resolve,

$$A_{(MT),i} = [c_i I + c_m (A_i)^{-1} + \sum_j c_j A_j (A_j)^{-1}]^{-1} \quad 3.13$$

$$\bar{C}_{(MT)} = C_M + \sum_i c_i (C_i - C_M) A_{(MT),i} \quad 3.14$$

Where C_i denotes the elastic strain tensor of inclusions, c_i the volume fraction of inclusions and $A_{(MT),i}$ the localized strain tensor of inclusions and I is the fourth order identity.

Models prepared for thermal conductivity, elastic modulus and coefficient of thermal expansion are preliminarily validated using previously published experimental literature [23,27]. Deviation in results is attributed to the modelling being performed assuming

perfectly spherical shaped inclusion particles whereas in reality, particles are found to be irregularly shaped. Trends and deviations are discussed in greater detail in Section 3.3.

3.2.2 Prediction of fracture toughness and energy release rate

There are various parameters that determine the overall fracture toughness of reinforced brittle composites via the activation of different fracture mechanisms. The microstructure of the composite, its constituent properties and the distribution of phases influence the fracture behavior of materials undergoing deformation by affecting the failure mechanisms. To better understand the fracture behavior, Li & Zhou have proposed analytical models through the use of a J-integral based approach and cohesive FEM simulations to predict the overall fracture toughness of brittle ceramic-based composites which is evaluated as a function of particle size, volume fraction percentages, constituent properties and interfacial bonding attributes [59,60] and modified for additional inclusions. Due to statistical measures this approach is applied on microstructures possessing random heterogenous phase distributions. The fracture toughness parameter is evaluated as a function of the critical energy release rate, effective elastic modulus and Poisson's ratio. For brittle materials, the fracture toughness is related to the critical energy release rate through the equation:

$$K_{IC}^2 = J_{IC} \frac{\bar{E}}{1-\bar{\nu}^2} \quad 3.15$$

Where \bar{E} and $\bar{\nu}$ are the effective elastic modulus and Poisson's ratio while J_{IC} is the critical energy release rate function. For a tortuous crack path where different types of fracture

sites, namely matrix cracking, interface debonding and particle cracking are present, the average energy release rate can be stated as:

$$J_{IC} = \frac{L}{W} \left(\varphi_{in} \frac{L_{in}}{L} + \varphi_m \frac{L_m}{L} + \varphi_p \frac{L_p}{L} \right) \quad 3.16$$

$$J_{IC} = \xi(Q, s, f) (\varphi_{in} H_{in} + \varphi_m H_m + \varphi_p H_p) \quad 3.17$$

Where W is the projected crack surface area in the direction of crack propagation. L_{in} , L_m , and L_p represent the crack arc lengths along the interface, within the matrix and intersecting the reinforcement material particles which equal the total crack length L . Solving Eqn. 3.16 is broken into two parts as highlighted in Eqn. 3.17. $\xi(Q, s, f)$ is defined as the crack length multiplication factor (CLMF). This factor allows the capturing the influence of interfacial compliance as a function of strength ratio Q , reinforcement particle size s and the reinforcement volume fraction f respectively. H_{in} , H_m , and H_p are the proportions of crack lengths that are associated with the interface debonding, matrix cracking and particle cracking. The analysis performed with the two equations described applies only to quasistatic crack growth in which crack speed will approach zero. Nevertheless, it is found that for brittle materials, which is the case for our study, the evaluation of J_{IC} can be performed by accounting for the crack speed via the use of dynamic calculations. There are two kinds of possible fracture types that can occur when a crack approaches an interface between matrix and reinforcement within a ceramic composite. Interface debonding is a key mechanism for crack deflection which is a result of weak interfacial bonding, smaller reinforcement particle size and greater roundness of particles. Second mode of fracture is particle cracking which is promoted by crack penetration. This type of failure typically results in catastrophic failure. This model can quantify the conditions which will allow the

two fracture mechanisms to be activated. This makes it possible to manipulate the design of microstructure to improve the fracture resistance of developed composites. The approach used for determining the activation of the mechanisms is based around the work of He and Hutchinson, Martin et al, which is an energy-based criteria which takes into account the works of each fracture type along different crack paths. A crack will grow when there is sufficient energy in the stress field which is needed to form new fracture areas. Therefore, the energy release rate of each type of fracture behavior would have to exceed the fracture energies of the interface and reinforcement for crack growth to be possible. Li and Zhou extended this work to incorporate the effects of size, shape and distribution of phases.

Characterization of the competition between the two fracture types (crack deflection and crack penetration) is done to quantify to the proportion of each mode occurring. He and Hutchinson presented a method to analyze the fracture behavior which involves analyzing a semi-infinite crack which is perpendicular to the planar bi-material interface. The solution of this analysis depends on the evaluating Dunder's parameters [79]. These parameters are evaluated by the following equations:

$$\alpha = f_1 \frac{[\mu_1(1-v_0)-\mu_0(1-v_1)]}{[\mu_1(1-v_0)+\mu_0(1-2v_1)]} + f_2 \frac{[\mu_2(1-v_0)-\mu_0(1-v_2)]}{[\mu_2(1-v_0)+\mu_0(1-2v_2)]} \quad 3.18$$

$$\beta = f_1 \frac{0.5[\mu_1(1-2v_0)-\mu_0(1-2v_1)]}{[\mu_1(1-v_0)+\mu_0(1-v_1)]} + f_2 \frac{0.5[\mu_2(1-2v_0)-\mu_0(1-2v_2)]}{[\mu_2(1-v_0)+\mu_0(1-v_2)]} \quad 3.19$$

Where μ_i and v_i are the shear modulus and Poisson's ratio for the matrix ($i=0$) and reinforcements ($i=1,2,\dots$).

To determine the activation of the fracture mechanisms, Li and Zhou have proposed a modified parameter that incorporates the effect of particle size, shape and phase distribution. This parameter identifies the type of fracture failure and is independent of crack extension lengths.

$$U = \frac{1-\beta^2}{a_0(1-\alpha)} [|c|^2 + |h|^2 + 2R_e(ch)] \rho^{-a_1} e^{\left(\frac{a_2}{0.5(s_1+s_2)}\right)} - \frac{\varphi_{in}}{\varphi_p} \quad 3.20$$

Where ρ is defined as the roundness of the reinforcement particle, s_i represents the reinforcement sizes; which leads to:

$$P_{jj} = (f_1 - f_1^2) e^{-\left(\frac{D}{s_1}\right)} + f_1^2 + (f_2 - f_2^2) e^{-\left(\frac{D}{s_2}\right)} + f_2^2 \quad 3.21$$

$$P_{ii} = [(1 - f_1) - (1 - f_1)^2] e^{-\left(\frac{D}{s_1}\right)} + (1 - f_1)^2 + [(1 - f_2) - (1 - f_2)^2] e^{-\left(\frac{D}{s_2}\right)} + (1 - f_2)^2 \quad 3.22$$

$$P_{ij} = \frac{(1-P_{jj}-P_{ii})}{2} \quad 3.23$$

These are the probabilistic functions for randomly located vectors with a defined length D which begins in each different phase present. Here, phase i is defined as the matrix with j considered as the reinforcements of volume fractions f_1 and f_2 . Additional reinforcements are included by manipulating these functions to consider the probability of encountering these inclusions when a crack is propagated. The coefficients c and h needed to perform these parametric studies are approximated as:

$$c = \frac{1}{2} \sqrt{\frac{1-\beta}{1+\alpha} \left(e^{\frac{-i}{2}} + e^{\frac{-3i\omega}{2}} \right)} \quad 3.24$$

$$h = \frac{1}{4} \sqrt{\frac{1-\beta}{1-\alpha}} \left(e^{\frac{-i\omega}{2}} - e^{\frac{-3i\omega}{2}} \right) \quad 3.25$$

The crack deflects at the interface when $U > 0$, otherwise it will penetrate into the reinforcement which will result in particle cracking. Coefficients c and h are greatly influenced by the crack incidence angle ω . Both c and h tend to become constant as $\omega > 60^\circ$. Veljkovic also reported that the error associated with c and h is within 1% when $0^\circ < \omega < 45^\circ$. Using this information, the probability of crack deflection is therefore defined as:

$$p = \frac{\int_{\omega_0}^{\pi/2} U d\omega}{\int_0^{\pi/2} |U| d\omega} \quad 3.26$$

Using the parameters discussed, we can predict K_{IC} by quantifying the probability of occurrence for each fracture mechanism over a defined crack length D [80–82]. Crack deflection can occur through either matrix cracking or interfacial debonding. Thus, the interfacial bonding strength and the fracture energies should be taken into account. The relation that accounts for these factors is empirically determined using:

$$H_{in} = \frac{\int_0^D P_{ij}(D) dx}{D} p \left(\frac{\varphi_{in}}{\varphi_m} \right)^{-a \ln Q} \quad 3.27$$

$$H_p = \left(\frac{\int_0^D P_{ij}(D) dx}{D} (1 - p) + \frac{\int_0^D P_{jj}(D) dx}{D} \right) \left(\frac{\varphi_{in}}{\varphi_m} \right)^{-b \ln Q} \quad 3.28$$

$$H_m = 1 - H_{in} - H_p \quad 3.29$$

Where H_m , H_{in} , and H_p are the proportions of matrix cracking, interface debonding and particle cracking, respectively. $a = 0.4$ and $b = 2$ are dimensionless parameters that have been predetermined by fitting relations to programmed CFEM results. Q is the interfacial bonding strength, which is ratio of interfacial cohesive strength and the average value of

the cohesive strengths of matrix and reinforcement. Q may be varied between 10^{-5} and 10^1 based on the strength of the interface bonds (where small Q represents ductile interfaces). As previously mentioned, prediction of fracture toughness K_{IC} requires evaluating of the crack multiplication factor $\xi(Q, s, f)$. This factor depends on variation in trajectory of heterogeneity-induced cracks which requires $\xi > 1$ for all cases. A simplified version that has been implemented when taking $\xi(Q=1)$ as a constant is presented:

$$\xi(s, f) = \frac{1-e^{D_2}}{e^{D_1}-e^{D_2}} e^{D_1 f} + \frac{e^{D_1}-1}{e^{D_1}-e^{D_2}} e^{D_2 f} \quad 3.30$$

where $D_1 = m_1 s + m_2$ and $D_2 = m_3 s^{m_4} + m_5$; The parameters $m_1 = 0.0175$, $m_2 = -1.483$, $m_3 = -4.7 \times 10^{-12}$, $m_4 = 6.695$ and $m_5 = -4.04$ have been set by curve fitting on the CFEM data and s is the average of the reinforcement particle sizes.

The effective properties of the homogenized region have been predicted using the Mori-Tanaka method scheme. The effective bulk modulus and shear modulus are defined as:

$$\bar{K} = K_0 + \frac{f_1(K_1-K_0)(3K_0+4\mu_0)}{3K_0+4\mu_0+3(1-f_1)(K_1-K_0)} + \frac{f_2(K_2-K_0)(3K_0+4\mu_0)}{3K_0+4\mu_0+3(1-f_2)(K_2-K_0)} \quad 3.31$$

$$\bar{\mu} = \mu_0 + \frac{5f\mu_0(\mu_1-\mu_0)(3K_0+4\mu_0)}{5\mu_0(3K_0+4\mu_0)+6(1-f)(\mu_1-\mu_0)(K_0+2\mu_0)} \quad 3.32$$

where, f is the volume fraction of the reinforcement K and μ are the bulk and shear modulus for matrix ($i=0$) and reinforcements ($i=1,2,\dots$) respectively.

The effective Young's modulus and Poisson's ratio for the homogenized region are defined as:

$$\bar{E} = \frac{9\bar{K}\bar{\mu}}{3\bar{K}+\bar{\mu}} \quad 3.33$$

$$\bar{v} = \frac{3\bar{K}-2\bar{\mu}}{6\bar{K}+2\bar{\mu}} \quad 3.34$$

The fracture toughness model prepared has been validated using published experimental work [23,27] and variations in results are attributed to irregular reported surface fracture energies. Patterns and discrepancies are discussed in greater detail in Section 3.3.

3.3 Numerical Simulations

This section presents the numerical results of the simulations carried out for single inclusion and hybrid alumina-based composite containing the selected reinforcement phases i.e. cBN & SiC. These results will highlight the resulting effective properties as a function of volume fraction and particle size. The threshold values to obtain the desired properties for our cutting tool application will also be determined based on material properties acquired from literature.

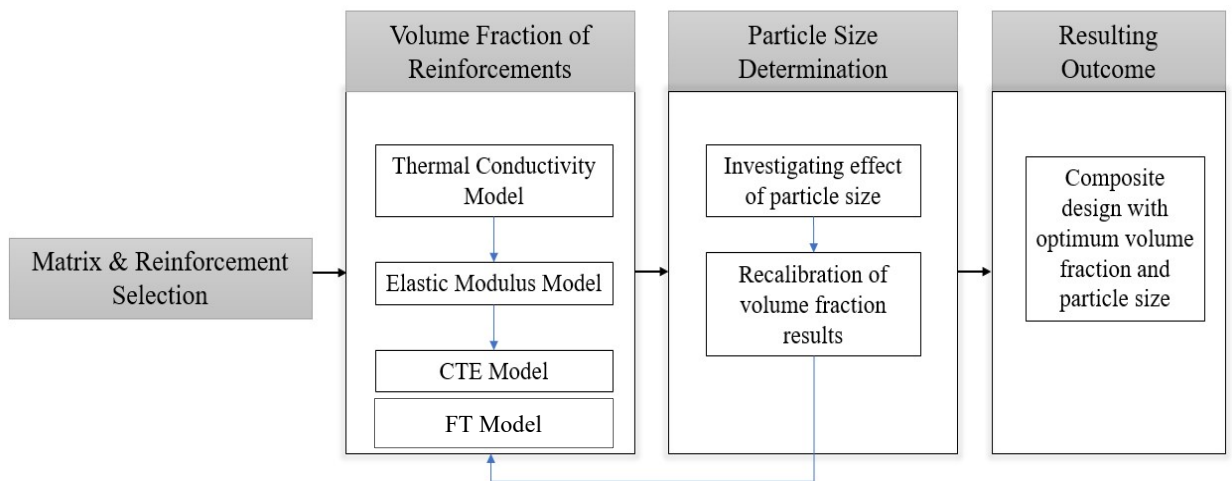


Figure 3.1 - Chronological map highlighting each step of the computational material design approach undertaken for ceramic matrix composite design.

Firstly, effective properties as a function of volume fraction will be presented to identify the amount of filler material needed to reach the threshold. In the second part, determination of the minimum required filler particle size to meet the properties target will be performed. We will be focusing on four key resulting properties; thermal conductivity, coefficient of thermal expansion (CTE), elastic modulus and fracture toughness. As a means of comparison, single-phase results will also be presented for each selected filler phase. The method of design is highlighted in Figure 3.1.

Since alumina is considered as a stand-alone cutting tool insert material very often within the industry, we have decided to design the composite with alumina as a benchmark.

Table 3.5 below lists the target properties threshold that has been determined to achieve:

Table 3.5 - Range of target properties for our proposed composite material design with comparison with pure alumina.

	Thermal Conductivity (W/m-K)	Elastic Modulus (GPa)	CTE ($10^{-6}/K$)	Fracture Toughness K_{IC} ($MPa.m^{1/2}$)
Alumina	25	150	7.1	3.96
Proposed Composite Material	$25 < K < 40$	$150 < E < 250$	$CTE < 7.1$	> 3.96

3.4 Single Inclusion Results

Initially, the models are run for single inclusion results only. Based on the reinforcements table and availability of material, three materials from the superior filler candidates have been selected. The results are discussed in the following section.

3.4.1 Effective Thermal Conductivity & CTE Determination

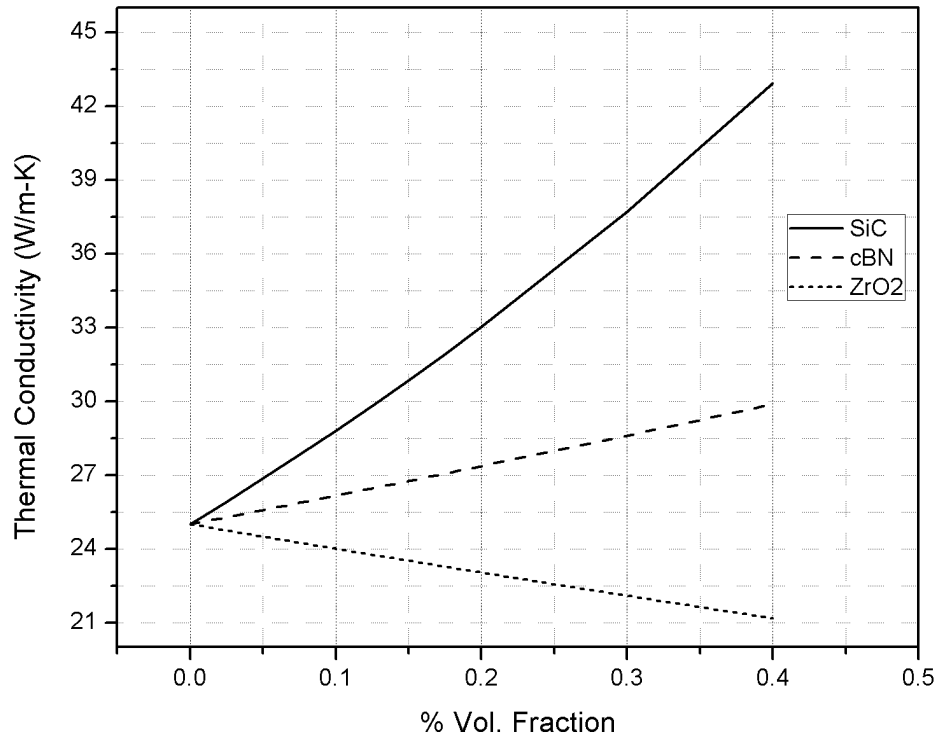


Figure 3.2 - Predicted thermal conductivity as a function of volume fraction of alumina based composite material with various independent fillers.

Figure 3.2 shows the effective thermal conductivity of various combination of fillers and Alumina matrix as a single inclusion composite. SiC and cBN fillers results in an increase of the effective thermal conductivity. Inclusion of zirconia has decreased thermal conductivity which was expected because of its reported inferior thermal properties. Similarly, effective CTE of the composite is lowered with the introduction of SiC and cBN, as shown in Figure 3.3. A lowered CTE is beneficial when considering the design of a cutting tool insert as it aids in the reduction of thermal shock at elevated temperatures.

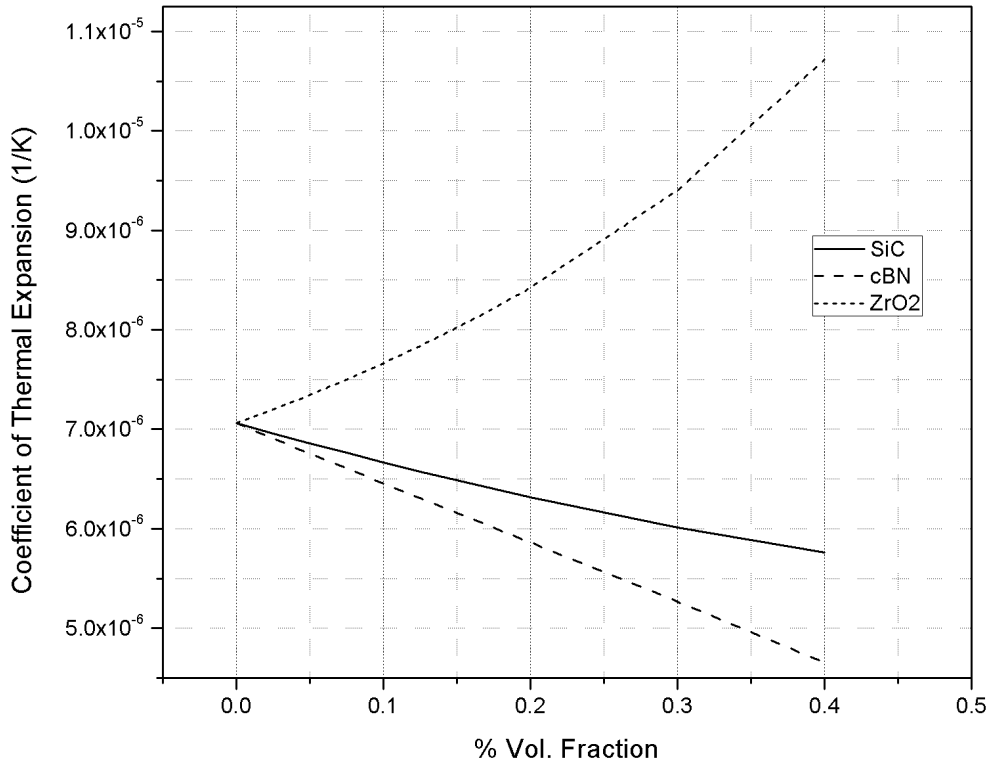


Figure 3.3 - Predicted coefficient of thermal expansion as a function of volume fraction of alumina based composite material with independent fillers.

3.4.2 Effective Elastic Modulus Determination

Effective elastic modulus reinforced alumina is improved with the introduction of SiC and cBN as shown in Figure 3.4. The relatively inferior elastic modulus of zirconia is resulting in reduction of elastic modulus of the composite material. With the single inclusion results, it seems silicon carbide and cubic boron nitride are the optimum filler candidates for the next phase; which is considering double inclusions.

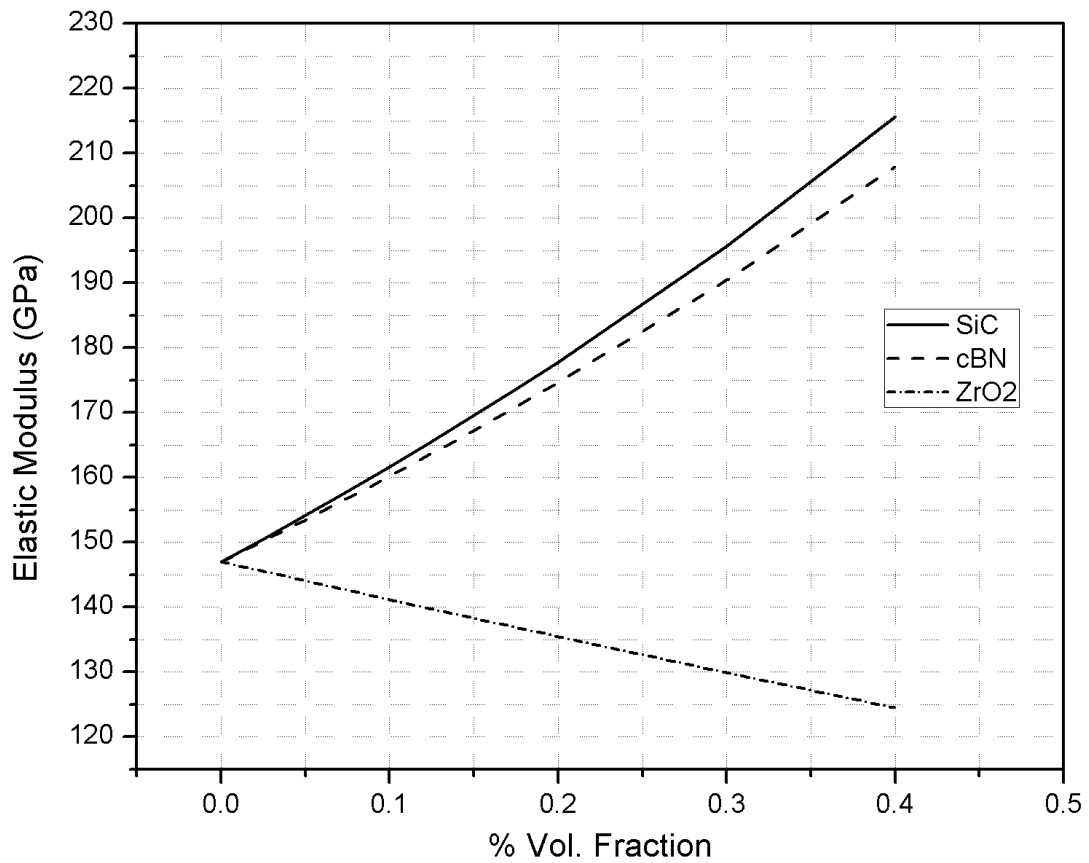
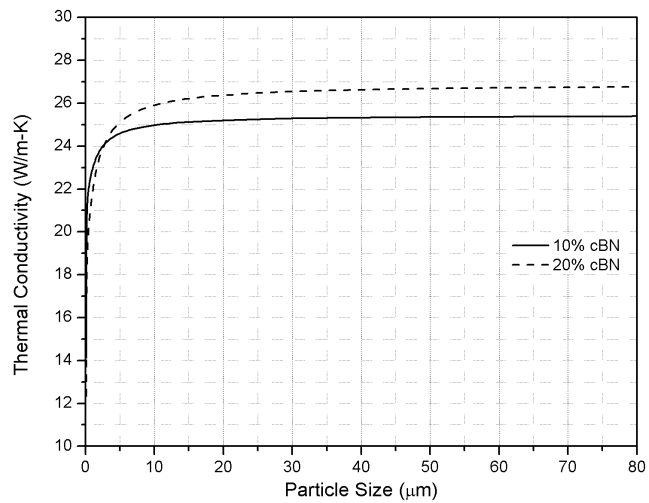


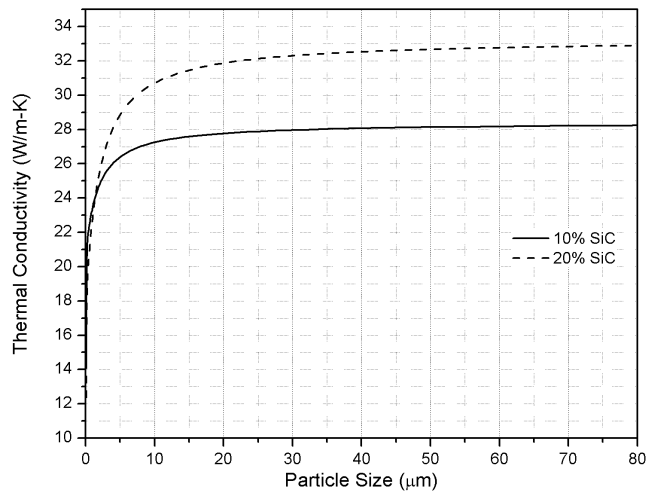
Figure 3.4 - Predicted effective elastic modulus as a function of volume fraction of alumina based composite with the addition of independent fillers.

3.4.3 Minimum Particle Size of Inclusion Study

After selecting the top two candidates, we have performed a study on the effect of particle size on the effective thermal conductivity. According to the computational model, the matrix is considered homogenous so its particle size effect is assumed to be independent.



a)



b)

Figure 3.5 - a) Effective thermal conductivity as a function of particle size of cBN reinforced alumina matrix composite. b) Effective thermal conductivity as a function of particle size of SiC reinforced alumina matrix composite.

The thermal interfacial resistance to be considered between matrix and fillers has been determined from surveyed literature [83]. As shown in the Figures 3.5a and 3.5b above, for both SiC and cBN cases the resulting thermal conductivity decreases at approximately 20 microns. A smaller particle size creates a larger contact surface area at the interface; the greater the area, the greater the thermal interfacial resistance. This leads to the drop in the effective thermal conductivity of the composite material. Therefore, it is important to select filler sizes beyond the minimum particle size to avoid a drop in thermal conductivity.

3.4.4 Effective Fracture Toughness Determination

Along with enhanced thermal properties, an effective cutting tool insert needs to have good fracture toughness properties. Enhanced fracture toughness can make the cutting tool insert more durable and prone to cracking at high cutting speeds resulting in greater tool life. The following graphs show the effective fracture toughness parameter of various single inclusion combinations as a function of volume fraction of inclusion. The constant parameters used for each case have been obtained from literature. Shape of inclusions are assumed to be perfectly spherical while the strength ratio is maintained constant.

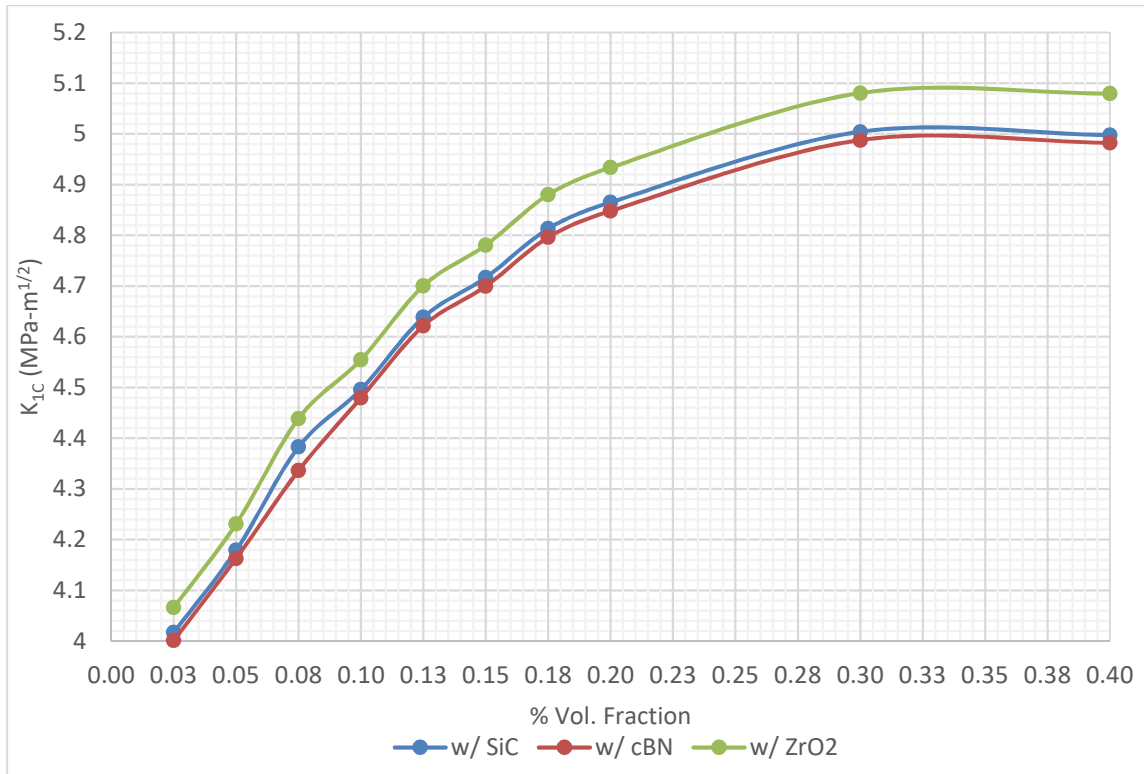


Figure 3.6 - Effective Fracture Toughness of Alumina Matrix w/ various inclusion candidates.

As shown in the figure above, an alumina composite reinforced with zirconia (zirconium oxide) exhibits enhanced fracture toughness compared with silicon carbide and cubic boron nitride with increasing volume fraction. This is attributed to the enhanced fracture toughness properties that are possessed by zirconia; incorporating zirconia into the system will reduce chances for particle cracking to occur due to its superior fracture surface energy. Embedding silicon carbide and cubic boron nitride are also improving the fracture toughness of the alumina base matrix composite. The greater elastic modulus values for these inclusion types greatly help in the improvement of the overall fracture toughness which is understandable when evaluating the J-integral equation. The decrease in the slope of the fracture toughness and volume fraction curves can be attributed to the greater number

of inclusion particles present within the system. The increased number of particles are resulting in a greater probability of failure due to particle cracking which could be a possible reason for the decrease in slope in the plotted data.

3.4.5 Exploring the Effect of Porosity

The porosity of the final material can also play a major role in the final effective properties of the composite material. Through the aid of computational modelling once again, the effect of porosity was investigated on Alumina-SiC case.

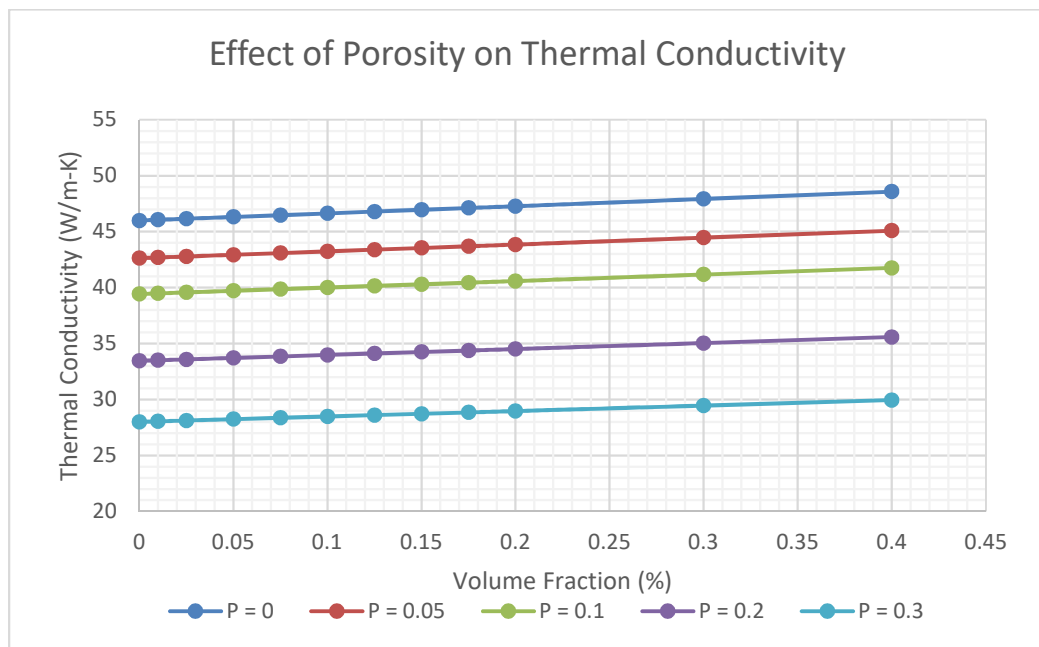


Figure 3.6 - Effect of porosity on the thermal conductivity of a Alumina-SiC composite.

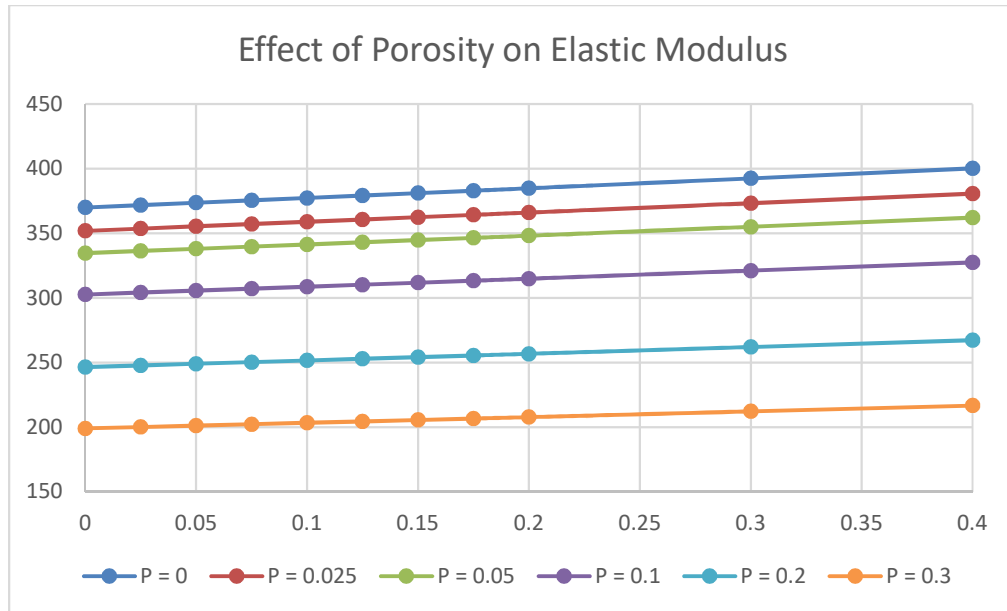


Figure 3.7 - Effect of porosity on the elastic modulus of a Alumina-SiC composite.

Increase in porosity will lead to a decrease in both elastic modulus and thermal conductivity therefore in order to avoid this issue the sintering of composites should be tuned in a way to reduce porosity as much as possible to avoid possible reduction of effective properties.

3.5 Double Inclusions

From the single inclusions study, we have concluded that the optimum reinforcements for a hybrid composite will be silicon carbide and cubic boron nitride. With these results, we have conducted a study for a composite with two reinforcements. Experimentally, we have observed slight cBN to hBN phase transformation when manufacturing the Al₂O₃-SiC-cBN composites using SPS. This transformation has been incorporated into our computational simulations by modifying the input properties of cBN inclusion. This is

because the transformation is occurring at the same locations and therefore does not have to be considered as an additional inclusion.

3.5.1 Effective Thermal Conductivity & CTE Determination

Figure 3.8 shows the effective thermal conductivity of the designed composite as a function of volume fraction of various combinations. As shown, the combination of alumina with SiC and cBN brings the effective thermal conductivity within the threshold around the 30% SiC & 20% cBN inclusion volume fraction region. The addition of silicon carbide affects the thermal properties considerably due to its superior thermal conductivity.

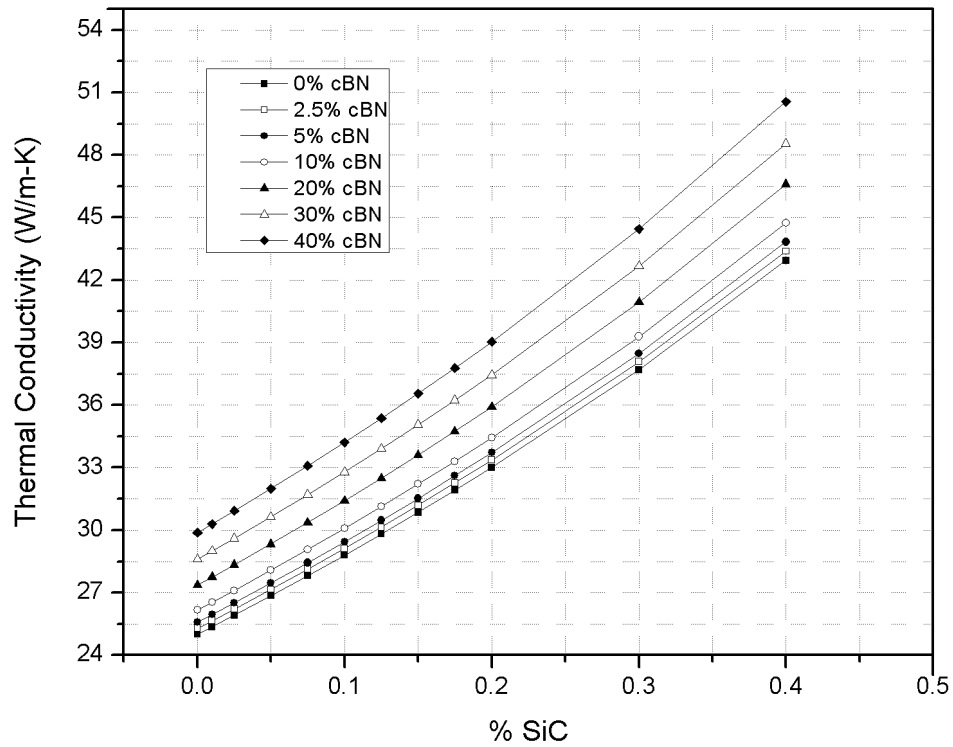


Figure 3.8 - Effective thermal conductivity as a function of volume fraction of a hybrid alumina matrix composite with reinforced SiC and cBN as filler materials.

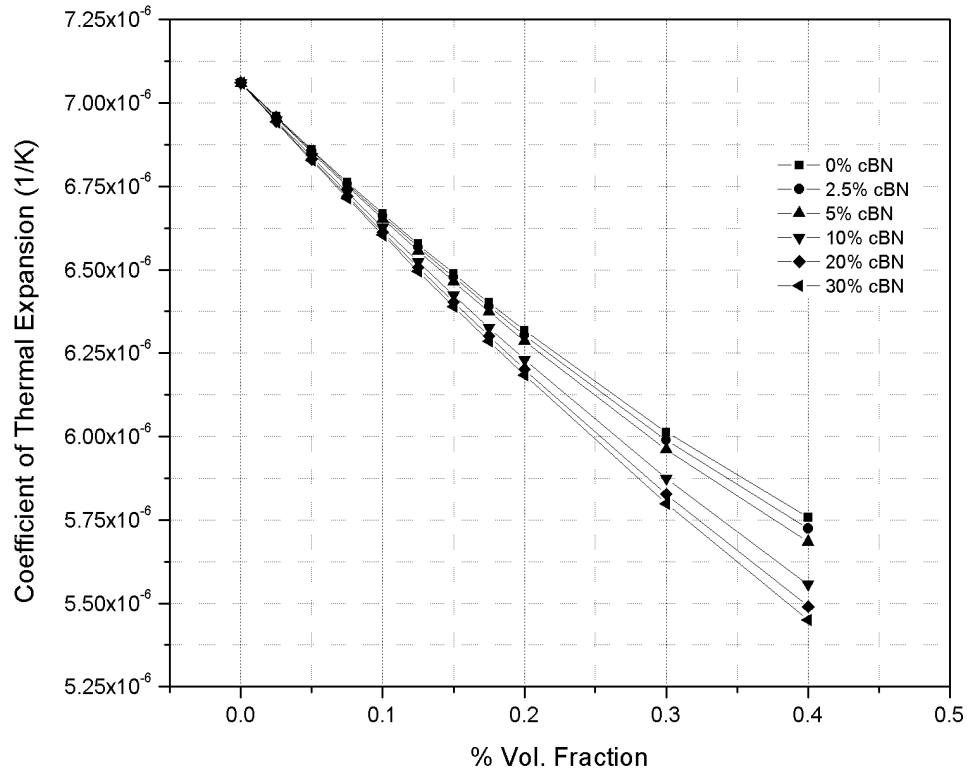


Figure 3.9 - Effective coefficient of thermal expansion as a function of volume fraction of an alumina based matrix composite with reinforced SiC and cBN filler materials.

A common issue with alumina based cutting tools is their weak resistance to thermal shocks due to its relatively poor thermal properties. The enhanced thermal conductivities of SiC and cBN improve the resulting thermal conductivity of the composite. To further improve the thermal performance of the composite during machining, the effective CTE should be reduced because of the inversely proportional effect of CTE on the thermal shock resistance. From Figure 3.9, it is clear that the reinforcements are reducing the effective CTE as volume fraction of the filler materials is increased.

The drop in coefficient of thermal expansion can be attributed to the low CTEs of both inclusions. The excellent thermal properties of SiC are desirable for our application and

the figure shows increase in SiC content is resulting in a much rapidly decreasing effective CTE of the composite.

3.5.2 Effective Elastic Modulus Determination

Another important aspect to consider is the structural integrity of the developed composite. Elastic modulus is an integral property which has a direct effect on the mechanical strength and toughness of the material. A stable elastic modulus can help improve the resistance to deformation during the cutting process. Figure 3.10 shows the effective elastic modulus as a function of volume fraction for varying SiC and cBN content. The base matrix and SiC as the first filler have been kept constant while the second filler, cBN, has been varied based on the candidates narrowed down. The superior elastic modulus properties of both silicon carbide and cBN will result in an improved effective elastic modulus of the composite. As reported in Figure 3.10, a combination of 30% SiC along with 20% cBN improves the elastic modulus significantly. Due to the high elastic modulus possessed by cBN, this combination is the most optimum out of the available candidate options to bring the elastic modulus within range. It is best to be around the base value to reduce any major effects on the overall strength and toughness.

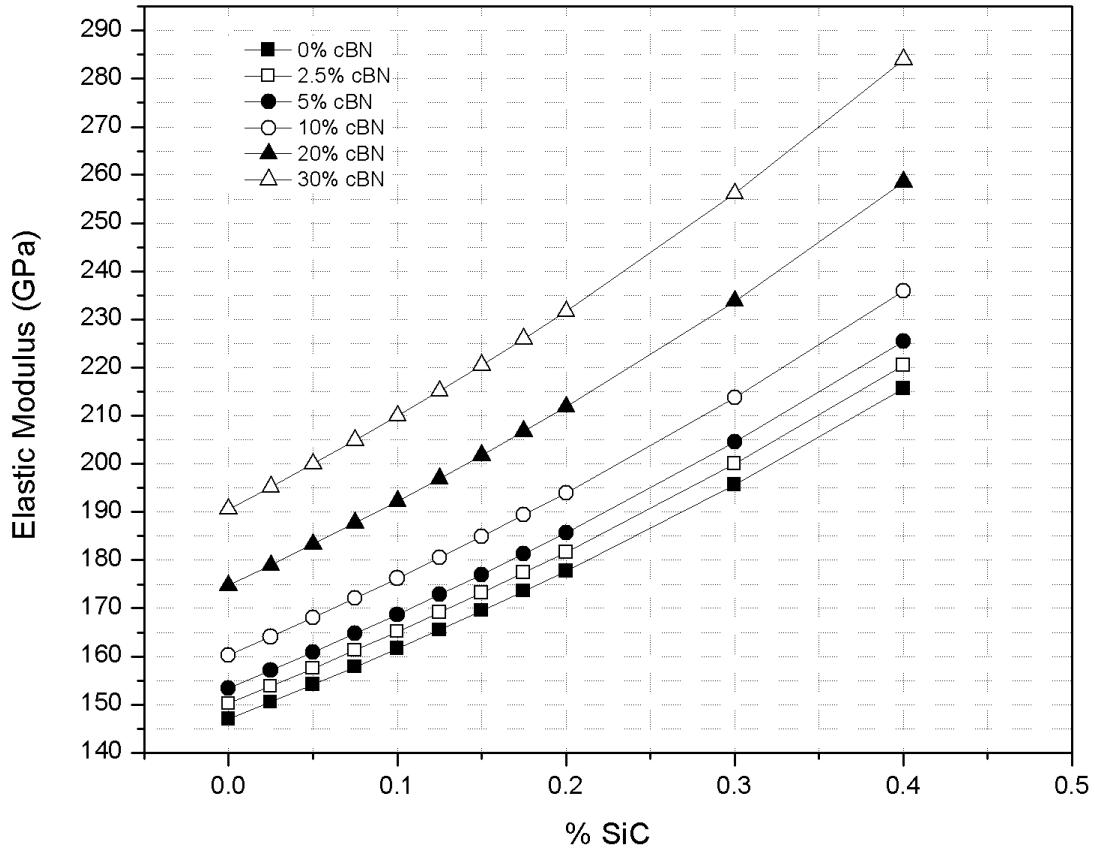


Figure 3.10 - Predicted effective elastic modulus as a function of volume fraction of an alumina matrix composite with reinforced cBN and SiC reinforced filler materials.

3.5.3 Effective Fracture Toughness Determination

Similarly, to improve the structural integrity of the proposed hybrid composite it is desirable to improve the overall fracture toughness. Enhanced fracture toughness leads to reduced crack propagation which is vital for an effective cutting tool insert as it improves the overall tool life which leads to a reduction of costs for replacement. The effective fracture toughness is predicted for the proposed hybrid alumina-silicon carbide-cubic boron nitride composite as a function of volume fraction.

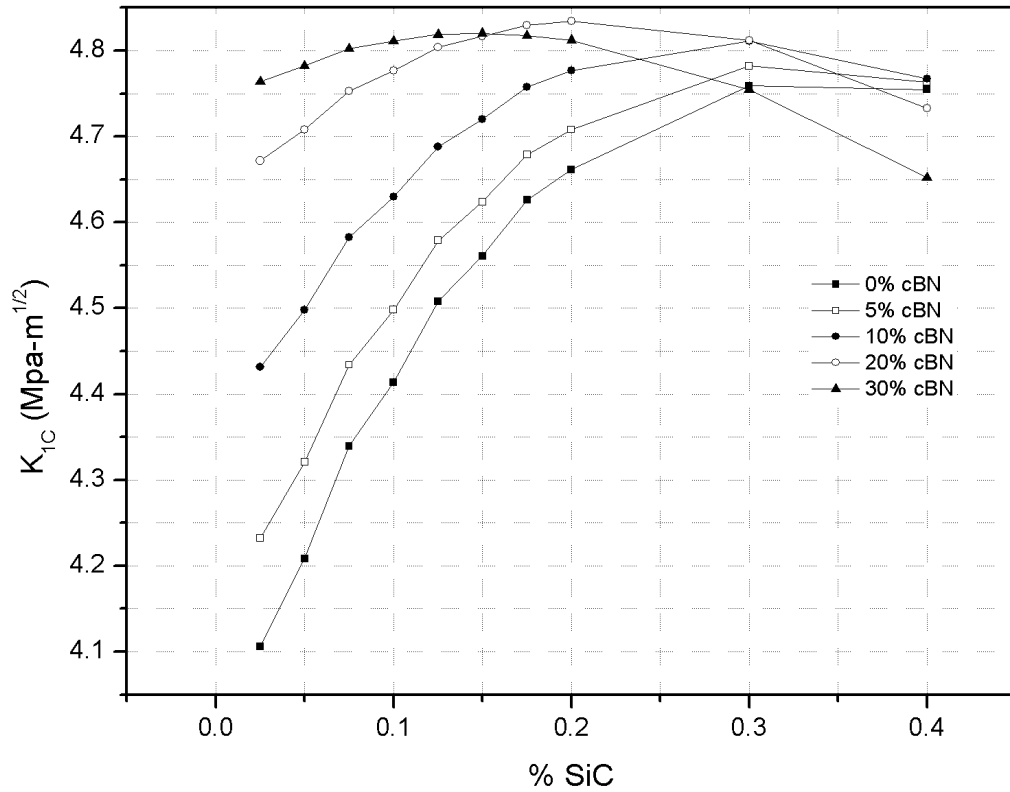


Figure 3.11 - Predicted effective fracture toughness as a function of volume fraction of an alumina matrix composite with reinforced cBN and SiC reinforced filler materials.

Increase in SiC and cBN content results in the overall increase of the effective fracture toughness. This is attributed to the superior fracture toughness values of both inclusions. Particle sizes for inclusions have been considered as equal to simplify the problem. The increase in fracture toughness can be pinpointed to enhanced elastic modulus of the composite because of the silicon carbide and cubic boron nitride inclusions. A decrease in fracture toughness is observed at increased volume fraction of inclusions, this can be explained by the greater amount of particles which is increasing the probability of fracture failure due to reinforcement particle cracking.

3.5.5 Minimum Particle Size of Inclusions Determination

Particle size plays a major role in the effective thermal conductivity of the developed material. Various studies have shown that a decrease in particle size leads to a drop in the resulting thermal conductivity. Keeping this in mind, simulations were performed to predict the thermal conductivity as a function of particle size. As seen in Figure 3.12, our numerical results show how a smaller particle size results in a decrease in thermal conductivity.

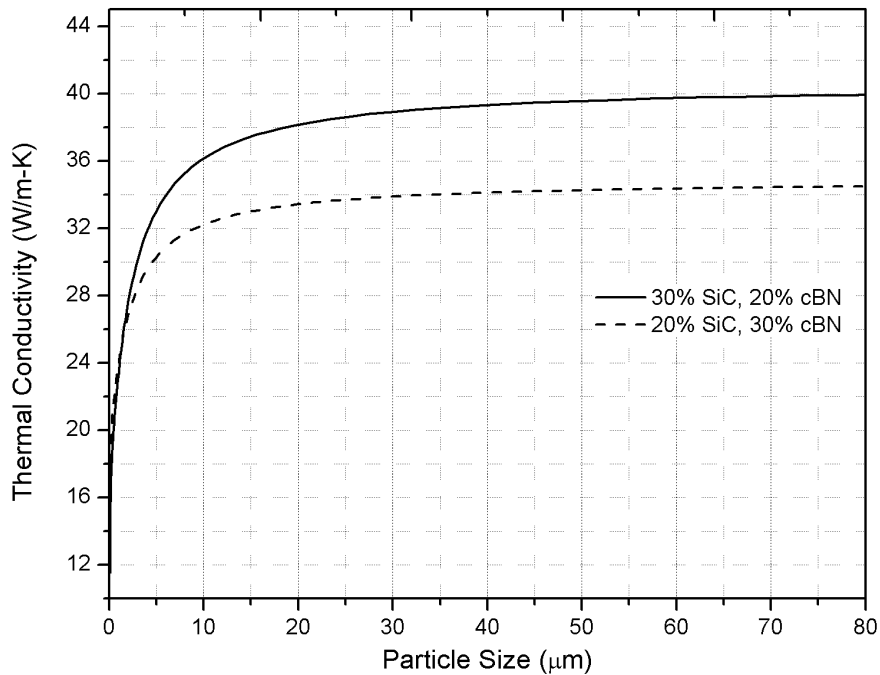


Figure 3.12 - Predicted effective thermal conductivity as a function of particle size of a hybrid alumina matrix composite with reinforced filler combinations i) 30% SiC and 20% cBN and ii) 20% SiC and 30% cBN.

This decrease in the thermal conductivity is associated with the fact that a smaller particle size is increasing the chances of phonon scattering. This increase in scattering leads to an increase in the interfacial resistance of the composite with results in a drop in thermal

conductivity. As discussed previously, a smaller particle size creates a larger contact surface area at the interface; this leads to an increase in thermal interfacial resistance. This results in the drop of the effective thermal conductivity of the composite material. Therefore, it is important to select filler sizes beyond the minimum particle size to avoid a drop in thermal conductivity.

3.6 Summary of Chapter

In this chapter,

- Various material candidates for ceramic based cutting tool inserts composites are compiled. Using Pugh's method, alumina is selected as the best possible matrix material. Similarly, the candidates with the inferior target properties are eliminated to filter out the weak options.
- Through the aid of computational models, the effective target properties are determined for the top 3 inclusion candidates as single inclusion cases. Minimum particle size required to avoid a drop in thermal conductivity is also determined for each case. In addition, the effect of porosity is also investigated where it was found the least amount of porosity percentage is desirable.
- The two best candidates are then carried forward into the hybrid composite study considering double inclusions. The effective targeted properties are determined and a minimum particle size study is performed to avoid a drop in thermal conductivity. With the selection of the best possible combinations, work is moved into the next phase of the project which is material development.

CHAPTER 4

MATERIAL DEVELOPMENT, CHARACTERIZATION & TESTING

4.1 Material Development

In order to validate the accuracy of the computational simulations an experimental phase is performed which will include characterization and determination of properties of the prepared composites. Pure alumina and alumina matrix composites with selected filler inclusions are manufactured using SPS (Spark Plasma Sintering). Based on the minimum particle size as predicted from numerical simulation, the inclusion particle sizes were selected at 40 microns to obtain the desired thermal conductivity. Measurement techniques for properties be discussed extensively in the experimental setup section. Lastly, the corresponding experimental results are tabulated and compared to the numerical simulation results.

As discussed previously in the material design section, the base matrix material for the hybrid composite is chosen to be alumina. For the reinforcement selection, cubic boron nitride and silicon carbide have been selected in line with our computational predictions due to their enhanced properties which will allow us to achieve our targeted properties values. Figure 4.1 shows the schematic which highlights each step in the material development process.

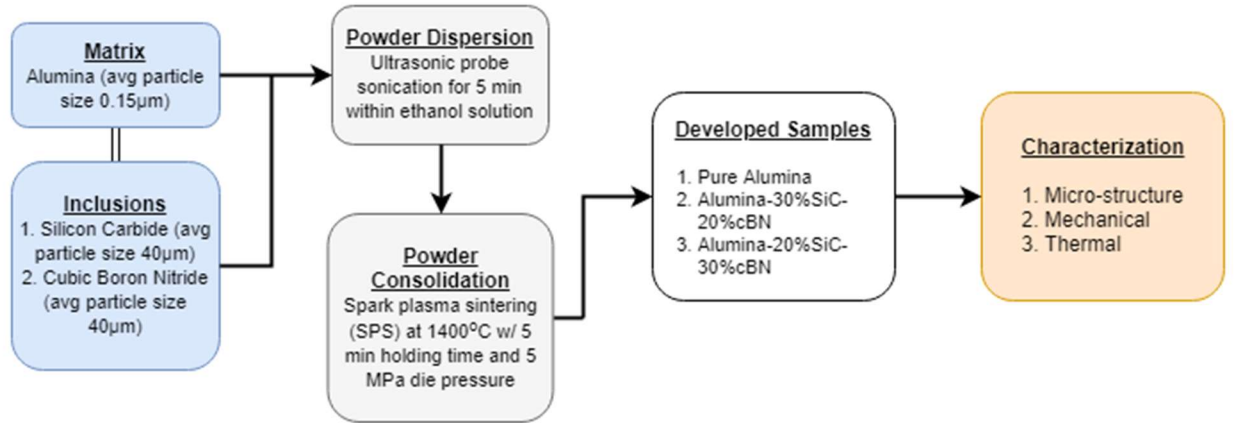


Figure 4.1 - Schematic displaying the step-by-step process undertaken for Material Development phase.

4.1.1 Manufacturing of Designed Composite

The alumina powder used was supplied by Chempur with an average particle size of 0.15 microns. The reinforcements were decided to be kept at equal size and were selected at an average particle size of 40 microns which is in line with the minimum particle size study performed computationally. The silicon powder supplied by Buehler while the cubic boron nitride was provided by Sigma. Cubic boron nitride powder has been acquired from Element Six, ABN800, USA. The fraction of matrix material is kept at a constant while the fraction of each reinforcement is varied. Table 4.1 is highlighting the details of the material development approach.

Table 4.1 - Types of samples developed using SPS.

Sample #	Matrix	Inclusion Types & Volume Fraction	Average Particle Sizes of Inclusions
1	Alumina (0.15 μ m)	None	None
2		30%SiC-20%cBN	40 μ m
3		20%SiC-30%cBN	40 μ m

The reinforcement materials are effectively dispersed into the alumina base matrix through the use of an ultrasonic probe sonicator (Model VC750, Sonics) mixed within an ethanol solution. Each sample prepared is probe sonicated for 5 minutes to allow effective dispersion. They are then left in a furnace at 80°C for 24h to allow the removal of the ethanol solution from the homogenized mixture.



Figure 4.2 - Ultrasonic probe sonicator (Model VC750, Sonics)

The designed composites were prepared using a 20 mm diameter graphite die using a Spark Plasma Sintering system from FCT, Germany. The samples are sintered at a fixed temperature of 1400°C, a heat rate of 100°C/min, holding time of 10 minutes and die pressure of 50 MPa. Parameters for sintering have been selected based on previous published works for similar composite design [23,27,62]. The graphite dies are used to produce disc shaped samples of approximately 8 mm height. Graphite sheet is kept between the die and sample to minimize the effect of friction which will allow easy ejection of the sintered samples.



Figure 4.3 - Spark Plasma Sintering system from FCT, Germany.

With the powder filled within the graphite die, it is then placed into the SPS chamber. A combination of passing current, applying heat and a mechanical axial load is forced onto the die simultaneously. The sintering temperature is measured and monitored using a

pyrometer placed at the bottom of a central hole in the upper punch. The pulse duration and pause time as well as the heating rate are fixed throughout all phases of the experiment. The samples' cross sections are prepared via grinding and polishing to be used for scanning electron microscopy.

4.1.2 Microstructure and Mechanical Characterization

i) Scanning Electron Microscopy

The microstructure and the overall constituent distribution of the reinforced composites are examined using a scanning electron microscope. Jeol JSM-6460LV scanning electron microscope equipped with energy-dispersive spectrometry (EDS) is used to observe the microstructures of the prepared composite samples. The samples are well grinded and polished to maximize quality of the capturing images. To obtain high quality microstructure images the surface of the samples is coated with a gold film to provide improved light penetration. This thin gold film is applied using a vacuum evaporation process. EDS scan technique is used to perform qualitative analysis of the microstructure as well as perform mapping to see the effectiveness of the dispersion process.

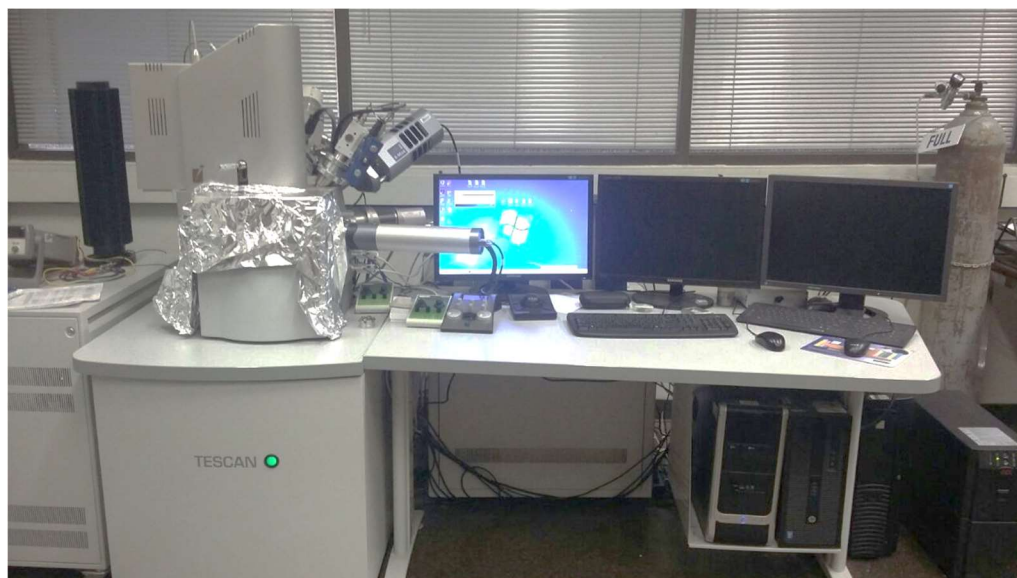


Figure 4.4 - Jeol JSM-6460LV scanning electron microscope equipped with energy-dispersive spectrometry (EDS).

X-ray diffraction analysis is used for phase characterization using the Rigaku desktop x-ray diffractometer model “Miniflex II” with copper radiation and a wavelength of 1.5418 angstroms. The XRD analysis range was selected from 20° to 100° based on results for similar materials found in literature.



Figure 4.5 - Rigaku desktop x-ray diffractometer model “Miniflex II”.

Raman spectroscopy results were acquired using a DXR2 Raman microscope. A 532-nm wavelength laser line is used as the excitation wavelength and the laser power used was 2.5 mW. The limits of spectra were selected from 100 to 3000 cm^{-1} at 25°C based on previous related work [23].



Figure 4.6 - A DXR2 Raman microscope.

ii) Microhardness and Determination of Elastic Modulus and Fracture Toughness

The micro hardness along with the associated properties such as modulus of elasticity & fracture toughness are measured using a Micro Hardness Tester supplied by Buehler instruments. A diamond indenter in the shape of a pyramid which is normal to the surface of the sample is driven down into the sample by applying an increasing load to a present value after which the load is gradually decreased until the material is back in its relaxed state. The indentation hardness is therefore defined as the mean contact pressure applied by the indenter onto the sample.



Figure 4.7 - Micro Hardness Tester supplied by Buehler instruments.

The microhardness value is supplied by the equipment itself after test completion while the diagonal and crack lengths of the indent are measured using the scope provided with the instrument. The modulus of elasticity and fracture toughness applying the data acquired using the equations as found within literature [84–89].

iii) Density

Density of the designed composite greatly depends on the constituents and the relative proportion of both matrix and inclusions. It is a key factor in the determination of the overall porosity of the manufactured material. The theoretical density of the of the matrix and reinforcement constituents can easily be determined composite in terms of the density and volume fraction via the rule of mixtures.

$$\rho_{th} = (\rho_m * v_m) + (\rho_{inc} * v_{inc}) \quad 4.1$$

Where ρ and v represent the density and volume fraction and where f and m are used to denote inclusion and matrix respectively. The experimental density is determined experimentally through the use of the Archimedes principle. This approach requires the determination of the mass of the composite material in both air and water.

With the determination of the theoretical and experimental densities, the percentage porosity of the composite can be calculated using Eqn. (4.2).

$$\%P = \left(\frac{\rho_{th} - \rho_{exp}}{\rho_{th}} \right) * 100 \quad 4.2$$

4.1.3 Thermal Characterization

i) Thermal Conductivity

C-Therm TCI Thermal Conductivity Analyzer as seen in the figure below is used to measure the thermal conductivity of various materials ranging from polymers, metals, rubbers and ceramics at room temperature at any given form of state, solid or liquid. This thermal conductivity equipment operates based on the modified transient plane source (MTPS) technique that uses a one-sided interfacial heat reflectance sensor that applies a momentary constant heat source to samples. The thermal conductivity of the designed composite samples is measured at room temperature. A set current is applied to the equipment's heating element which results in the rise of the interfacial temperature between the sensor and material. This fluctuation of temperature causes a change of voltage in the sensor element. The rise in voltage is used to quantify the thermal effusivity and thermal conductivity of the sample. These properties are proportional to the rate of increase in the sensor's voltage.



Figure 4.8 - C-Therm TCI Thermal Conductivity Analyzer.

ii) Coefficient of Thermal Expansion

Coefficient of thermal expansion of a material can be defined as the strain induced in the material due to a per unit rise of temperature. The coefficient of thermal expansion (CTE) of the developed composites is measured using a Mettler Toledo Thermal mechanical analyzer (TMA/SDTA 1 LF/1100). A thermal mechanical analyzer is used to measure the changes in dimensions of the sample due to variation of temperature. TMA is used to evaluate the coefficient of thermal expansion of the material as well as softening, crystallization and solid-solid transitions.



Figure 4.9 - Mettler Toledo Thermal mechanical analyzer (TMA/SDTA 1 LF/1100).

4.2 Microstructure & Mechanical Characterization

Properties of the composite depend on various parameters. These parameters include the interaction between the matrix and the inclusion, the dispersion of the inclusions into the matrix and the final resulting microstructure. Therefore, after manufacturing of the composite samples, various tests have been conducted to characterize the material which will allow us to know if the material has been sintered properly. Characterization of samples is done using three techniques; SEM (Scanning Electron Microscopy), XRD (X-ray Diffraction) and Raman Spectroscopy.

4.2.1 SEM Analysis

The prepared composites were analyzed under the scanning electron microscope to observe the microstructure and the dispersion of inclusions. Initially, the pure alumina sample is viewed through the SEM at the cross section of the sample.

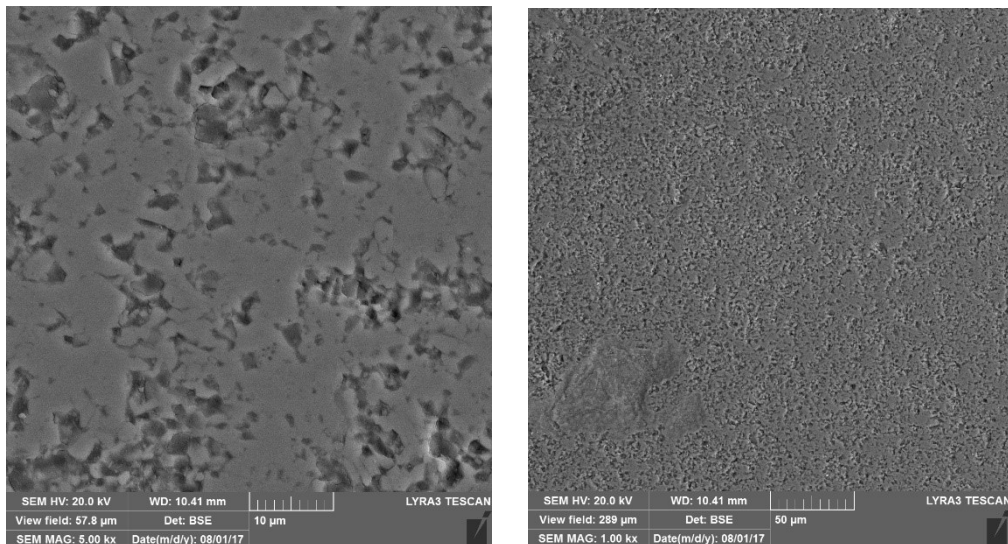
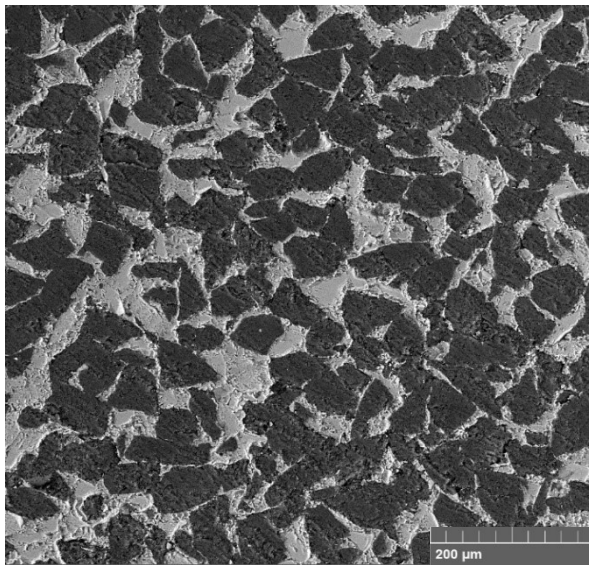
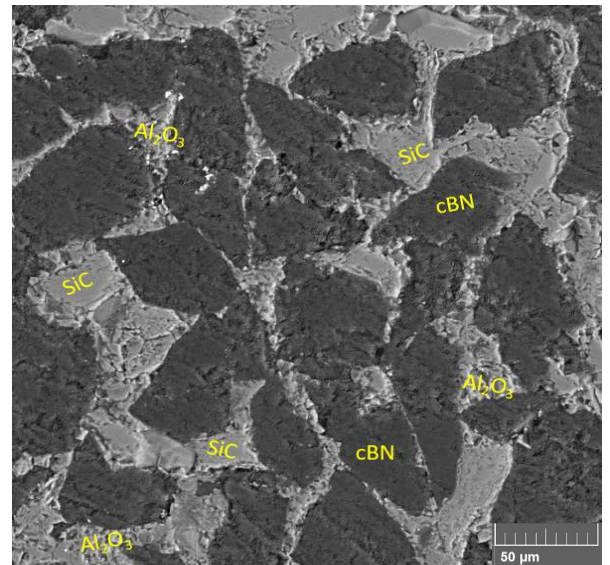


Figure 4.10 - SEM image of a pure alumina sample.

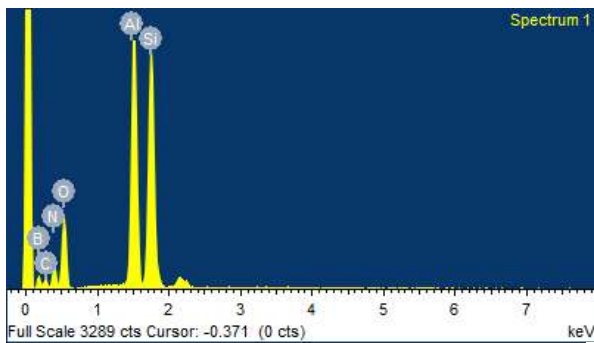
Due to the defined sintering parameters used in SPS there is some visible pores which leads to presence of porosity which is quantified in the density section. Furthermore, the small particle size alumina selected may also be attributed to presence of porosity in the pure alumina sample. As seen in the figure below, the inclusions of SiC and cBN have been embedded into the alumina matrix.



a)



b)



c)

Element	Weight%	Atomic%
B K	33.08	37.23
C K	34.67	35.13
N K	29.79	25.88
O K	2.09	1.59
Al K	0.21	0.10
Si K	0.16	0.07
Totals	100.00	100.00

Figure 4.11 - a) SEM image of an Al₂O₃-30%SiC-20%cBN at 400x magnification. b) SEM image of an Al₂O₃-30%SiC-20%cBN at 1000x magnification with each constituent specified. c) EDS analysis highlighting the presence of elements within the composite material (performed at 400x).

Figure 4.11 displays the microstructure of Al_2O_3 -30cBN-20SiC composite at different magnifications. The filler materials (shown in black color) of cubic boron nitride and silicon carbide have been fully embedded into the white alumina matrix. The presence of small pores is attributed to the holding time used in the sintering process as well as the brittle nature of the composite which may have led to removal of material during preparation of sample. EDS analysis shows the presence of each element within the composite to confirm the composite composition.

To further confirm the presence of the desired elements, EDS mapping is done for Figure 4.11 with 1000x magnification to highlight the location of elements within the frame. As shown, it is found that the fillers have dispersed well within the alumina matrix which means there is more homogeneity in properties of the material.

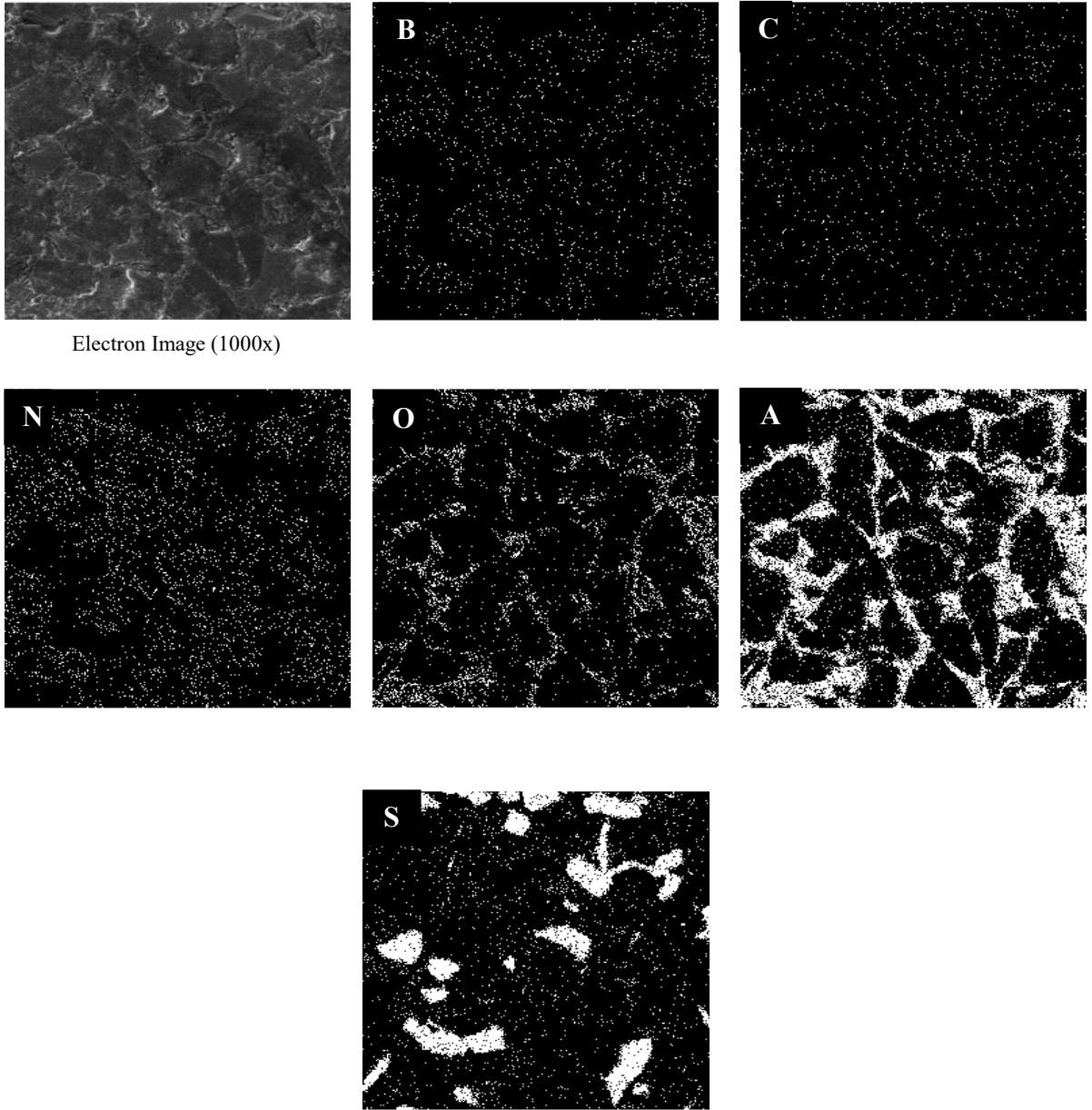
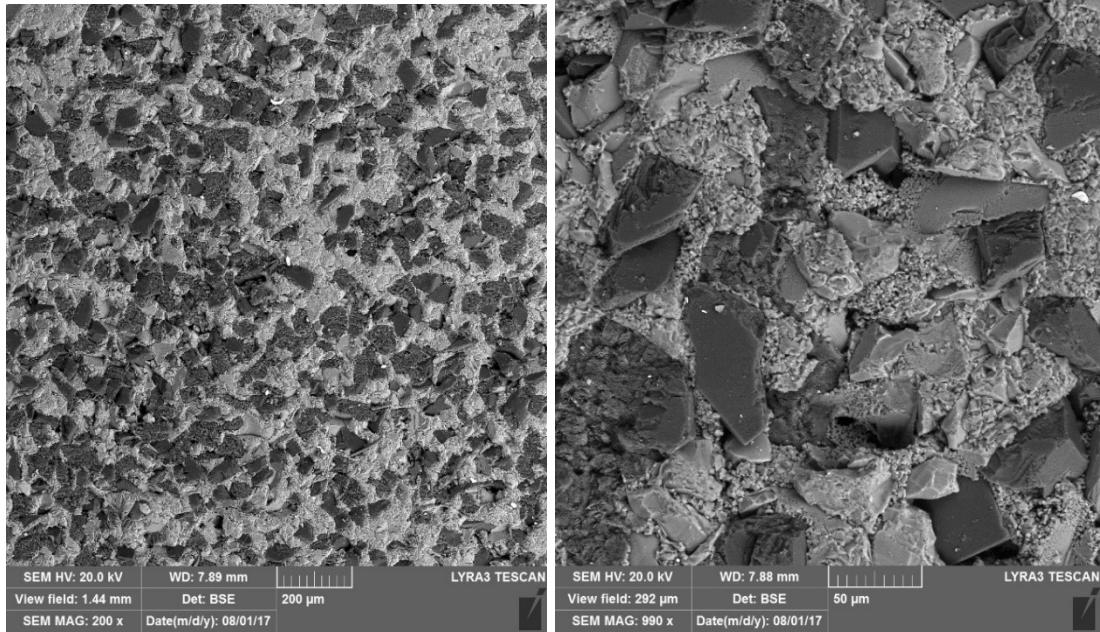


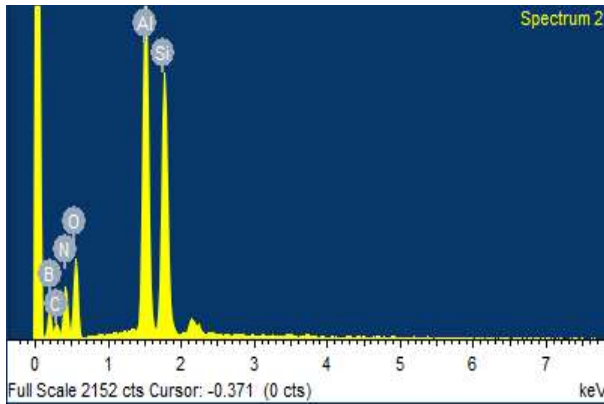
Figure 4.12 - EDS mapping performed at 1000x highlighting the presence and location of each element within the Al_2O_3 -30%SiC-20%cBN composite material.

Furthermore, the SEM results for the remaining samples (Alumina-20%SiC-30%cBN) are shown next.



a)

b)



Element	Weight%	Atomic%
B K	40.08	48.62
C K	10.52	11.49
N K	23.42	21.92
O K	16.28	13.35
Al K	5.32	2.58
Si K	4.38	2.04
Totals	100.00	

c)

Figure 4.13 - a) SEM image of an Al₂O₃-20%SiC-30%cBN at 400x magnification. b) SEM image of an Al₂O₃-20%SiC-30%cBN at 1000x magnification with each constituent specified. c) EDS analysis highlighting the presence of elements within the composite material (performed at 400x).

4.2.2 X-ray Diffraction Analysis

To further characterize the prepared composite, XRD analysis is performed on all prepared samples. Figure 4.14 show the diffractograms obtained for pure alumina and two prepared Al_2O_3 -SiC-cBN hybrid samples.

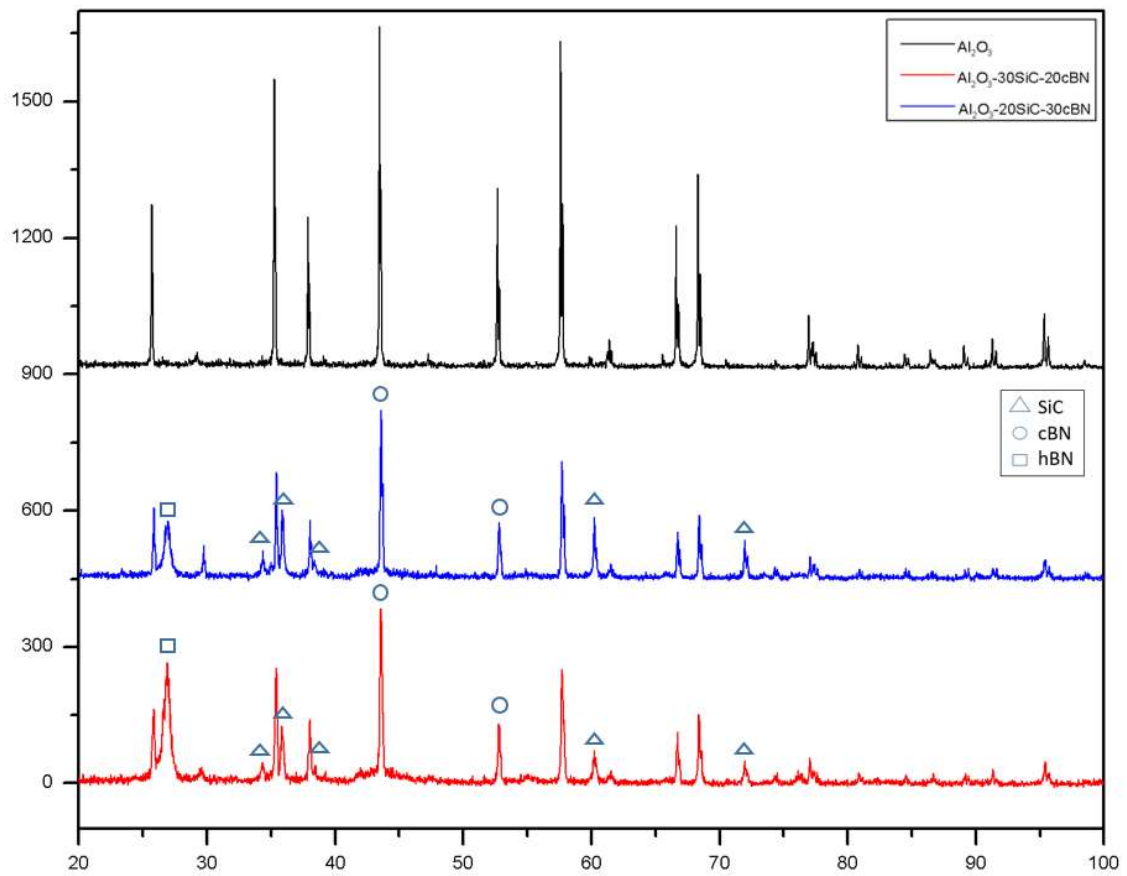


Figure 4.14 - X-ray diffraction analysis/comparison of the three samples a) Pure Al_2O_3 , b) Al_2O_3 -30%SiC-20%cBN, c) Al_2O_3 -20%SiC-30%Cbn (with 42 μm avg. particle size).

The obtained peaks at certain diffraction angles are compared with the values for Al₂O₃, SiC and cBN. As shown in the figure, a peak of hBN is formed as cBN content is increased. This is attributed to the sintering process; due to the presence of large SiC particles present within the mixture there are areas of thermomechanical stresses present within the microstructure at high temperature. These stresses are therefore transforming a small amount of cBN phase to hBN. This phenomenon is also presented in the work of Irshad and co-authors in which they have reported phase transformation due to larger particle size of the base matrix. The occurring phase transformation is taken into consideration and the variation in modelling results is attributed to this factor.

4.2.3 Raman Spectroscopy Analysis

Our findings from XRD analysis showed how a certain amount of cBN has phase transformed to hBN during the sintering process. To validate these results, we have conducted Raman tests to confirm whether this phenomenon is actually taking place or a different reaction between fillers has occurred. The presence of peaks at 800 & 990 cm⁻¹ are those that are attributed to the SiC phase. Broad peak initiating at approximately 1367 cm⁻¹ highlights the presence of cBN that phase within the material. The broad nature of the peak has led to the understanding that only a small amount of phase transformation has occurred. Therefore, it is concluded that the Raman results validate the phenomenon captured within the XRD analysis.

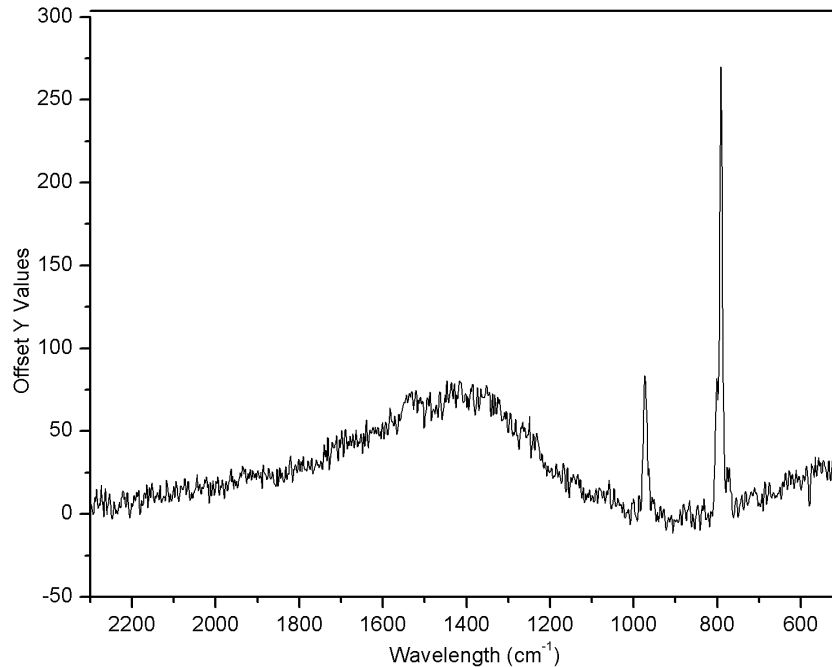


Figure 4.15 - Raman spectroscopy results of manufactured Al₂O₃-30%SiC-20%cBN.

4.2.3 Density & Porosity Determination

Design of a composite material is greatly influenced by its density which depends on the relative proportions of the matrix and inclusions embedded into the system. The effective density has a direct relation with porosity present within the material which can have an effect on the effective properties of the composite. Table shows the theoretical and measured density values of the developed materials. It can be seen that the experimental and theoretical density have a slight variation with each other which is attributed to the slight porosity present within the samples. This porosity present may be due to the sintering parameters that were selected for the SPS process. This porosity % is considered to be within the acceptable range and will not cause great variation between numerical and experimental results.

Table 4.2 - Measured & theoretical density of samples along with associated porosity.

Matrix	Filler Type/Vol%	Measured Density (g/cm³)	Theoretical Density (g/cm³)	Porosity %
Alumina	None	3.879 ± 0.457	3.96	2.05%
	30% SiC-20% cBN	3.194 ± 0.325	3.318	3.73%
	20% SiC-30% cBN	3.104 ± 0.723	3.207	3.21%

4.2.4 Micro Hardness, Modulus of Elasticity and Fracture Toughness

Hardness is a key property when going through the process of characterizing a composite material. This indicates the ability of a material to withstand local deformation when a fixed load is applied. In this work, the microhardness of the samples has been measured at 300g and 500g loadings. Testing has been conducted multiple times at different areas on the face of the prepared composite samples and microhardness along with standard deviation are reported. Results are tabulated below. The results highlight an improvement in hardness because of the introduction of the inclusions into the base matrix system.

Table 4.3 - Hardness test results and the associated elastic modulus, fracture toughness values.

Matrix	Filler Type/%	Vickers Micro Hardness (GPa)		Elastic Modulus (GPa)	Fracture Toughness K_{IC} (MPa.m ^{1/2})
		At 300g		Average	Average
		Average	Standard Deviation		
Alumina	None	19.12	1.502	146.987	3.96
	30% SiC-20% cBN	21.44	1.274	189.376	4.42
	20% SiC-30% cBN	22.97	2.563	174.11	4.21

An improvement in elastic modulus and fracture toughness is observed in the alumina-30%SiC-20%cBN composite as is expected based on the numerical simulations performed. However, there is a decreased elastic modulus and fracture toughness noticed in the alumina-20%SiC-30%cBN. This is attributed to the increased content of cBN reinforced into the composite. It is observed that after a certain limit of cBN inclusion percentage there is a drop noticed in the structural properties of the composite material. Variations between the numerical results and experimental data are attributed to the porosity present within the developed composites. The sintering parameters that the numerical models are not able to incorporate. Also, the numerical model assumes the shape of inclusions to be

perfectly spherical along with perfect distribution of the inclusions embedded into the matrix which may be a reason for the small variation in results. The comparative ratios between the effective composite and the matrix material are shown in the figures below:

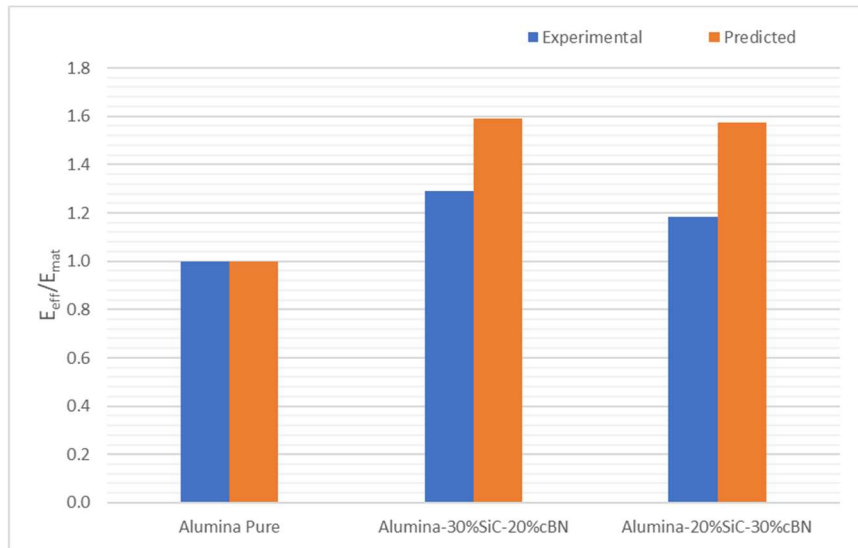


Figure 4.16 - E_{eff}/E_{mat} ratios between effective and matrix elastic modulus values (Experimental & Numerical).

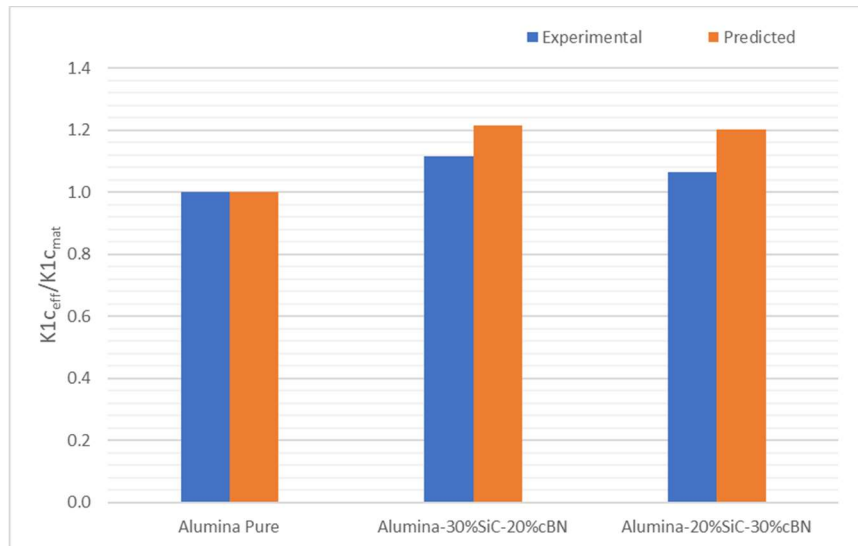


Figure 4.17 - $K_{1C_{eff}}/K_{1C_{mat}}$ ratios between effective and matrix fracture toughness values (Experimental & Numerical).

4.3 Thermal Characterization

4.3.1 Effective Thermal Conductivity

The effective thermal conductivity of the developed composites has been measured. The sintered pure alumina was measured and the numerical simulation results were recalibrated based on the sample reading.

The CTI thermal conductivity analyzer has been used to measure the thermal conductivity values of the developed composite materials and pure alumina. The table below presents the thermal conductivity results; as expected the enhanced inclusions have provided a considerable increase to the effective thermal conductivity of the composites. It is observed that increasing SiC content within the matrix provides a greater improvement in thermal conductivity in comparison to increasing the cBN content.

Table 4.4 - Thermal conductivity values of samples determined experimentally and computationally.

<i>Sample #</i>	<i>%Al₂O₃</i>	<i>%SiC</i>	<i>%cBN</i>	<i>Experimental K (W/m-K)</i>	<i>Standard Deviation %</i>	<i>Computational K (W/m-K)</i>
1	100	0	0	25.68	0.71	25.68
2	50	30	20	36.86	1.08	40.95
3	50	20	30	32.79	1.71	37.45

Variations between the numerical and experimental values can be attributed to certain assumptions and factors that are involved in the design process. For example, the numerical models assume inclusions to be perfectly spherical shapes while that is not the case in a

real-life scenario. It also assumes equivalent particle sizes to be perfectly distributed within the alumina matrix while in reality, powders are supplied by average particle size. Furthermore, the thermal interfacial resistance between the matrix and the inclusions has been acquired from literature. The thermal interfacial resistance depends on the characteristics of the interface and can fluctuate for the same material due to change in various parameters. All of these factors may be resulting in the variation in results however these variations are considered to be in an acceptable range.

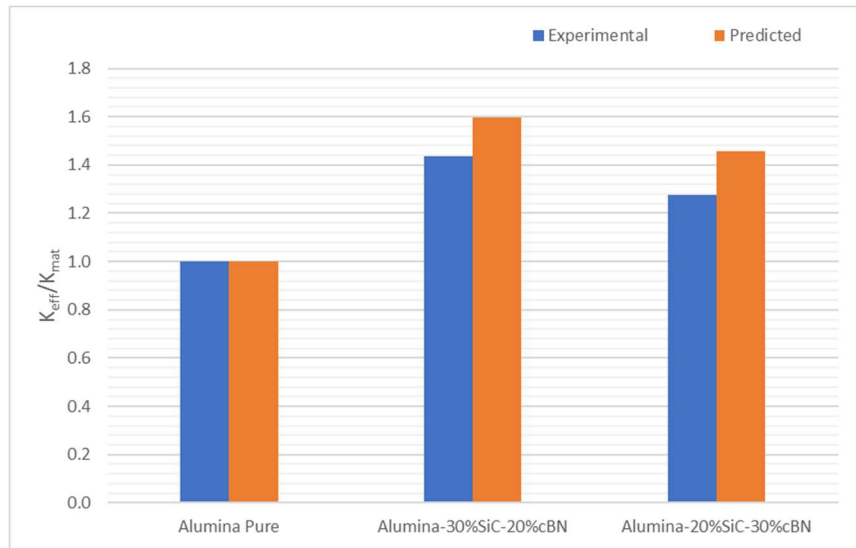


Figure 4.18 - K_{eff}/K_{mat} ratio of effective and matrix thermal conductivity of samples (Experimental & Numerical).

4.3.2 Coefficient of Thermal Expansion (CTE)

The CTE is a key property when considering the design of cutting tool inserts. An enhanced CTE can greatly improve the thermal shock resistance of a material and therefore one of the objectives of this work was to decrease the CTE of the designed composite to reduce expansion of the material when exposed to high temperatures. The Mettler Toledo Thermal

Mechanical Analyzer has been used to evaluate the effective coefficient of thermal expansion values of the developed samples i.e. sintered composites and pure alumina. Table presents the results of the conducted CTE tests of all samples. It can be seen that the CTE values of the inclusions has reduced the effective CTE of the composites.

Table 4.5 - Effective CTE values of samples determined experimentally and computationally.

<i>Matrix</i>	<i>Filler Type/%</i>	<i>Effective CTE ($10^{-6} /K$)</i>	
		<i>Experimental</i>	<i>Computational</i>
Alumina	None	7.06	7.06
	30% SiC-20% cBN	5.41	6.19
	20% SiC-30% cBN	5.21	6.10

The figure below shows the improvement in CTE in both experimental and predicted cases in comparison to the base matrix alumina.

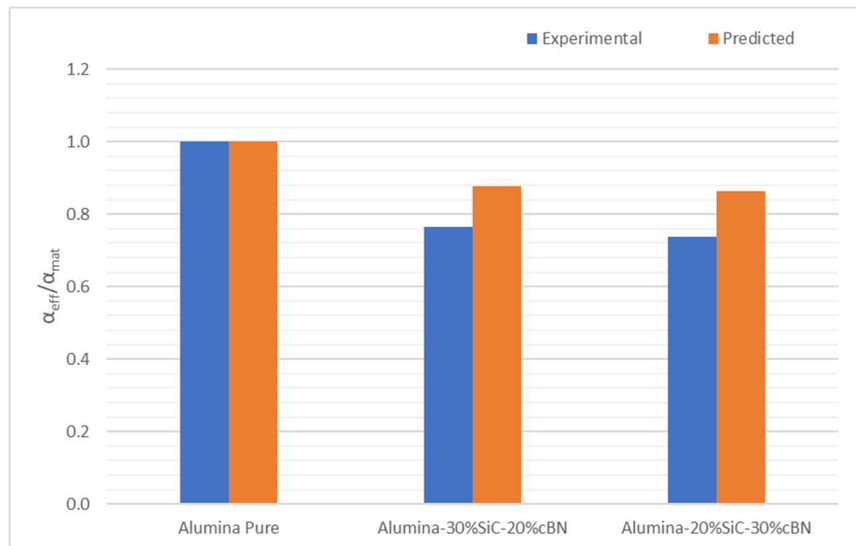


Figure 4.19 - $\alpha_{eff}/\alpha_{mat}$ ratio of effective and matrix CTE of samples (Experimental & Numerical).

4.4 Summary of Results

The overall compiled results of properties determination are presented in the table below:

Table 4.6 - Comparison of Computational Results and Experimental Results of alumina-SiC-cBN hybrid composite design with respect to the selected alumina matrix.

	<i>Pure Alumina</i>	<i>Alumina-30%SiC-20%cBN</i>		<i>Alumina-20%SiC-30%cBN</i>	
	<i>(Matrix)</i>	<i>Predicted</i>	<i>Experimental</i>	<i>Predicted</i>	<i>Experimental</i>
Effective Thermal Conductivity (K_{eff}) (W/m-K)	25.7	40.95	36.86	37.45	32.79
K_{eff}/K_{mat}	1	1.59	1.43	1.46	1.28
Effective CTE (α_{eff})($10^{-6}/K$)	7.06	5.83	5.41	6.18	5.21
$\alpha_{eff}/\alpha_{mat}$	1	0.83	0.77	0.88	0.74
Effective Elastic Modulus (E_{eff})(MPa)	147	233.77	189.38	231.64	174.11
E_{eff}/E_{mat}	1	1.59	1.29	1.58	1.18
Effective K_{IC} (Mpa.m ^{1/2})	3.96	4.81	4.42	4.75	4.41
K_{ICeff}/K_{ICmat}	1	1.22	1.12	1.20	1.06

4.5 Summary of Chapter

In this chapter, the following has been discussed:

- Types of matrix and inclusion materials used in the development of material.
- Details of composite sample development techniques, characterization methods and experimental property measurements of material (mechanical and thermal).
- Results of material characterization, mechanical and thermal property measurement tests performed on the developed composite samples.
- Comparative analysis as a means of validation of the property estimation results obtained from the numerical modelling done in the material design phase.

The following chapter will present the description of the coupled thermal-structural performance evaluation of the designed composite material as a cutting tool insert in a simulated cutting process through the aid of finite element modelling. The results obtained from the analysis for the composite material will be compared with various benchmark materials.

CHAPTER 5

PERFORMANCE EVALUATION OF THE PROPOSED

CUTTING TOOL INSERT

5.1 Introduction

This chapter discusses the performance evaluation of the proposed ceramic based composite material when considered for the application of cutting tool inserts. The newly proposed alumina-based composite material is analyzed and compared with its fellow cutting tool insert competitors, such as standalone alumina and ZTA (zirconia toughened alumina) inserts. The new composite material possesses enhanced thermal and structural properties in accordance to cutting tool insert design while also possessing the economic and environmental benefits of alumina.

The performance evaluation of the composite cutting tool inserts when considered for the turning of a high-strength steel will be done through a coupled thermal-structural analysis. This study will be done with the aid of FEM (finite element modelling) as the problem was idealized as a 3-dimensional steady-state thermal-structural finite element model. A steady-state thermal stress analysis will allow the simulation of the heat flux being generated at the cutting edge due to frictional forces occurring during machining and the flow of heat within the insert. This flow of heat into the system results in increased temperature and greater stress gradients throughout the body. Uneven temperatures within

the cutting edge and the rest of the body will cause sticking of chip to the face of the insert and result in poorer chip quality [90,91]. In addition, a high CTE can result in greater deformation of the insert which can lead in thermal shock failure due to the fluctuation of temperature.

5.2 Mathematical Models

The mathematical models used in the fully coupled thermal-structural stress performance analysis is presented in this chapter.

For the thermal part of the analysis, the basic energy will be utilized to determine the temperature field as shown in Eq. (5.1):

$$C_p u \cdot \nabla T = \nabla(k \nabla T) + Q \quad 5.1$$

Where C_p is the heat capacity, k is the thermal conductivity of the constituents present within the system, ∇T and Q are the temperature difference and the heat source within the system. Thermal insulation is governed by equation (5.2) which will not allow the flow of heat in any given direction.

$$-n(-k \nabla T) = 0 \quad 5.2$$

Here, n is a unit vector which is normal to the boundary. To simulate the process of dry cutting, the body i.e. the cutting insert will be defined with a convective heat transfer of air to simulate a portion the heat generated to escape from the body. The general heat flux into and out of the body is defined by the following equation:

$$-n(-k \nabla T) = h_c (T_c - T) \quad 5.3$$

Where h_c is the convective heat transfer coefficient and T_c is the temperature of the surrounding environment respectively. T is defined as the initial temperature at any given point on the surface of the boundary.

Regarding the steady-state structural analysis, the stress-strain constitutive behavior is defined by:

$$-\nabla u * \sigma = F * v \quad 5.4$$

$$\sigma_y - \sigma_0 = c: (\varepsilon - \varepsilon_0 - \varepsilon_{Th} - \varepsilon_p) \quad 5.5$$

In these equations, σ is the Cauchy stress, $F * v$ is the body load, ε is the total strain value, ε_{Th} is the strain generated due to the thermal loading and ε_p is the effective plastic strain generated. σ_y is the yield stress of the material, ∇u is the displacement gradient and c is the elastic stiffness matrix. The mathematical relationships for the strains are given by:

$$\varepsilon = \frac{1}{2} [(\nabla u)^T + \nabla u] \quad 5.6$$

$$\varepsilon_{Th} = \alpha(T - T_{ref}) \quad 5.7$$

$$\varepsilon_p = \lambda \frac{dQ}{d\sigma} \quad 5.8$$

Considering the time-dependent structural analysis, the stress-strain constitutive behavior will become the following:

$$\rho \frac{d^2 u}{dt^2} - \nabla \sigma = F v \quad 5.9$$

$$\sigma = J^{-1} F S F^T \quad 5.10$$

Where S is the second Piola-Kirchoff stress and the remaining variables are defined as,

$$F = (1 + \nabla u) \quad 5.11$$

$$J = \det(F) \quad 5.12$$

$$S - S_0 = c: (\varepsilon - \varepsilon_0 - \varepsilon_{Th} - \varepsilon_p) \quad 5.13$$

$$\varepsilon = \frac{1}{2} [(\nabla u)^T + \nabla u + \nabla u (\nabla u)^T] \quad 5.14$$

To remove the possibility of rigid-body motion, the area where the insert is fitted onto the tool arm is considered to be constrained in all directions. Therefore, a roller support boundary condition is applied on the boundary in focus as shown in the equation below.

$$n \cdot u = 0 \quad 5.15$$

The equations are summarized by the following,

$$[f_{Thermal}] = [K_1][t] \quad 5.16$$

$$[f] = [K_2][d] - [f_{TF}] \quad 5.17$$

Where f_{Therm} is defined as the thermal load which may be applied as a heat source, heat flux or conduction or convection of heat. K_1 is function matrix of the effective thermal conductivity of the material and geometry dimensions. t is the temperature distribution matrix which contains the unknown variables. f_{TF} is defined as the thermal force and is a function of the temperature distribution t , CTE and the effective elastic modulus of the composite. f is the applied nodal forces which will be varied based on the cutting tool machining experimental data extracted from literature. K_2 is a matrix defined as a function

of the elastic modulus of the composite and geometry dimensions; d is the nodal displacement matrix which is also an unknown.

5.3 Coupled Thermal-Structural Analysis

The coupled thermal and structural analysis of the composite cutting tool insert has been evaluated using FEM. Excellent thermal performance of a cutting insert will lead to an improvement of the tool life of the insert due to better resistance to thermal shock which can be associated to better flow of temperature through the insert. In addition, the stresses generated due to the combined effect of the heat flux and mechanical loading on the cutting edge will be analyzed. The simulated cutting process will provide the critical stress zone as a function of time and the total von Mises stresses can help identify if the material is suitable for the designated cutting process. It is important to avoid a large difference in temperature to avoid the sticking of chip formation onto the insert. As the chip forms and moves away from the edge, it is possible for it to stick onto the cooler face therefore a greater difference in temperature will increase the likelihood of chip sticking to occur. Greater temperature gradients will also lead to greater probability of thermal shock occurrence. Therefore, it is vital to understand the temperature and stress distribution within the cutting tool insert and compare the composite performance with the benchmark material.

5.4 Finite Element Modelling

5.4.1 Geometry Model

The selected mathematical models have been selected for the coupled thermal-structural stress analysis and have been implemented through the use of COMSOL Multiphysics. The 3D geometrical model (generated using SOLIDWORKS) for the cutting tool insert, as shown in the figure below, is a standard sized triangular shaped insert with three cutting edges and fitted onto the tool holder in the middle [92].

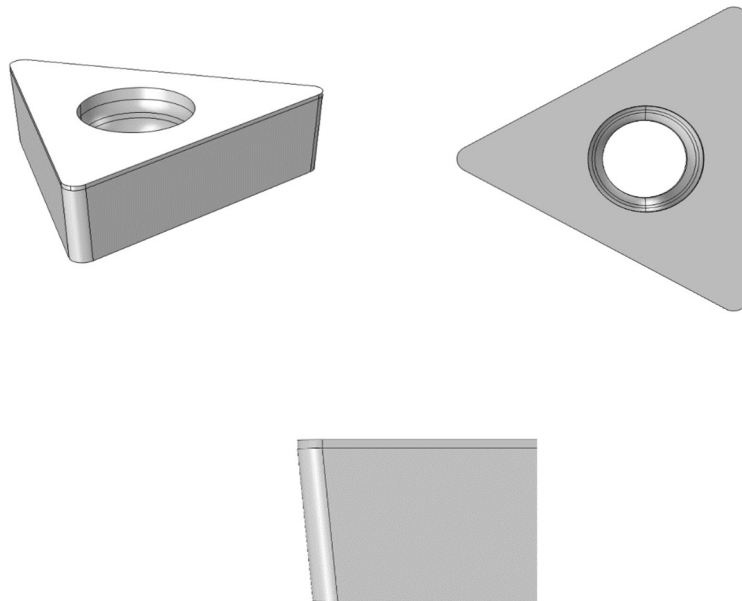


Figure 5.1 - Geometry model of the cutting tool insert developed using SOLIDWORKS.

The triangular insert is dimensioned 20 mm with a 60-degree angle on each edge and a height of 5 mm. The fitting hole to attach the insert to the tool holder is a varying diameter design as is standard for an industry-level cutting tool insert with a diameter of 6.35 mm

for a depth of 0.24 mm on top level and a diameter 4.76 mm for the remaining depth. The cutting edge has a length of 0.240 mm with an angle on the flank face of 3 degrees.

5.4.2 Material Model

The material properties used for the ceramic based composite material model have obtained for the experimental material characterization and testing described in the previous chapter. The selected ceramic based composite consists of an alumina matrix with 30% silicon carbide and 20% cubic boron nitride inclusions. The benchmark material which was selected as pure alumina was also developed in this work and the determined properties have been used for comparative analysis. In addition, ZTA (zirconia toughened alumina) material properties will also be considered for comparison when analyzing the designed composite material. ZTA material properties have been determined from previously published literature and insert manufacturer catalogues [93]. These properties are summarized in table 5.1 located below.

5.4.3 Boundary Conditions

Initially, the cutting tool insert will be constrained in all directions at the area where the insert is attached to the tool holder i.e. the hole. With the cutting tool insert in place, a varying heat flux (as shown in figure) as a function of time that has been extracted from literature is applied to the cutting edge surface for a period of 120 seconds with the following conditions: Cutting speed $V_c = 142$ m/min (900 rpm), feed rate $f = 0.14$ mm/rot, and cutting depth $a_p = 1.0$ mm [94].

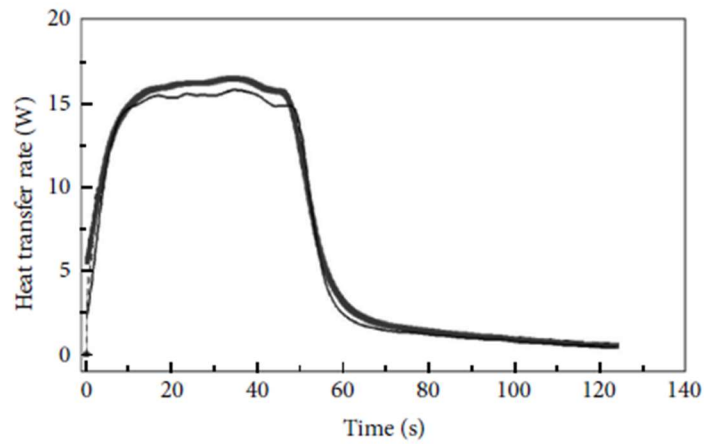


Figure 5.2 - Heat transfer loading applied onto cutting edge as a function of time. [94]

To simulate real-life dry cutting heat transfer cutting conditions, free and natural convective heat transfer has been applied to the entire body of the model with a heat transfer coefficient of air, which is $10 \text{ W/m}^2\text{-K}$, to simulate the heat moving from the body of the insert into the surrounding air at room temperature (298 K).

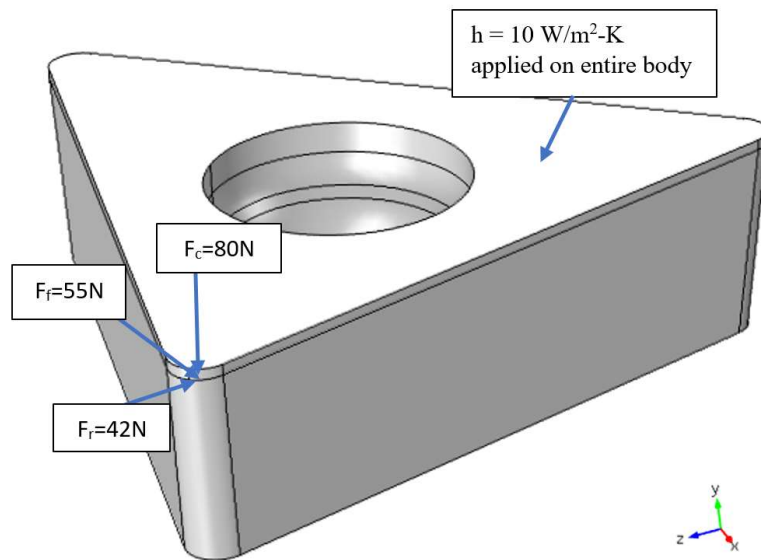


Figure 5.3 - Description of the additional boundary conditions applied onto the insert.

In addition to the thermal loadings, a cutting tool insert is also subjected to mechanical loadings during a cutting process. Therefore, forces developed on the cutting edge during the turning process of a high-strength material have been obtained from experimental literature data for a competitor insert [95]. These forces are divided into its three components in its respective direction i.e. cutting force, radial force and frictional force.

Table 5.1 - Material properties used to define the material model.

<i>Material</i>	<i>Elastic Modulus (GPa)</i>	<i>Poisson's Ratio</i>	<i>Tensile Strength (MPa)</i>	<i>Thermal Conductivity (W/m²-K)</i>	<i>CTE (1/K)</i>	<i>Fracture Toughness K_{IC} (MPa-m^{1/2})</i>
<i>Alumina</i>	147	0.22	665	25	7.06	4.0
<i>ZTA</i>	350	0.23	-	20	8.3	5
<i>Proposed Composite Material</i>	189.4	0.21	-	36.86	5.41	4.42

5.4.5 Meshing

Meshing has been performed using tetrahedral shaped elements on the finite element model with 6500 elements initially. After the mesh convergence test the number of elements has been increased to 25996 elements. The mesh has been resized to finer elements at the critical zone which the cutting edge area and also where the zones where greater stresses

were generated over time. Mesh convergence tests have been performed using the von Mises stress distribution and the temperature profile of the of the finite element model. The mesh convergence was finalized when both the von Mises stress distribution and temperature profile became constant with respect to the size of mesh. The study has been performed at the minimum amount of elements required to keep the results constant in order to optimize the computational time of the coupled thermal structural analysis.

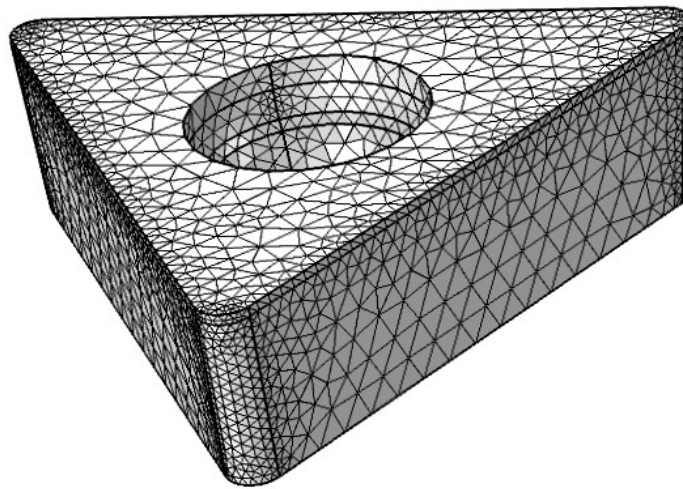


Figure 5.4 - Meshing of the cutting tool insert geometry.

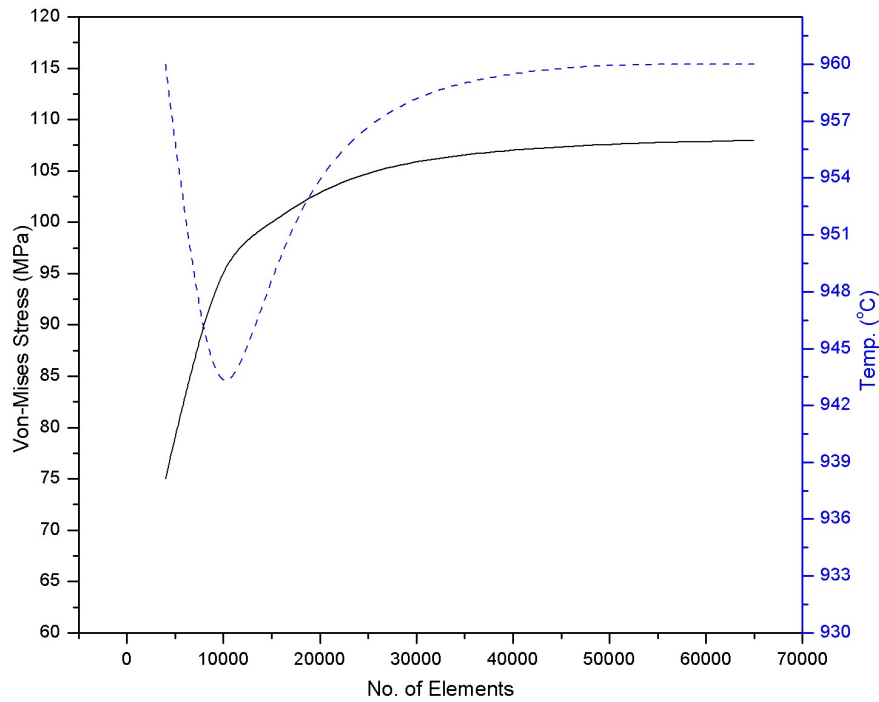


Figure 5.5 - Mesh convergence analysis for von-Mises stress and temperature.

5.5 Results and Discussion

Results have been obtained when the heat flux has been applied onto the cutting edge and the stresses distribution and temperature profile are observed as a function of time for each case. The duration of the dry cutting process was taken as 120 seconds with the results being recorded at every 0.1 second interval for better analysis. In addition, the surrounding temperature has been maintained at 25°C with the application of a convective heat transfer coefficient to allow heat to escape into the surrounding from the body therefore simulating dry cutting conditions. Three cases will be presented with each being comparatively analyzed in terms of temperature profile and stresses distribution.

5.5.1 Alumina Insert

The first case is that of standard standalone alumina; which is considered for use as a cutting tool insert due its good structural properties and chemical inertness. Results have been obtained as a function of time as the heat flux and the mechanical pressure loading is applied.

The heat flux begins to heat up the cutting edge and temperature increases rapidly and begins spreading around the edge. The heat entering through the cutting edge induces thermal stresses onto the insert. As shown in figure 5.6 the temperature starts increasing in the cutting edge as time increases. This is attributed to the frictional forces acting on the edge due to contact between workpiece and cutting edge. These frictional forces lead to the increase in temperature in cutting edge which spreads away from the edge as time goes on. The temperature is maximum at approximately 40 seconds; this is expected due to the heat flux boundary condition.

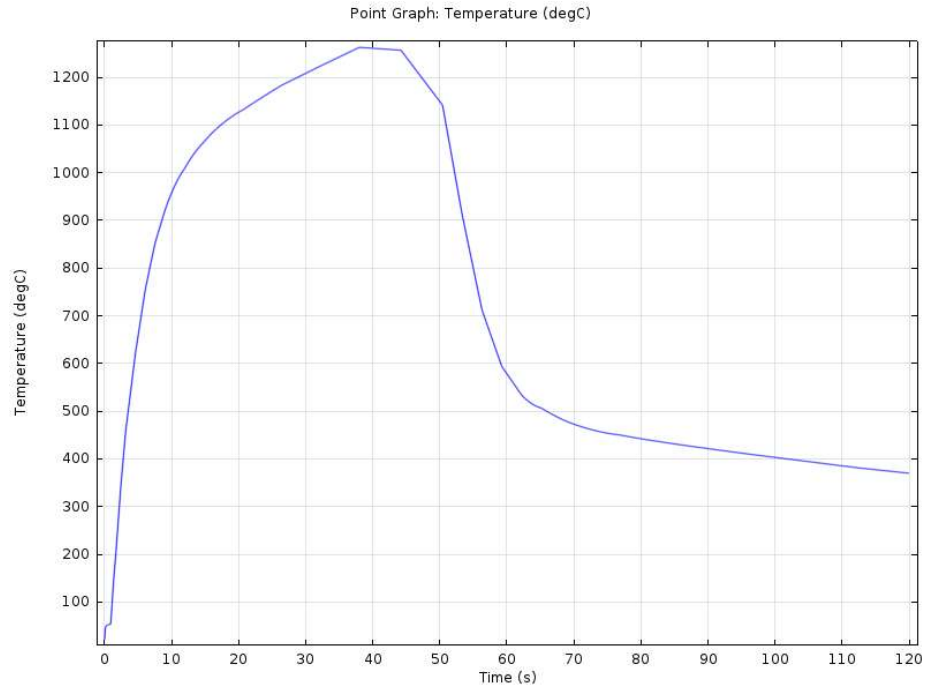


Figure 5.6 - Temperature profile of the cutting edge during the cutting process.

Figure 5.7 shows the temperature distribution of the cutting tool insert as a function of the distance away from cutting edge moving to the bolt fitting area at time of maximum temperature. It is observed that there is a temperature gradient between the cutting edge and the rest of the insert body. This gradient can cause mismatch in thermal expansion within the body which can result in failure from thermal shock.

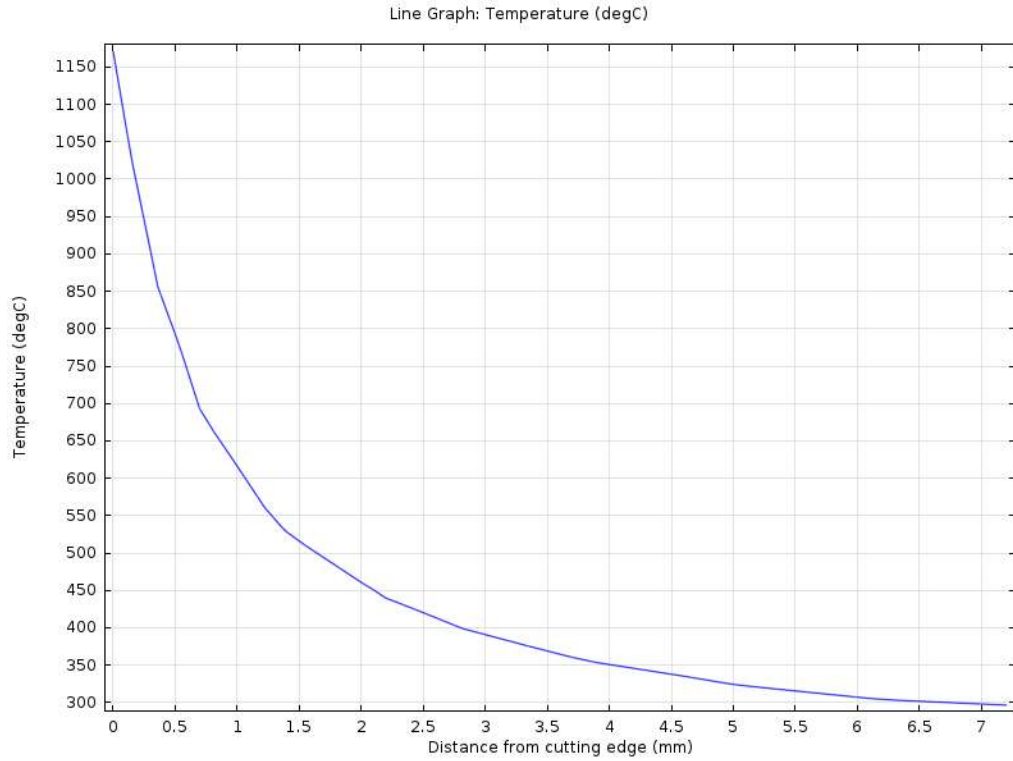


Figure 5.7 - Temperature profile as a function of distance moving away from the cutting edge towards the center.

In addition to temperature profile, it is important to monitor the von-Mises stresses generated within the insert during the cutting process. The von-Mises stress distribution can provide a clear indication of where the insert will be susceptible to failure.

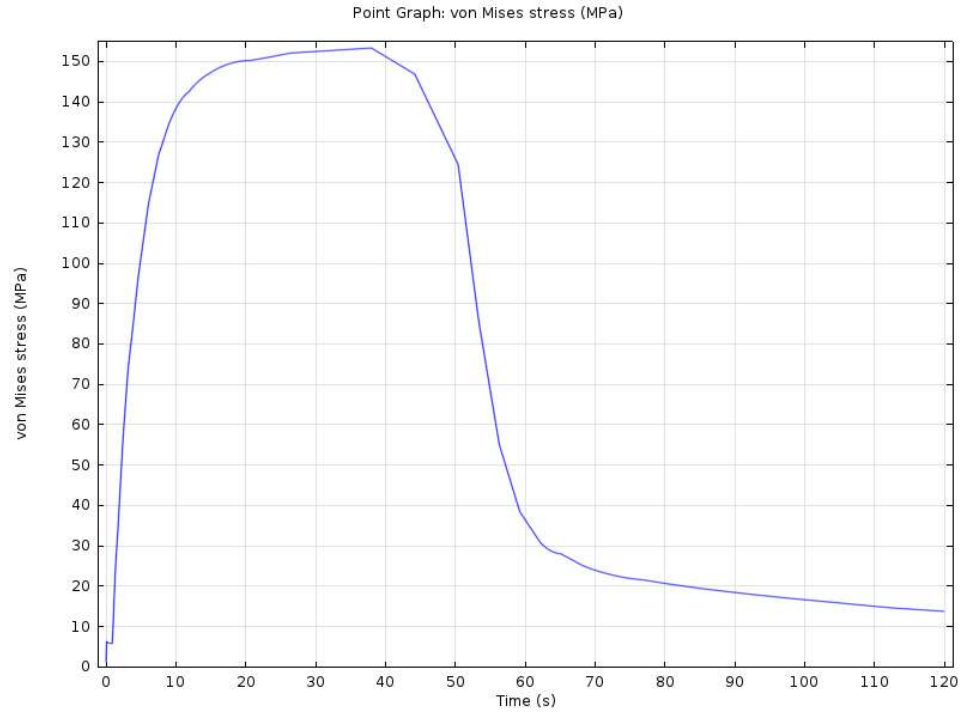


Figure 5.8 - Von-Mises stress distribution at the cutting edge of the tool insert during the cutting process.

The stresses being generated during the cutting process are due to a combination of both the thermal and mechanical loading. The region susceptible to failure varies over time as after approximately 60 seconds the critical region becomes the fitting area which is constrained in all directions. The CTE has a great effect on the stress distribution because a higher CTE will result in greater deformation of the body which will generate greater stresses.

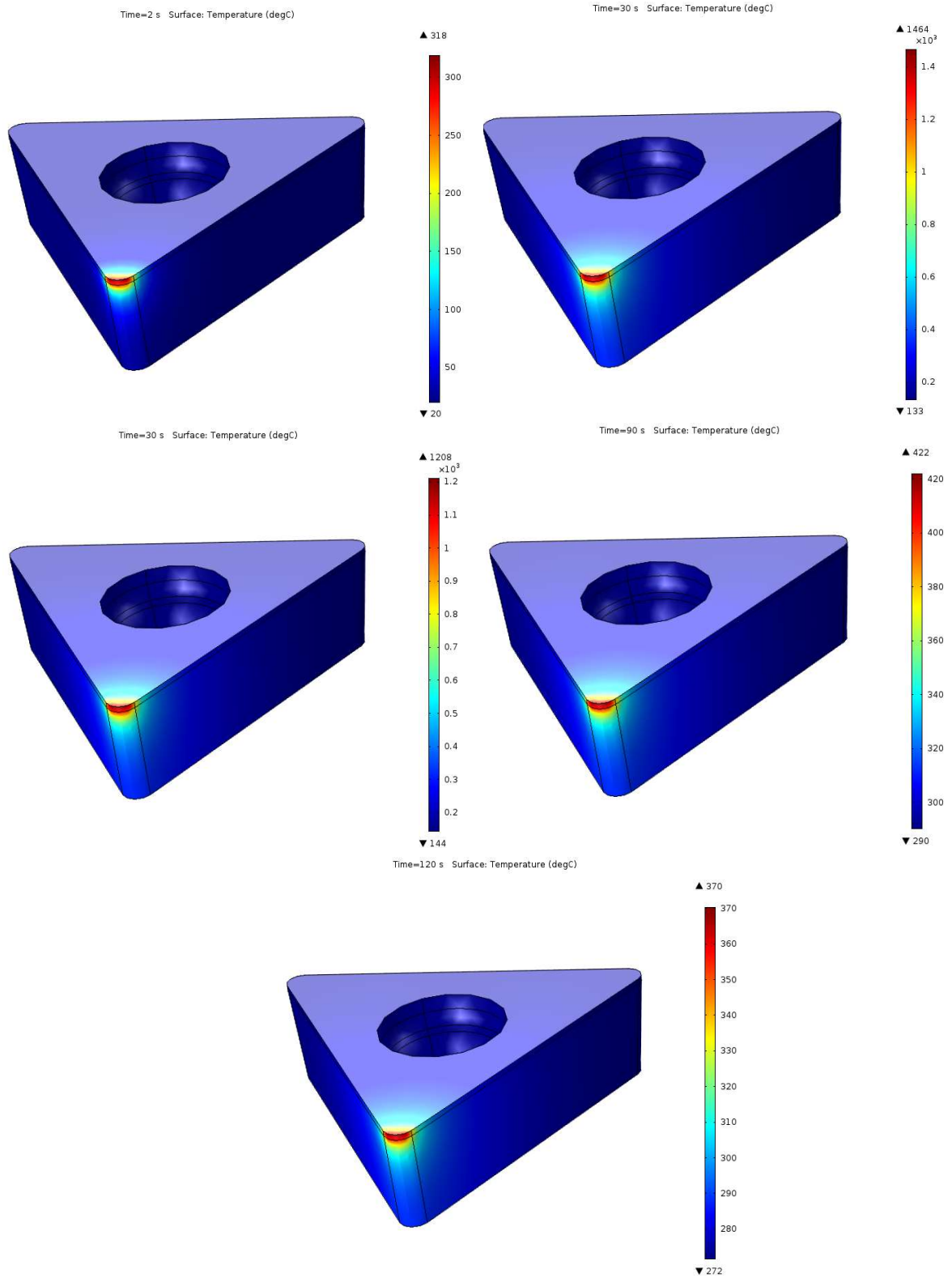


Figure 5.9 - Temperature profile of the alumina insert at different times during simulated cutting process

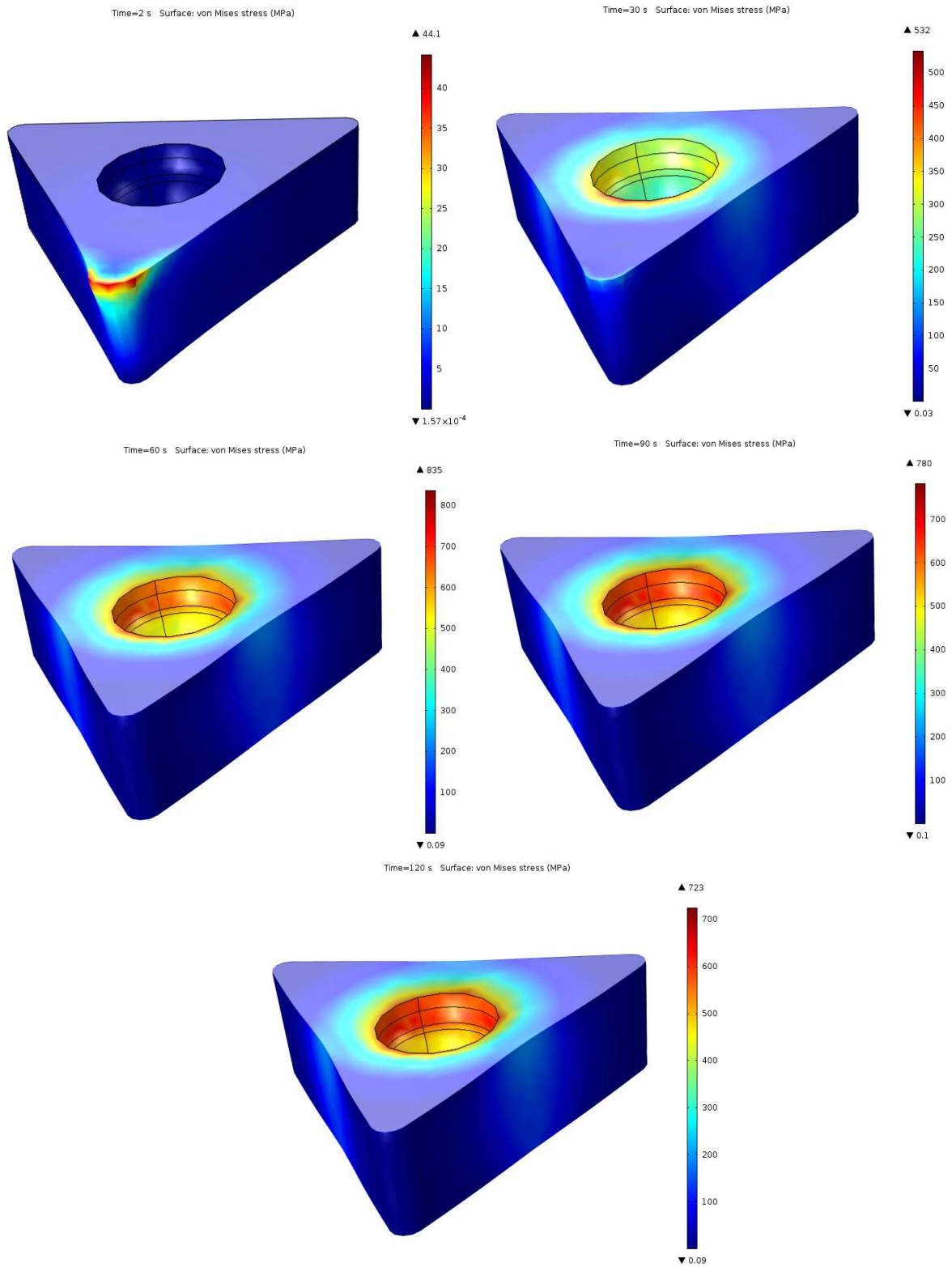


Figure 5.11 - Von-Mises stress distribution of the alumina insert at different times during the simulated cutting process.

5.5.2 ZTA Insert

The second case analyzes the performance of zirconia-toughened alumina (ZTA) insert under similar loadings. ZTA inserts are considered for as cutting tools due to their enhanced fracture toughness which is attributed to the phase transformation of zirconia at high temperature which restricts elongation of crack formations. Results are presented as a function of time during the application of heat flux and mechanical pressure.

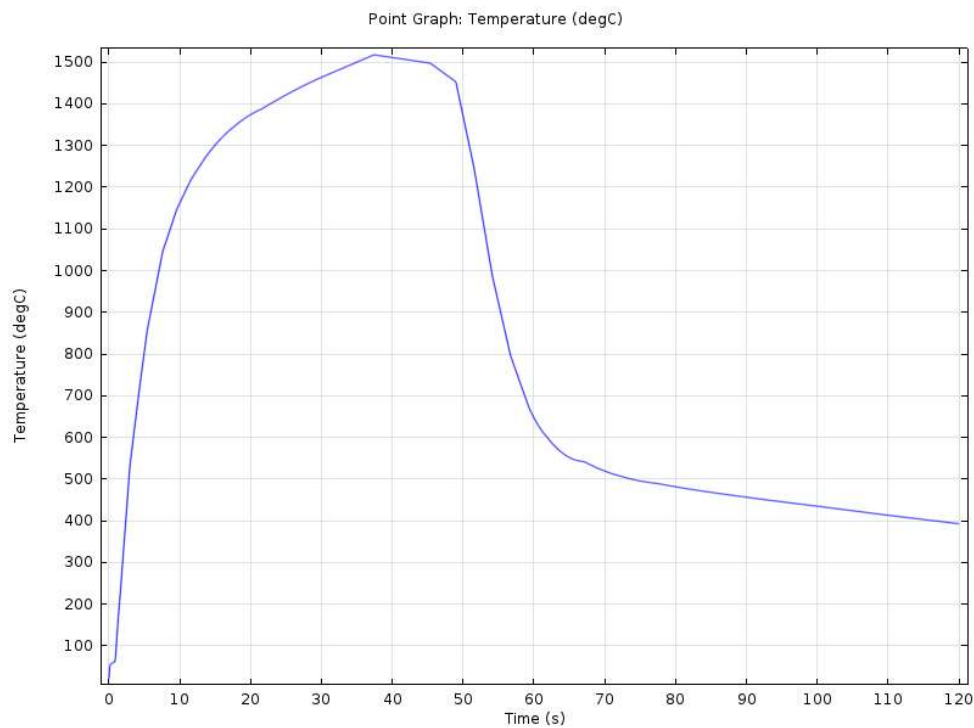


Figure 5.11 - Temperature profile of the cutting edge of ZTA insert during cutting process.

Figure 5.11 above shows the temperature profile of the cutting edge as a function of time. The temperature is at its maximum when heat flux is highest. It is observed that the temperature of ZTA insert is higher compared to the alumina insert at the cutting edge. The temperature gradient observed as temperature is recorded away from the cutting edge is

found to be larger as compared to alumina. This is attributed to the poor thermal conductivity of ZTA because of poor thermal properties of the reinforced zirconia. This temperature gradient can lead to sticking of chip formation on tool face which can lead to permanent damage on the insert.

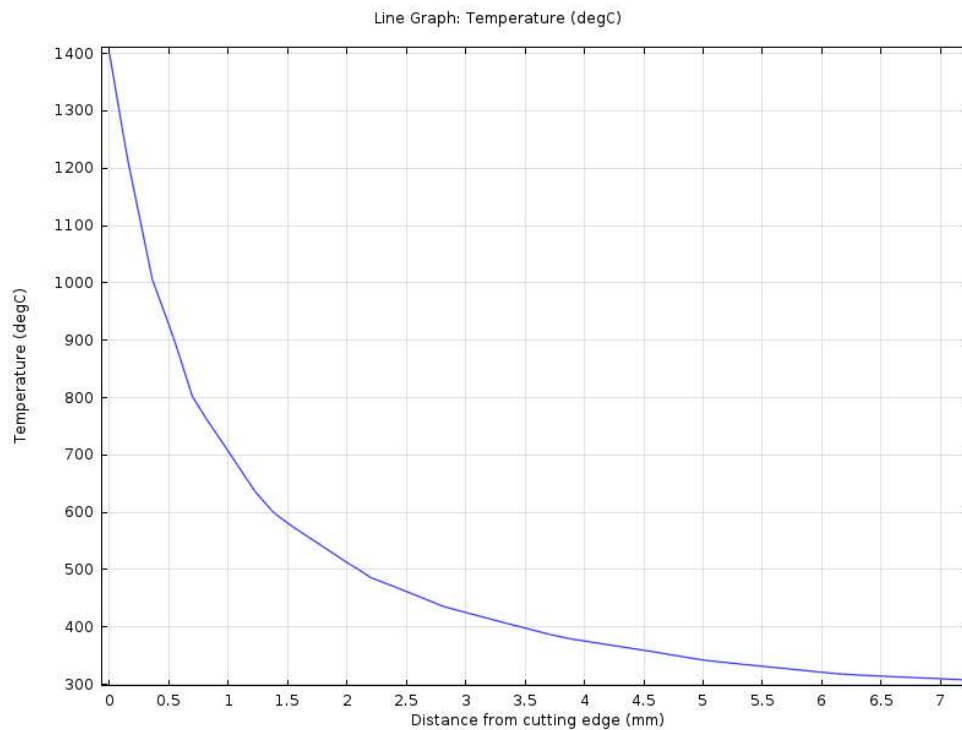


Figure 5.12 - Temperature profile as a function of distance moving from cutting edge towards the center of the ZTA insert.

Analysis of the von-Mises stress distribution at the cutting edge as a function of time show that there are greater stresses being generated as compared to the alumina insert. This is attributed to the relatively low elastic modulus of the reinforced zirconia present in the ZTA insert which is causing greater stresses being generated within the insert.

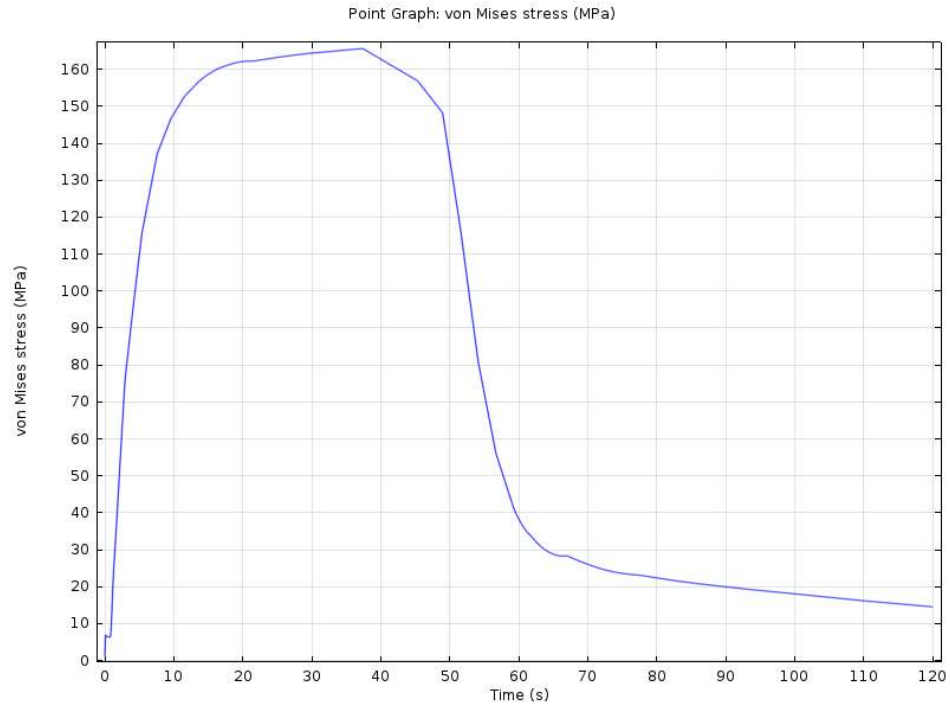


Figure 5.13 - Von-Mises stress distribution at the cutting edge of ZTA insert as a function of time.

The von-Mises stress distribution of the insert shows that critical stresses shift from edge to the fitting area over time which is due to the constraints applied. The critical stresses are relatively higher as compared to the alumina insert which is assumed to be due to the poor effective CTE of the ZTA insert which is allowing greater deformation due to the thermal loading and susceptible to thermal shock loading.

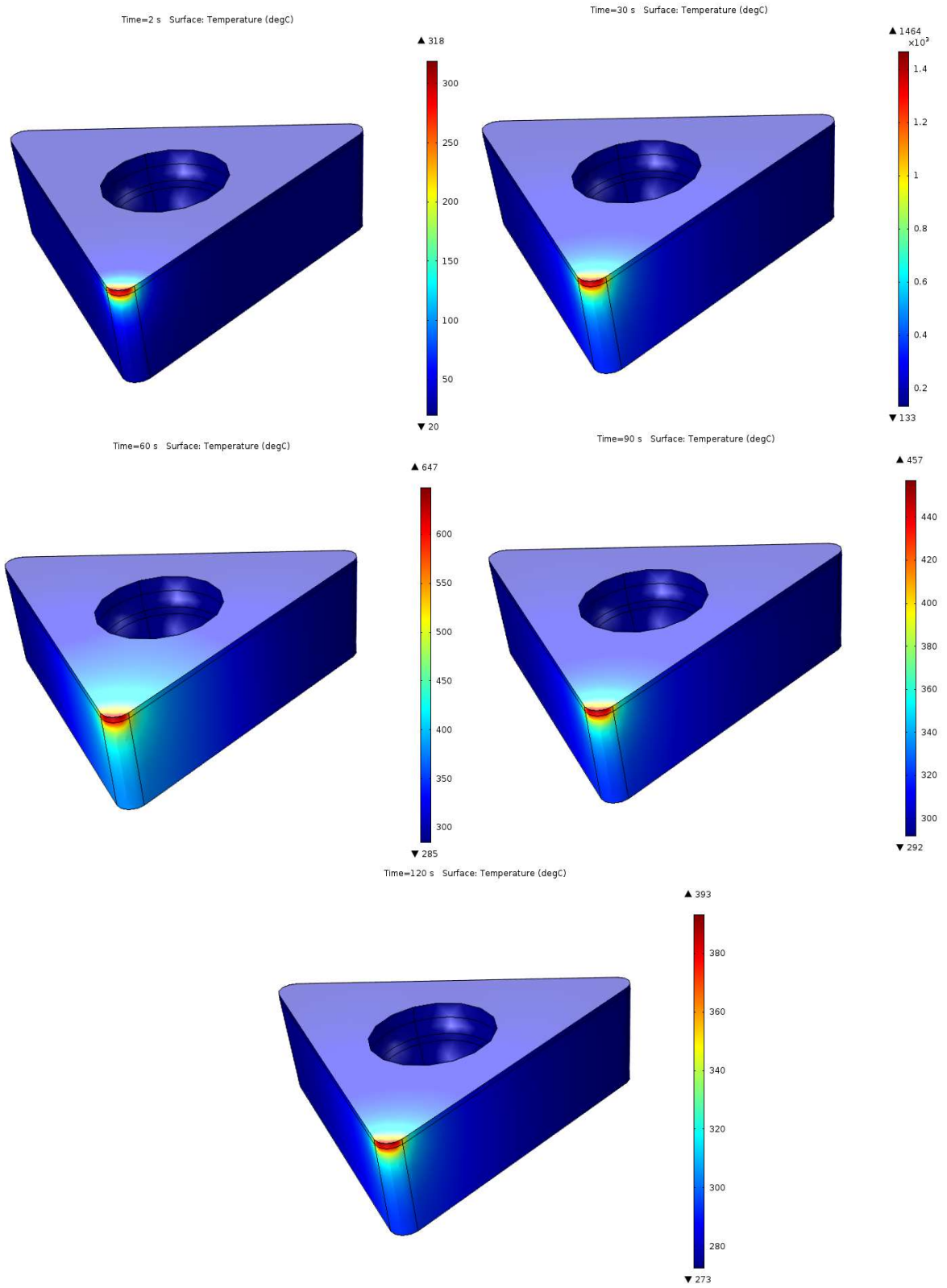


Figure 5.14 - Temperature profile of ZTA insert at different times during simulated cutting process.

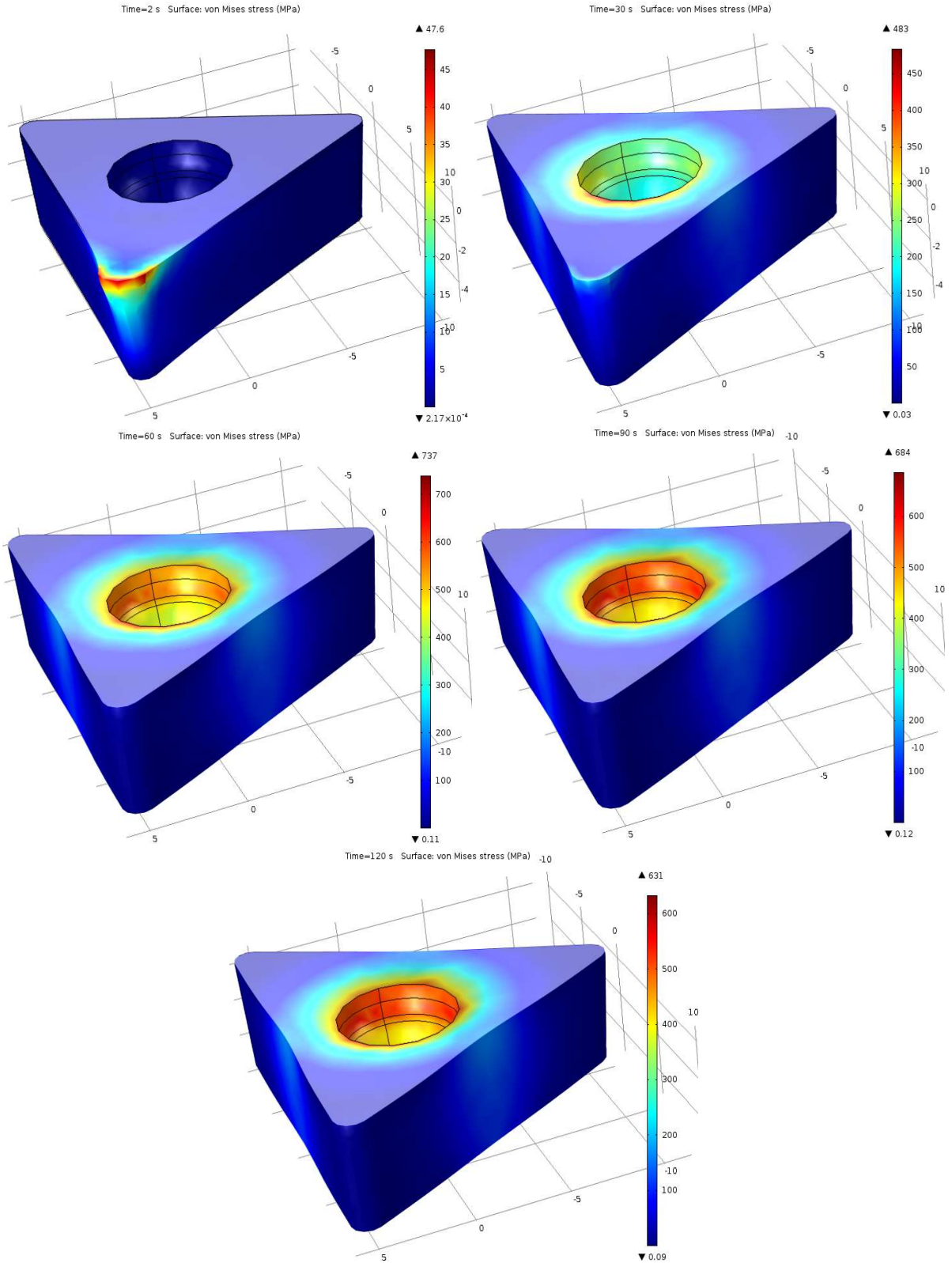


Figure 5.15 - Von-Mises stress distribution of ZTA insert at different times during simulated cutting process.

5.5.3 Designed Ceramic Composite Insert

The third and final case is analyzing the designed ceramic composite material considered for cutting tool insert in comparison with the previous cases. The proposed composite material is a $\text{Al}_2\text{O}_3\text{-30\%SiC-20\%cBN}$ with enhanced thermal and structural properties. Results are presented with the analysis of temperature profile and stress distributions as a function of time during a simulated cutting process.

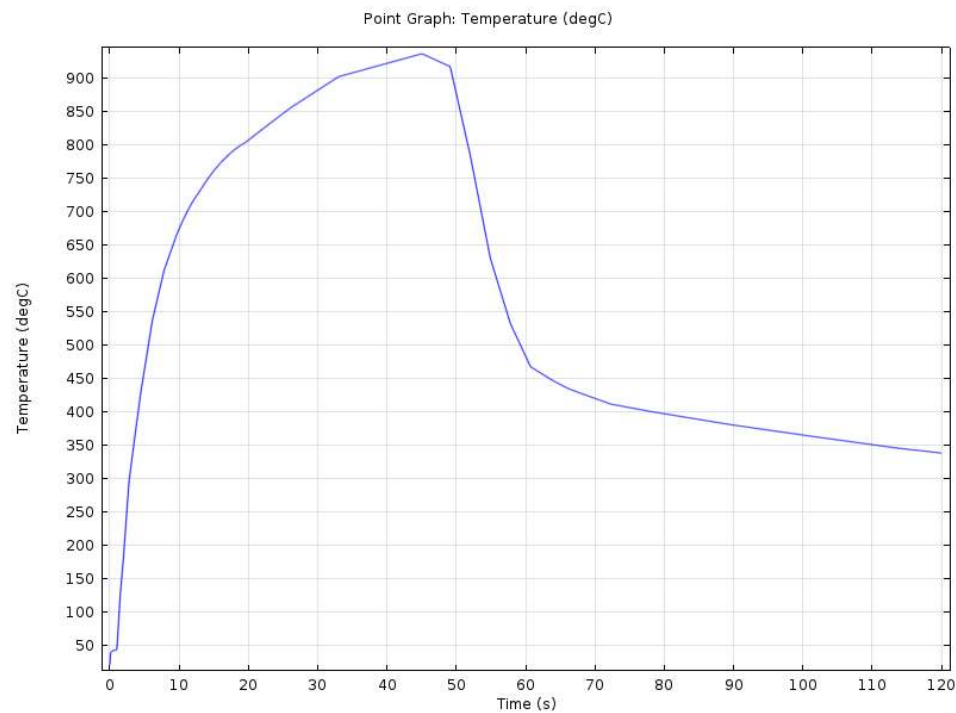


Figure 5.16 - Temperature profile at the cutting edge of the proposed insert as a function of time.

Figure 5.16 above shows the temperature profile of the insert cutting edge during the cutting process of a high strength profile steel. It is observed that the temperature at the point of highest heat flux is found to be much less as compared to the two previous cases of alumina and ZTA inserts. This is attributed to the superior thermal conductivity of the

designed composite which is allowing the temperature to quickly flow away from the cutting edge.

This phenomenon is further validated in the figure which shows the temperature profile as a function of distance moving away from the cutting edge. The temperature gradient of the designed composite material is less compared to the previous cases.

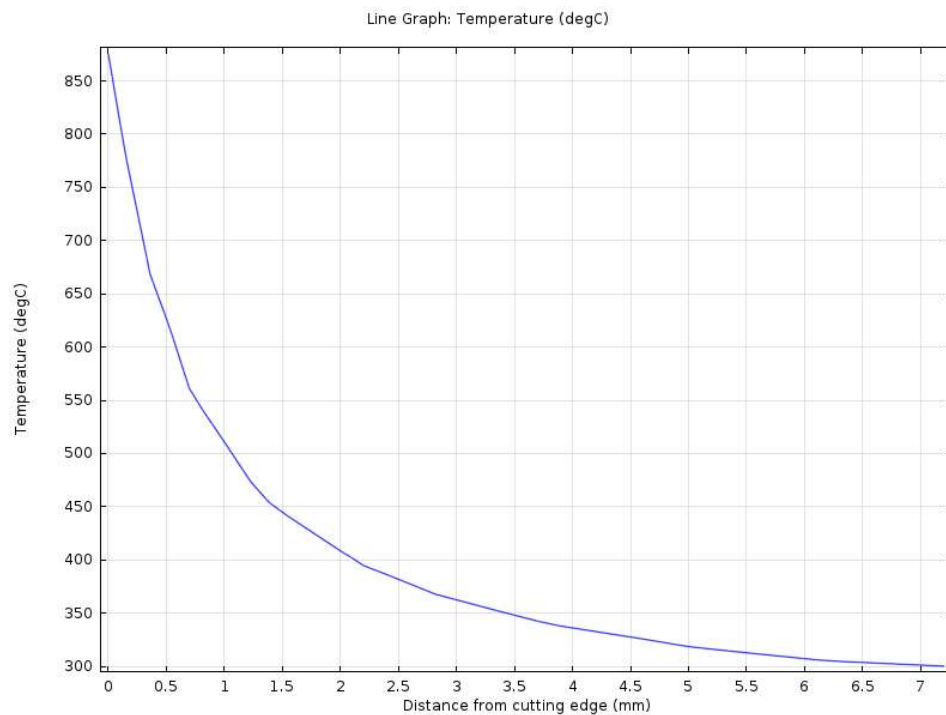


Figure 5.17 - Temperature profile as a function of distance from cutting edge to the center of proposed insert.

Next, the von-Mises stresses generated within the proposed cutting tool will be analyzed. It is important to monitor the stresses generated on the cutting edge as reduced stresses can lead to fewer chances of failure of the insert and improve the tool life of the cutting tool insert.

The von-Mises stress distribution of the Al₂O₃-SiC-cBN composite insert during the cutting process is shown below. At the cutting edge, it is found that there are considerably less stresses imposed on the designed insert when compared to the alumina and ZTA inserts. This is due to the enhanced elastic modulus of the composite along with the decreased CTE which is reducing the amount of deformation caused by the loadings imposed during the cutting process.

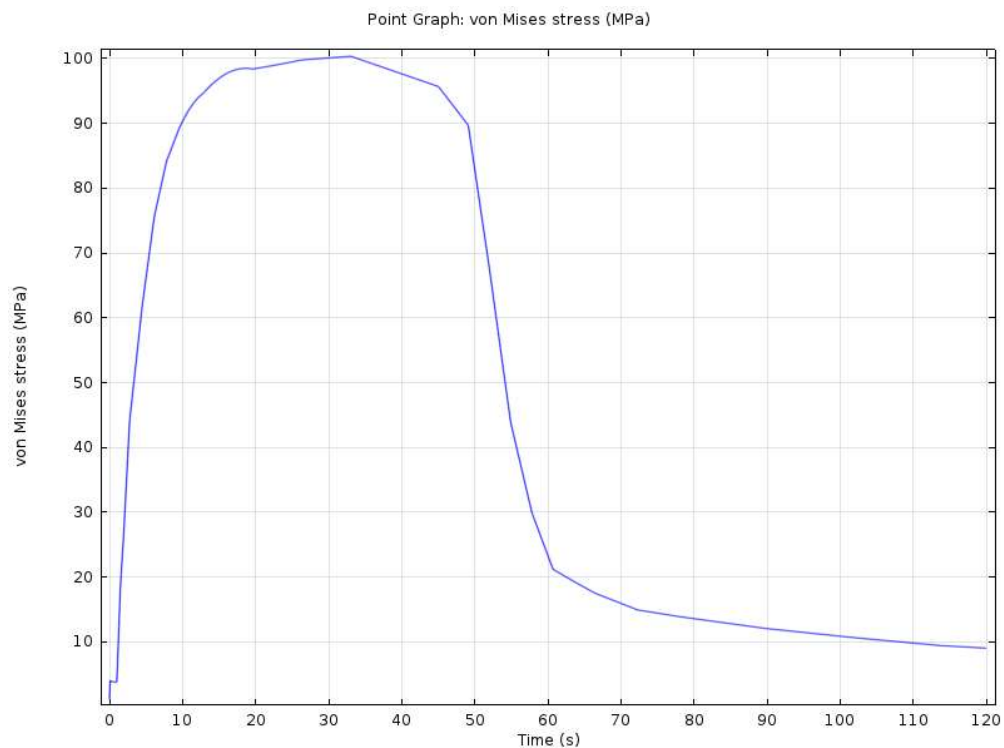


Figure 5.18 - Von-Mises stress distribution at the cutting edge of proposed insert during the cutting process.

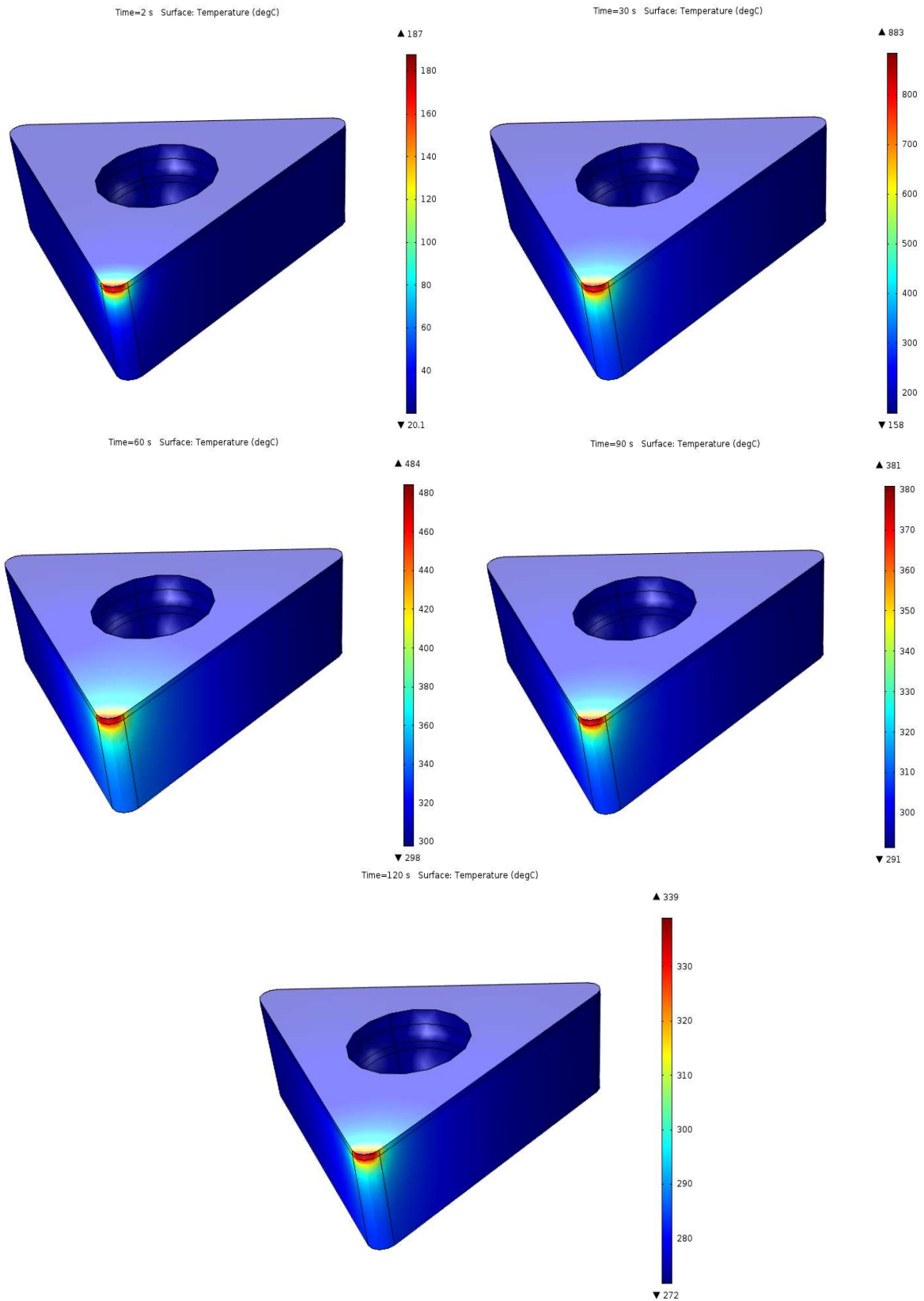


Figure 5.19 - Temperature profile of proposed insert at different times during simulated cutting process.

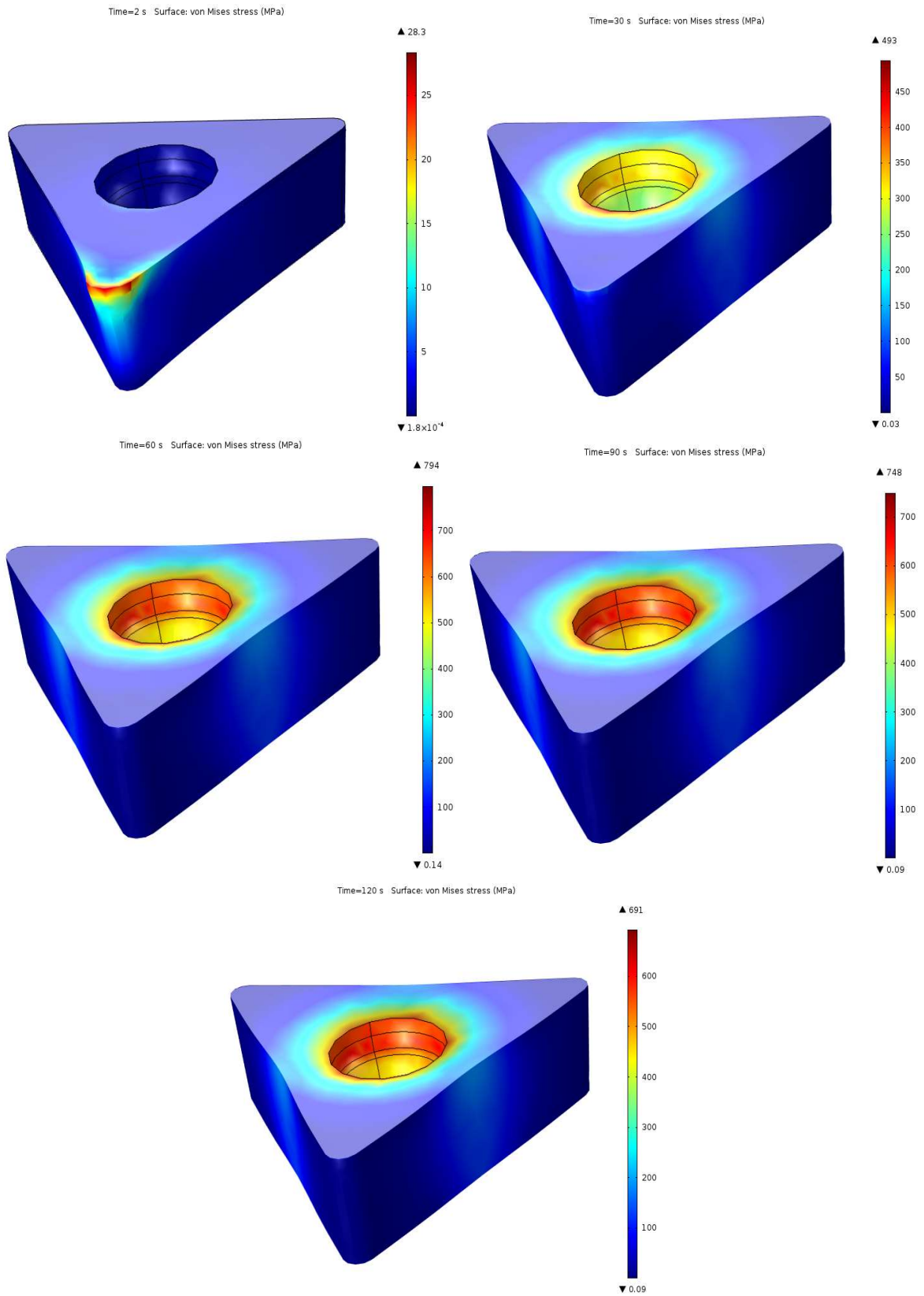


Figure 5.20 - Von-Mises stress distribution of the proposed insert at different times of simulated cutting process

5.6 Model Validation

The developed model has been implemented on the work done previously by KISKU on the investigation of the temperature profile of a coated and uncoated cemented carbide insert due to the heat flux introduced during the cutting process [96]. The same material model and boundary conditions have been used and the corresponding results are in good agreement with the reported results in reviewed work.

5.7 Summary of Chapter

This chapter has discussed the following:

- The performance designed and developed Al₂O₃-SiC-cBN composite when considering for use as cutting tool inserts is evaluated.
- FEM is considered to model the thermal performance of the composite when subjected to a cutting process of predetermined cutting speed, feed rate and depth of cut.
- As a means of comparison, alumina and ZTA inserts' performance is evaluated along with the designed composite.
- The thermal performance of the Al₂O₃-SiC-cBN composite is found to be better compared to the two other cases.
- Structural performance is also found to have been improved due to the presence of comparatively reduced stresses on the cutting edge of the designed composite.

CHAPTER 6

CONCLUSIONS & RECOMMENDATIONS

6.1 Conclusions

An innovative ceramic composite material for cutting tool insert applications is introduced through this work. The proposed material will possess enhanced thermal conductivity, elastic modulus, fracture toughness and lower CTE while retaining the environmental and economic advantages of alumina to improve the performance of cutting tool inserts considered for high speed machining.

Material design has been carried out using a computational approach through the aid of numerical models used in predicting the effective target properties of particulate composites as a function of inclusion volume fraction and particle size. Best matrix and inclusion material candidates are selected based on application and optimal combinations are determined through simulations. The material was designed as a hybrid alumina matrix composite with silicon carbide and cubic boron nitride inclusions to perform as an enhanced and cost-effective cutting tool insert.

Spark plasma sintering (SPS) was used to develop three material samples for material design validation, two alumina based composites (with 30% silicon carbide, 20% cubic boron nitride and 20% silicon carbide, 30% cubic boron nitride 40 μ m particle size inclusions, respectively) and one pure alumina (0.15 μ m matrix particle size). From

material testing, the developed composites were found to have improved thermal conductivity, elastic modulus, fracture toughness and lower CTE when compared with pure alumina with minimal porosity present. SEM scans showed the silicon carbide and cubic boron nitride inclusions to be fully dispersed into the alumina matrix. XRD patterns of the samples were observed and an additional peak was identified. The identified additional peak was associated with a phase transformation of cBN to hBN during the sintering process. The cause of transformation was hypothesized to be due to the presence of thermo-mechanical stresses present during the SPS process because of the additional silicon carbide inclusions within the matrix. For confirmation purposes, Raman spectroscopy was performed and it was observed that there was small transformation of cBN therefore confirming the XRD findings. This transformation is taken into account and the numerical simulations are recalibrated.

Lastly, performance evaluation is carried out to assess the capabilities of the composite material during a high-speed machining process in comparison to alumina and ZTA. Finite element method (FEM) is considered for the performance evaluation to assess the thermal-structural performance of the selected composite in a simulated cutting process. Normal working conditions were simulated where the temperature profile and localized stresses were analyzed as a function of time. The newly proposed $\text{Al}_2\text{O}_3\text{-SiC-cBN}$ composite material demonstrated more robust performance than alumina and ZTA due to the enhanced thermal and structural target properties. The temperature and stress analysis of the composite cutting tool insert highlighted greater thermal shock resistance and structural integrity of the composite material which reduces the risk of critical failure and enhances tool life.

6.2 Recommendations

Another critical area to focus in the design of cutting tools is to analyze the wear performance of the material. Therefore, a thorough tribological analysis is needed to assess the wear properties of the designed composite and identifying the types of wear failure which may occur during machining operations. Custom-made dies for spark plasma sintering can allow for manufacturing of cutting tool insert shaped samples which can allow carrying out of experimental performance testing using standard lathe machines as well as environmental impact studies.

Process optimization of spark plasma sintering may be performed to fine-tune the sintering parameters to reduce the percentage of unnecessary porosity present within the composite and stop the minimal phase transformation of the cBN inclusion. In addition, the fracture toughness model considered in this work is able to handle quantification of different modes of fracture failure. Therefore, an experimental study of determining the fracture failure modes of the composite may be undertaken to add another dimension to the existing work.

With the numerical models validated through means of experimental work, additional particulate composite combinations may be considered. Other matrix and inclusion candidates can be selected and their effect on the performance of the composite can be investigated for the selected application.

References

- [1] Emerging Economies to Fuel Global Machine Tools and Cutting Tools Market - Aerospace Manufacturing and Design, (n.d.). <http://www.aerospacemanufacturinganddesign.com/article/emerging-economies-fuel-global-machine-tools-and-cutting-tools-market-061513/> (accessed March 25, 2018).
- [2] Cutting Tools and Market Trends in the USA, (n.d.). <https://www.makino.com/about/news/Cutting-Tools-and-Market-Trends-in-the-USA/175/> (accessed March 25, 2018).
- [3] Grzesik, Wit. *Advanced Machining Processes of Metallic Materials : Theory, Modelling and Applications*. Amsterdam, NL: Elsevier Science, 2008. ProQuest ebrary. Web. 20 March 2017. Copyright © 2008. Elsevier Science. All rights reserved., (2017).
- [4] Krishan K. Chawla, *Composite materials: Science and Engineering*, 1998. doi:DOI 10.1007/978-1-4757-2966-5.
- [5] S. George, *Cutting Tools Application*, (2002) 153.
- [6] *ADVANCED ARENA: Why Ceramic Cutting Tools?* | 2012-02-01 | Ceramic Industry, (n.d.). <https://www.ceramicindustry.com/articles/92178-advanced-arena--why-ceramic-cutting-tools-> (accessed March 25, 2018).
- [7] G.A. Schneider, G. Petzow, *Thermal Shock and Thermal Fatigue Behavior of Advanced Ceramics*, Springer Netherlands, 1993.
- [8] R. Wertheim, A. Layyous, J. Harpaz, *Development and Application of New Cutting Tool Materials*, Proc. Conf. Improv. Mach. Tool Performance, San Sebastian, Spain. (1998) 303–313.
- [9] M.A. Yallese, K. Chaoui, N. Zeghib, L. Boulanouar, J.F. Rigal, *Hard machining of hardened bearing steel using cubic boron nitride tool*, J. Mater. Process. Technol. 209 (2009) 1092–1104. doi:10.1016/j.jmatprotec.2008.03.014.
- [10] Y. Sahin, *Comparison of tool life between ceramic and cubic boron nitride (CBN) cutting tools when machining hardened steels*, J. Mater. Process. Technol. 209 (2009) 3478–3489. doi:10.1016/j.jmatprotec.2008.08.016.
- [11] D.A. Stephenson, J.S. Agapiou, *Metal Cutting Theory and Practice*, n.d.
- [12] K. Geric, *Ceramics Tool Materials With Alumina Matrix*, Mach. Des. 3 (2010) 367–372.
- [13] E.D. Whitney, *Ceramic cutting tools : materials, development, and performance*, Noyes Publications, 1994.

- [14] C. Engineering, S. Proceedings, Alumina-Sic Whisker Composites, c (1986) 1182–1186.
- [15] J.L. Ortiz-Merino, R.I. Todd, Relationship between wear rate, surface pullout and microstructure during abrasive wear of alumina and alumina/SiC nanocomposites, *Acta Mater.* 53 (2005) 3345–3357. doi:10.1016/j.actamat.2005.03.031.
- [16] L. Fabbri, E. Scafè, G. Dinelli, Thermal and elastic properties of alumina-silicon carbide whisker composites, *J. Eur. Ceram. Soc.* 14 (1994) 441–446. doi:10.1016/0955-2219(94)90082-5.
- [17] C. Xu, X. Ai, C.H.- Wear, undefined 2001, Fabrication and performance of an advanced ceramic tool material, Elsevier. (n.d.).
- [18] J. Li, J. Sun, L.H.-M.S. and E. A, undefined 2002, Effects of ductile cobalt on fracture behavior of Al₂O₃-TiC ceramic, Elsevier. (n.d.).
- [19] Q. Dong, Q. Tang, W.L.-M.S. and E. A, undefined 2008, Al₂O₃-TiC-ZrO₂ nanocomposites fabricated by combustion synthesis followed by hot pressing, Elsevier. (n.d.).
- [20] S. Song, X. Ai, J. Zhao, C.H.-M.S. and E. A, undefined 2003, Al₂O₃/Ti(C_{0.3}N_{0.7}) cutting tool material, Elsevier. (n.d.).
- [21] A.S. Kumar, A.R. Durai, T. Sornakumar, Wear behaviour of alumina based ceramic cutting tools on machining steels, *Tribol. Int.* 39 (2006) 191–197. doi:10.1016/j.triboint.2005.01.021.
- [22] A. Senthil Kumar, A. Raja Durai, T. Sornakumar, Development of alumina-ceria ceramic composite cutting tool, *Int. J. Refract. Met. Hard Mater.* 22 (2004) 17–20. doi:10.1016/j.ijrmhm.2003.10.005.
- [23] H.M. Irshad, B.A. Ahmed, M.A. Ehsan, T.I. Khan, T. Laoui, M.R. Yousaf, A. Ibrahim, A.S. Hakeem, Investigation of the structural and mechanical properties of micro-/nano-sized Al₂O₃ and cBN composites prepared by spark plasma sintering, *Ceram. Int.* 43 (2017) 10645–10653. doi:10.1016/j.ceramint.2017.05.325.
- [24] D. Jianxin, C. Tongkun, L.L.-J. of the E.C. Society, undefined 2005, Self-lubricating behaviors of Al₂O₃/TiB₂ ceramic tools in dry high-speed machining of hardened steel, Elsevier. (n.d.).
- [25] D. Jianxin, L. Lili, L. Jianhua, ... Z.J.-... J. of M.T., undefined 2005, Failure mechanisms of TiB₂ particle and SiC whisker reinforced Al₂O₃ ceramic cutting tools when machining nickel-based alloys, Elsevier. (n.d.).
- [26] K. Broniszewski, J. Wozniak, M. Kostecki, A. Olszyna, Properties of Alumina - Graphene Oxide Composites, *Mater. Today Proc.* 2 (2015) 370–375. doi:10.1016/j.matpr.2015.04.034.

- [27] S.S. Akhtar, L.T. Kareem, A.F.M. Arif, M.U. Siddiqui, A.S. Hakeem, Development of a ceramic-based composite for direct bonded copper substrate, *Ceram. Int.* 43 (2017) 5236–5246. doi:10.1016/j.ceramint.2017.01.049.
- [28] E.A. Almond, Towards improved tests based on fundamental properties., *Natl. Lab. Met. Soc.* (1981) 161–9.
- [29] E.M. (Edward M. Trent, P.K. Wright, *Metal cutting*, Butterworth-Heinemann, 2000.
- [30] G.T. Smith, *Cutting tool technology : industrial handbook*, Springer, 2008.
- [31] T.N. Tiegs, P.F. Becher, Thermal Shock Behavior of an Alumina-SiC Whisker Composite, *J. Am. Ceram. Soc.* 70 (1987) C-109-C-111. doi:10.1111/j.1151-2916.1987.tb05017.x.
- [32] M.H. Rahman, H.M.M. Al Rashed, Characterization of Silicon Carbide Reinforced Aluminum Matrix Composites, *Procedia Eng.* 90 (2014) 103–109. doi:10.1016/j.proeng.2014.11.821.
- [33] D. Jianxin, L. Lili, L. Jianhua, Z. Jinlong, Y. Xuefeng, Failure mechanisms of TiB₂ particle and SiC whisker reinforced Al₂O₃ ceramic cutting tools when machining nickel-based alloys, *Int. J. Mach. Tools Manuf.* 45 (2005) 1393–1401. doi:10.1016/j.ijmachtools.2005.01.033.
- [34] S.Y. Luo, Y.S. Liao, Y.Y. Tsai, Wear characteristics in turning high hardness alloy steel by ceramic and CBN tools, *J. Mater. Process. Technol.* 88 (1999) 114–121. doi:10.1016/S0924-0136(98)00376-8.
- [35] Y.K. Chou, C.J. Evans, M.M. Barash, Experimental investigation on CBN turning of hardened AISI 52100 steel, *J. Mater. Process. Technol.* 124 (2002) 274–283. doi:10.1016/S0924-0136(02)00180-2.
- [36] L. Przybylski, B. Slodki, *High speed machining (HSM) - The effective way of modern cutting*, (2002).
- [37] J. Kopac, Advanced tool materials for high-speed machining, *Proc. 12th Int. Sci. Conf. Achiev. Mech. Mater. Eng.* (2003) 1119–1128.
- [38] H. Schulz, T. Moriwaki, High-speed Machining, *CIRP Ann.* 41 (1992) 637–643. doi:10.1016/S0007-8506(07)63250-8.
- [39] M.A. Davies, T.J. Burns, T.L. Schmitz, *High-Speed Machining Processes: Dynamics on Multiple Scales*, (n.d.).
- [40] C.C. Poe, Fracture Toughness of Fibrous Composite Materials, 3 (1984) 1759–1766.
- [41] J. Pittari, G. Subhash, J. Zheng, V. Halls, P. Jannotti, The rate-dependent fracture toughness of silicon carbide- and boron carbide-based ceramics, *J. Eur. Ceram.*

Soc. 35 (2015) 4411–4422. doi:10.1016/j.jeurceramsoc.2015.08.027.

- [42] I. Doghri, L. Tinel, Micromechanical modeling and computation of elasto-plastic materials reinforced with distributed-orientation fibers, *Int. J. Plast.* 21 (2005) 1919–1940. doi:10.1016/J.IJPLAS.2004.09.003.
- [43] T. Mori, K. Tanaka, Average stress in matrix and average elastic energy of materials with misfitting inclusions, *Acta Metall.* 21 (1973) 571–574. doi:10.1016/0001-6160(73)90064-3.
- [44] M. Rosenfeld, D. Kwak, M. Vinokur, A fractional step solution method for the unsteady incompressible navier-stokes equations in generalized coordinate systems, *J. Comput. Phys.* 94 (1991) 102–137. doi:10.1016/0021-9991(91)90139-C.
- [45] W. Jiajun, Y. Xiao-Su, Effects of interfacial thermal barrier resistance and particle shape and size on the thermal conductivity of AlN/PI composites, *Compos. Sci. Technol.* 64 (2004) 1623–1628. doi:10.1016/J.COMPSCITECH.2003.11.007.
- [46] C.-W. Nan, R. Birringer, D.R. Clarke, H. Gleiter, Effective thermal conductivity of particulate composites with interfacial thermal resistance, *J. Appl. Phys.* 81 (1998) 6692. doi:10.1063/1.365209.
- [47] S.S. Akhtar, M.U. Siddiqui, R. Kabeer, A. Hakeem, L. Kareem, A.F. Arif, A computational and experimental study on the effective properties of Al₂O₃-Ni composites, *Int. J. Appl. Ceram. Technol.* 14 (2017) 766–778. doi:10.1111/ijac.12674.
- [48] Y.M. Shabana, N. Noda, Numerical evaluation of the thermomechanical effective properties of a functionally graded material using the homogenization method, *Int. J. Solids Struct.* 45 (2008) 3494–3506. doi:10.1016/J.IJSOLSTR.2008.02.012.
- [49] M.U. Siddiqui, A.F.M. Arif, Generalized effective medium theory for particulate nanocomposite materials, *Materials (Basel)*. 9 (2016). doi:10.3390/ma9080694.
- [50] R. Emilia, A simple approach for determining the in situ fracture toughness of, (2001) 1889–1891. doi:10.1023/A:1012870110675.
- [51] P.P. Camanho, G. Catalanotti, Analytical Model for the Prediction of the Fracture Toughness of Multidirectional Laminates, 16th Int. Conf. Compos. Mater. (2007) 1–4.
- [52] T. Zhou, C. Huang, H. Liu, J. Wang, B. Zou, H. Zhu, Crack propagation simulation in microstructure of ceramic tool materials, *Comput. Mater. Sci.* 54 (2012) 150–156. doi:10.1016/j.commatsci.2011.10.039.
- [53] F. Cesari, L. Esposito, F.M. Furgiuele, C. Maletta, A. Tucci, Fracture toughness of alumina-zirconia composites, *Ceram. Int.* 32 (2006) 249–255. doi:10.1016/j.ceramint.2005.02.012.

- [54] G.A. Gogotsi, Fracture toughness of ceramics and ceramic composites, *Ceram. Int.* 29 (2003) 777–784. doi:10.1016/S0272-8842(02)00230-4.
- [55] D. Wang, J. Zhao, J. Zhao, A. Li, X. Chen, Microstructure-level modeling and simulation of the flexural behavior of ceramic tool materials, *Comput. Mater. Sci.* 83 (2014) 434–442. doi:10.1016/j.commatsci.2013.11.049.
- [56] M. Basista, W. Węglewski, Modelling of Damage and Fracture in Ceramic Matrix Composites – an Overview 1, *J. Theor. Appl. Mech.* 44 (2006) 455–484.
- [57] A. Leonardi, F. Furgiuele, R.J.K. Wood, S. Syngellakis, Numerical analysis of brittle materials fractured by sharp indenters, *Eng. Fract. Mech.* 77 (2010) 264–276. doi:10.1016/j.engfracmech.2009.08.003.
- [58] C.R. Chen, J. Pascual, F.D. Fischer, O. Kolednik, R. Danzer, Prediction of the fracture toughness of a ceramic multilayer composite - Modeling and experiments, *Acta Mater.* 55 (2007) 409–421. doi:10.1016/j.actamat.2006.07.046.
- [59] Y. Li, M. Zhou, Prediction of fracture toughness of ceramic composites as function of microstructure: I. Numerical simulations, *J. Mech. Phys. Solids.* 61 (2013) 472–488. doi:10.1016/j.jmps.2012.09.013.
- [60] Y. Li, M. Zhou, Prediction of fracture toughness of ceramic composites as function of microstructure: II. analytical model, *J. Mech. Phys. Solids.* 61 (2013) 489–503. doi:10.1016/j.jmps.2012.09.011.
- [61] G. Xie, Spark Plasma Sintering: A Useful Technique to Develop Large-Sized Bulk Metallic Glasses, *J. Powder Metall. Min.* 2 (2013) 2–4. doi:10.4172/2168-9806.1000e109.
- [62] Z. Shen, M. Johnsson, Z. Zhao, M. Nygren, Spark Plasma Sintering of Alumina, *J. Am. Ceram. Soc.* 85 (2002) 1921–1927. doi:10.1111/j.1151-2916.2002.tb00381.x.
- [63] N. Alumina, Spark-Plasma Sintering of Silicon Carbide Whiskers (SiC), *Processing.* 2300 (2004) 2297–2300.
- [64] L. Gao, H. Wang, J. Hong, H. Miyamoto, K. Miyamoto, Y. Nishikawa, S.D.D. Torre, Mechanical Properties and Microstructure of Nano-SiC–Al₂O₃ Composites Densified by Spark Plasma Sintering, *J. Eur. Ceram. Soc.* 19 (1999) 609–613. doi:10.1016/S0955-2219(98)00232-5.
- [65] J.H. Chae, K.H. Kim, Y.H. Choa, J.I. Matsushita, J.W. Yoon, K.B. Shim, Microstructural evolution of Al₂O₃-SiC nanocomposites during spark plasma sintering, *J. Alloys Compd.* 413 (2006) 259–264. doi:10.1016/j.jallcom.2005.05.049.
- [66] F. De Genua, V.M. Sglavo, High strength engineered alumina-silicon carbide laminated composites by Spark Plasma sintering, *Procedia Eng.* 10 (2011) 2621–2626. doi:10.1016/j.proeng.2011.04.437.

- [67] N. Tamari, T. Tanaka, K. Tanaka, I. Kondoh, M. Kawahara, M. Tokita, Effect of Spark Plasma Sintering on Densification and Mechanical Properties of Silicon Carbide, *J. Ceram. Soc. Japan.* 742 (2000) 740–742. doi:10.2109/jcersj.103.740.
- [68] V.M. Sglavo, F. De Genua, A. Molinari, F. Casari, Alumina/silicon carbide laminated composites by spark plasma sintering, *J. Am. Ceram. Soc.* 92 (2009) 2693–2697. doi:10.1111/j.1551-2916.2009.03247.x.
- [69] J. Zhang, R. Tu, T. Goto, Spark plasma sintering of Al₂O₃-cBN composites facilitated by Ni nanoparticle precipitation on cBN powder by rotary chemical vapor deposition, *J. Eur. Ceram. Soc.* 31 (2011) 2083–2087. doi:10.1016/j.jeurceramsoc.2011.05.019.
- [70] F. Ye, Z. Hou, H. Zhang, L. Liu, Y. Zhou, Spark plasma sintering of cBN/ β -SiAlON composites, *Mater. Sci. Eng. A.* 527 (2010) 4723–4726. doi:10.1016/j.msea.2010.04.034.
- [71] M. Hotta, T. Goto, Effects of cubic BN addition and phase transformation on hardness of Al₂O₃-cubic BN composites, *Ceram. Int.* 37 (2011) 1453–1457. doi:10.1016/j.ceramint.2010.09.058.
- [72] J. Zhang, R. Tu, T. Goto, Evaluation of CVD-deposited SiO₂ as a sintering aid for cubic boron nitride consolidated with alumina by spark plasma sintering, *J. Am. Ceram. Soc.* 95 (2012) 2827–2832. doi:10.1111/j.1551-2916.2012.05269.x.
- [73] M. Hotta, T. Goto, Densification and microstructure of Al₂O₃ – cBN composites prepared by spark plasma sintering, *J. Ceram. Soc. Japan.* 116 (2008) 744–748. doi:10.2109/jcersj2.116.744.
- [74] Y. Zhao, M. Wang, Effect of sintering temperature on the structure and properties of polycrystalline cubic boron nitride prepared by SPS, *J. Mater. Process. Technol.* 209 (2009) 355–359. doi:10.1016/j.jmatprotec.2008.02.005.
- [75] Y. Li, G. Qiao, Z. Jin, Machinable Al₂O₃ / BN composite ceramics with strong mechanical properties, *Mater. Res. Bull.* 37 (2002) 1401–1409.
- [76] H.M. Irshad, B.A. Ahmed, M.A. Ehsan, T.I. Khan, T. Laoui, M.R. Yousaf, A. Ibrahim, A.S. Hakeem, Investigation of the structural and mechanical properties of micro-/nano-sized Al₂O₃ and cBN composites prepared by spark plasma sintering, *Ceram. Int.* 43 (2017) 10645–10653. doi:10.1016/j.ceramint.2017.05.325.
- [77] Online Materials Information Resource - MatWeb, (n.d.). <http://www.matweb.com/> (accessed March 25, 2018).
- [78] Y. Xu, Y. Tanaka, M. Goto, Y. Zhou, K. Yagi, Thermal conductivity of SiC fine particles reinforced Al alloy matrix composite with dispersed particle size, *J. Appl. Phys.* 95 (2004) 722–726. doi:10.1063/1.1632022.
- [79] S. Schmauder, M. Meyer, H.F. Fischmeister, Correlation Between Dundurs $\hat{\alpha}^{\text{TM}}$ Parameters and Elastic Constants I- I-, *Z. Metallkd.* 83 (1992) 524–528.

- [80] Fracture Toughness / Fracture Energy Data for Ceramics - NIST Ceramics Data Portal, (n.d.). <https://srdata.nist.gov/CeramicDataPortal/ftmain> (accessed March 25, 2018).
- [81] A.G. Evans, B.J. Dalgleish, P.G. Charalambides, *J. Am. Ceram. Soc.* 73 (1990) 2419–2429.
- [82] R.W. Trice, J.W. Halloran, Influence of microstructure and temperature on the interfacial fracture energy of silicon nitride/boron nitride fibrous monolithic ceramics, *J. Am. Ceram. Soc.* 82 (1999) 2502–2508. doi:10.1111/j.1151-2916.1999.tb02110.x.
- [83] D. Smith, S. Fayette, Thermal resistance of grain boundaries in alumina ceramics and refractories, *Am. Ceram. Soc.* 86 (2003) 105–111. doi:10.1111/j.1151-2916.2003.tb03285.x.
- [84] G.D. Quinn, Fracture Toughness of Ceramics by the Vickers Indentation Crack Length Method: A Critical Review, *Mech. Prop. Perform. Eng. Ceram. II Ceram. Eng. Sci. Proc.* 27 (2008) 45–62. doi:10.1002/9780470291313.ch5.
- [85] N. Meredith, M. Sherriff, D.J. Setchell, S.A.V. Swanson, Measurement of the microhardness and young's modulus of human enamel and dentine using an indentation technique, *Arch. Oral Biol.* 41 (1996) 539–545. doi:10.1016/0003-9969(96)00020-9.
- [86] D. Chicot, *Tricot, Mechanical properties of ceramics by indentation: principle and applications*, *Ceram. Mater.* (2010) 115–153.
- [87] T. Oungkulsolmongkol, P. Salee-Art, W. Buggakupta, Hardness and Fracture Toughness of Alumina-Based Particulate Composites with Zirconia and Strontia Additives, *J. Met. Mater. Miner.* 20 (2010) 71–78.
- [88] D. Chicot, D. Mercier, F. Roudet, K. Silva, M.H. Staia, J. Lesage, Comparison of instrumented Knoop and Vickers hardness measurements on various soft materials and hard ceramics, *J. Eur. Ceram. Soc.* 27 (2007) 1905–1911. doi:10.1016/j.jeurceramsoc.2006.06.011.
- [89] L. Ćurković, V. Rede, K. Grilec, *Mulabdić*, Hardness and fracture toughness of alumina ceramics, *Proc. Conf. (6AD)* 40–45.
- [90] C. Shet, X. Deng, Finite element analysis of the orthogonal metal cutting process, *J. Mater. Process. Technol.* 105 (2000) 95–109. doi:10.1016/S0924-0136(00)00595-1.
- [91] M. Putz, G. Schmidt, U. Semmler, M. Dix, M. Bräunig, M. Brockmann, S. Gierlings, Heat flux in cutting: Importance, simulation and validation, *Procedia CIRP.* 31 (2015) 334–339. doi:10.1016/j.procir.2015.04.088.
- [92] Insert Designation Chart - provides ANSI and ISO designation code definitions for carbide insert shapes, relief angles, tolerances, chipbreaker codes, hole types, size values, thickness values, radius values, wiper lead angle, wiper clearance angle,

cutti, (n.d.). <http://www.carbidedepot.com/formulas-insert-d.htm#edgeprep> (accessed March 25, 2018).

- [93] Z. Bin Shamsudin, DEVELOPMENT OF CERAMIC CUTTING TOOL INSERT OF ALUMINA (Al_2O_3) AND ZIRCONIA (ZrO_2) FOR TURNING HARDENED TOOL STEEL, (n.d.) 45.
- [94] M. Ribeiro, S. Metrevelle, M. De Lima, Á.R. Machado, M. Bacci, G. Guimarães, S.R. De Carvalho, A. Jo, Analyses of Effects of Cutting Parameters on Cutting Edge Temperature Using Inverse Heat Conduction Technique, 2014 (2014).
- [95] M. Günay, M.E. Korkmaz, N. Yaşar, Finite element modeling of tool stresses on ceramic tools in hard turning, *Mechanika*. 23 (2017) 432–440. doi:10.5755/j01.mech.23.3.14363.
- [96] R. a M.C. Kisku, “ Modelling of Temper Ature Profile in Turning With Uncoated and Coated Cemented Carbide Ins Ert ,” (n.d.).

Vitae

Name: :Taha Waqar

Nationality: :Pakistani

Date of Birth: :10/25/1994

Email: :tahawaqar@gmail.com

Address: :280, K2, Wapda Town, Lahore, Pakistan, 54000

Academic Background: **B.S. (Mechanical Engineering)**
January 2016
King Fahd University of Petroleum and Minerals
Dhahran, Saudi Arabia

Publications:

- [1] Waqar, T., Akhtar, S. S., Hakeem, A., Arif, A. F., & Al-Athel, K. (2017).
Material Design and Development of Ceramic-based Composite For Cutting Tool
Inserts. *ICCE*.